AN ABSTRACT OF THE THESIS OF

John Anthony Starkovich (Name) for the Doctor of Philosophy (Degree)

in Chemistry (Major) presented on October 2, 1973 (Date)

Title: ELECTRODE DOUBLE LAYER MEASUREMENTS AND VOLTAMMETRY OF SOME ORGANOSULFUR COMPOUNDS IN SULFOLANE

Abstract approved: Redacted for privacy

Dr. Harry Freund

A new pulse method for measuring differential double layer capacitances has been developed in this work. The technique is based on the determination of the cell time constant which, for an ideally polarized test electrode-solution interface, is composed of the double layer capacitance and solution resistance. By applying small step voltage changes to a cell, an exponentially decaying current due to the charging of the double layer is observed. A propagation of errors analysis indicated that when the charging current had decayed to 50-25% of its peak value the maximum relative precision in the double layer capacitance could be achieved.

The pulse capacitance technique was implemented using a three-electrode potentiostat of conventional design built with integrated circuit operational amplifiers. The instrumentation and technique

were tested on cell circuit RC analogs and the accuracy of the capacitance measurements was within the precision of the measurement themselves, $\pm$ 3%. Double layer capacitance measurements made on a Hg-1.0 M KCl interface yielded results that agreed within experimental error with the accepted literature values.

The method was used to determine the double layer capacitance-potential curves for interfaces formed between electrodes of various materials and solutions of 0.10 M tetraethylammonium perchlorate in sulfolane. The simple RC model of the double layer was not applicable for these interfaces and a more complex model for the double layer was assumed which allowed for a small faradaic current to flow.

Except for a capacity hump anodic of the potential of zero charge, the capacitance-potential curve for mercury in sulfolane is similar in shape to those obtained for the electrode in other nonaqueous solvents. The value of the capacity maximum is about 30μf/cm^2. The capacity-potential curve was integrated by numerical summation to give the surface charge density and interfacial tension relative to the maximum value as a function of electrode potential. The parabolic relationship between interfacial tension and electrode potential was checked and found to agree closely with results obtained from polarographic drop time measurements. Capacitance-potential curves were also measured for gold, glassy carbon, and platinum. The double layer

capacitances for these electrodes were usually higher than for mercury and had larger faradaic current corrections.

Some of the advantages of the capacitance technique over the AC bridge technique are that the method is applicable to solutions of both high and low conductivities and that correction in the capacitance determination can be made for a non-ideally polarized interface. The technique can be implemented using instrumentation commonly used for fast scan voltammetry, thus not requiring a special instrument useful only for double layer capacitances.

The voltammetric potential ranges accessible in sulfolane with tetrathylammonium perchlorate supporting electrolyte are very large. The range available with mercury is +0.1 to -3.3 v, while for gold, glassy carbon, and platinum the ranges are +1.2 to -3.2, +1.3 to -3.3 and +1.6 to -3.0 v as measured with respect to a silver-silver ion reference electrode in the solvent.

Voltammetric waves were observed for n-butyl mercaptan, -sulfide, -disulfide and phenyl disulfide. The substances gave reasonably well-defined peaks with characteristic peak potentials. Anodic waves were observed for the mercaptan and sulfide on gold, glassy carbon and platinum electrodes. Cathodic waves were observed for butyl disulfide. All electrode reactions involving the aliphatic sulfur compounds appeared irreversible. Phenyl disulfide could be reversibly reduced on mercury.

Electrode Double Layer Measurements and Voltammetry of Some Organosulfur Compounds in Sulfolane

by

John Anthony Starkovich

A THESIS

submitted to

Oregon State University

in partial fulfillment of
the requirements for the
degree of

Doctor of Philosophy

June 1974

APPROVED:

Redacted for privacy

Professor of Chemistry
in charge of major

Redacted for privacy

Chairman of Chemistry

Redacted for privacy

Dean of Graduate School

Date thesis is presented October 2, 1973

Typed by Cheryl E. Curb for John Anthony Starkovich

ACKNOWLEDGMENTS

The author is deeply indebted to Dr. Freund for his personal help and guidance throughout the course of this work. The author also wishes to thank the other faculty members and fellow graduate students for their advice and helpful discussions. A research grant from the Pacific Northwest Pulp and Paper Association for partial support of this work and a grant of computer time from the Oregon State University Computer Center are gratefully acknowledged.

A special debt of gratitude are due my wife, Dixie, and my son, Chris, for their understanding, patience and unfailing moral support.

TABLE OF CONTENTS

TABLE OF CONTENTS (Cont.)

LIST OF TABLES

LIST OF FIGURES

LIST OF FIGURES (Cont.)

ELECTRODE DOUBLE LAYER MEASUREMENTS AND VOLTAMMETRY OF SOME ORGANOSULFUR COMPOUNDS IN SULFOLANE

I. LITERATURE

A. Introduction

Sulfolane is a relatively new nonaqueous solvent that appears to have many physical and chemical properties which could make it an industrially important and useful laboratory solvent. There is much current interest in learning more about its properties and use as a chemical reaction medium. There is also interest in examining its electrochemical properties and use as a medium for carrying out electrochemical reactions. Some solution conductances and potentiometric measurements have been made, but little voltammetric work has been performed in the solvent, and electrode-solution interfacial properties which are important to electrode reaction kinetics and voltammetric studies are generally lacking.

When the research for this dissertation was undertaken, the goal was to learn more about the electrochemical properties of sulfolane and explore the possibility of using the solvent as a medium for voltammetric analyses of electroactive organic materials. The research has dealt specifically with measuring electrode-solution interfacial capacities of the solvent using an innovative technique

developed in this work and obtaining voltammetric information on a few organosulfur compounds.

B. Sulfolane

Physical and Chemical Properties

Sulfolane (tetrahydrothiophene 1, 1-dioxide, or tetramethylene sulfone, or TMS) is a cyclic sulfone. It was first synthesized in 1916 through oxidation of tetrahydrothiophene with permanganate (40). The material was not much studied until around the mid-1930's when workers interested in petroleum refining discovered some of its valuable solvent properties. There were numerous patents granted during this period concerning various commercial methods for synthesizing TMS, but market development samples of the solvent were not available until the late 1950's. Thus much of the work reported with this solvent has been reported only in the last decade or so.

Sulfolane is commercially prepared today by the catalytic hydrogenation of 3-sulfolene (2, 5-dihydrothiophene 1, 1-dioxide), which is itself produced commercially through the reaction between butadiene and sulfur dioxide (67).

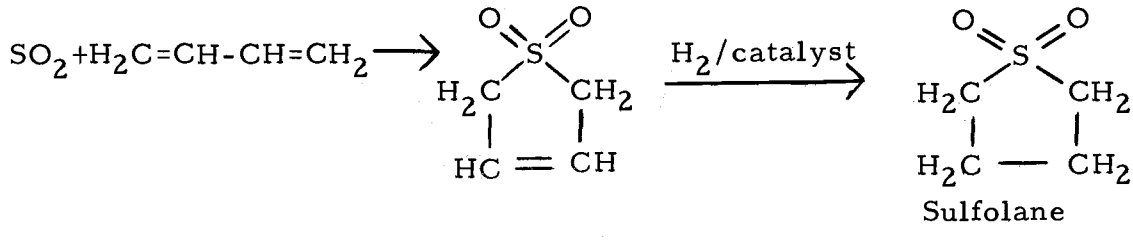

Some of the physical properties of sulfolane are listed in Table 1. TMS is a clear, colorless solid at usual room temperatures, but melts around 28°C. The solid resembles ice in appearance and the liquid is similar to water but much more viscous. Unlike ice and water, though, sulfolane has a mesophase. While the solvent solidifies around 28°C, it does not immediately crystallize at normal pressures, but remains in a liquid crystal state until around 17°C (45). The solvent's heat and entropy of fusion are very low, 2.73 Kcal per mole and 1.2 calories per degree, respectively, indicating that there is little difference between solid and liquid sulfolane near the melting temperature.

The low heat of fusion for solid TMS is responsible for an exceptionally large cryoscopic constant. The molal freezing point lowering constants for typical solvents, such as water, cyclohexane and benzene, range from 2 to 20° Kelvin per mole. This constant for sulfolane is 66.2. This large cryoscopic constant coupled with its near room temperature melting point led early workers to believe that sulfolane would find wide use as a solvent for molecular weight determinations. Subsequent discovery of the mesophase damped these expectations.

If one were to choose three adjectives to best characterize sulfolane, they would be polar, aprotic, and inert. As a class of organic solvents, the sulfones rank second after amides as solvents

Table 1. Some properties of sulfolane.

Property	Value	Reference
Molecular Weight	120.17	
Melting Point, ^{o}C.	28.37, 27.4-27.8	2, 76
Boiling Point, ^{o}C/mm	117/1	46
Critical Temperature, ^{o}K	801	76
Critical Pressure, Atm.	52.2	76
Dielectric Constant, at 30^{o}C	43.36, 43.3	79, 81
Density, g/ml at 40^{o}C	1.2525	79
Viscosity, centipoise, at 40^{o}C	7.91	79
Surface Tension, dyne cm^{-1} at 30^{o}C	49.46, 49.5	46, 79
Refractive Index, at 30^{o}C	1.4820	81
Dipole Moment, debye, in benzene at 25^{o}C	4.82	18
Molar Volume, cm^{3} at 30^{o}C	95.2	79
Specific Conductance, Mhos cm^{-1} at 30^{o}C	2-5 x 10^{-9}	77
Heat Capacity, C_p, cal g^{-1} deg^{-1}	0.31	76
Heat of Fusion, cal/g at 26^{o}C	2.73	10
Entropy of Fusion, e. u. at 26^{o}C	1.2	77
Heat of Vaporization, cal/g at 100^{o}C	125	76
Cryoscopic Constant, deg Kg. mole^{-1}	-66.2, -64.8	2, 10
LD_{50}, g Kg^{-1}, oral in mice	1.9-2.5	9, 75

with high dielectric constants. Sulfolane has a dipole moment of 4.69 debye and a high dielectric constant of 44. Both properties put TMS in the polar solvent category and somewhere in the upper part of this group. Most classes of organic compounds and polymers are soluble in or miscible with sulfolane (49) with the exception of paraffinic and naphthenic compounds and styrene and methacrylate polymers. Solubilities of inorganic materials in TMS are lacking. Salts that do dissolve to some extent are extensively dissociated (10, 24, 27, 33, 53) owing to the high dielectric constant of TMS.

Chemists requiring an aprotic solvent of low basicity in the Bronsted sense can look to sulfolane. Bordwell (7) has measured the proton acidities of a number of sulfones and found the pK_a for tetramethylene sulfone to be greater than 31 in DMSO at 25°C. Benoit (5) has reported the heat of solution for TMS in water to be 1.6 Kcal $mole^{-1}$ and Hall (41) has found sulfolane to have a proton basicity (pK_{BH+}) of -12.88. While both of these measurements reflect a solvent of very low proton basicity, Jones (48) has found TMS to be a better Lewis base. He was able to isolate a 1:1 complex between TMS and boron trifluoride and Langford (55) has observed complexes between some cobalt salts and TMS.

Despite sulfolane's apparent electron donor properties, the solvent is perhaps one of the most chemically and thermally stable organic solvents available today. TMS is thermally stable up to

220°C. At this temperature it starts decomposing to sulfur dioxide and unsaturated polymeric material (21). The decomposition rate at this temperature, though, is less than 0.01% per hour. No chemical reaction has been observed between sulfolane and potassium carbonate, sodium acetate, 25% aqueous sodium hydroxide and copper or iron strips after five hours of exposure at reflux temperatures (76). However, at 140-150°C, TMS will react with 93% sulfuric acid. At this temperature it will also react with aluminum chloride (49) to evolve HCl and H_2S. Sulfolane is non-reactive with metallic zinc, acetic and hydrochloric acids, but is reduced by lithium aluminum hydride and will undergo vapor phase hydrogenation over a catalyst at 350°C (65). Other reactions reported for TMS include a Grignard reaction (76), reduction to a sulfide (6) and reduction by sodium and potassium metals (83) to produce butane sulfinate.

When one considers the solvent properties of TMS and its low toxicity (9, 34, 75), one should expect to find the solvent being used in many applications. This is the case. There are numerous applications using sulfolane in various purification procedures. These range from large scale commercial processes, such as Shell's Sulfinol Process (31, 76), to laboratory size extraction methods. TMS has also been used as a solvent for metathesis, isomerization, and polymerization reactions. A discussion of many of these applications and specific uses can be found in references (67, 76) and will

not be pursued here. Specialty applications, such as the use of TMS as a dielectric material in high capacity electrical condensers and as a hydraulic fluid, etc., are also covered in these sources.

Electrochemical Work in Sulfolane

There have appeared in the literature many articles concerned with electrochemistry in sulfolane. The earliest of these papers had to do with using conductance measurements in determining the extent of ion pairing in TMS (10, 33). Other conductance work in sulfolane centered around collecting conductance information for a large number of salts and determining ion solvation and transport numbers (24, 25, 27, 33, 53). Della Monica's (26) group seems to have been the only one to have performed any conductometric titrations in sulfolane, though it was not for any analytical purpose.

Since Burwell's early conductance work in TMS, there has been some interest shown in potentiometric measurements in the solvent. Morman (66) has demonstrated that TMS can be used as a non-leveling medium for strong acid potentiometric titrations as well as for very weak base (such as caffeine) titrations. Coetzee (14) has also performed potentiometric acid-base titrations in TMS. The only other published papers concerned with potentiometric measurements in sulfolane appear to be those of Monica (26) and Benoit (3) in which the equilibria between silver ion and some halide ions were discussed.

No routine analytical potentiometric titration methods have been reported nor has there been any work published concerning the use of specific ion electrodes other than the glass electrode in this solvent.

Other types of electrochemical experiments performed in TMS have included polarography, voltammetry and electrical double layer capacitance measurements. Hill (see Bibliography in reference 43) was apparently the first person to point out that polarography in TMS was possible, but Headridge et al. (43) seem to have been the first to report on their polarographic studies in the solvent. They were interested in observing trends in the ease with which inorganic materials were electrochemically reduced or oxidized in TMS. Desbarres, Pichet and Benoit (28) found a reversible electrode couple that could be used as a convenient nonaqueous reference electrode in sulfolane and reported half-wave potentials relative to their reference electrode for some of the same metal species that Headridge had studied. Other workers (4, 15, 42, 77) have also been interested in the solvation and medium effects in sulfolane. Martinmaa (61) has combined ESR spectroscopy and polarography to study the products generated from the electrolysis of nitrobenzenes in sulfolane. This has been the only work concerned with organic electrode reactions in TMS. In all of the electrochemical work mentioned, only working electrodes of platinum and mercury have been used and no fast scan or cyclic voltammetric experiments have been performed in TMS.

Lawrence and Parsons (56, 57) have been the only workers who have shown interest in studying the nature of the electrical double layer in sulfolane solutions. Using the AC impedance bridge technique that was developed by Grahame (38, 39) for aqueous solutions, they measured double layer capacitances at the mercury-sulfolane interface for solutions of sodium perchlorate and potassium hexafluorophosphate. It is clear that if sulfolane is to be a useful solvent in which to carry out quantitative voltammetric analyses, the nature of the interface between electrodes of other materials and different electrolytic solutions must be studied.

C. Electrical Double Layer

Electrode-Solution Interfacial Models

The study of heterogeneous equilibria and the physical properties of surfaces is an old endeavor that is currently of much interest. One area of this research that is being actively pursued is the study of electrode-solution interfacial regions. Interest in this area stems generally from two sources, electrodynamicists and analytical chemists. It has been known for some time now that the electrode-solution interface can play an important role in determining the kinetics and equilibria of electrode reactions and thus is of interest to electrokineticists studying electrochemical processes. Analytical

chemists have found that the presence of the double layer region can in many instances determine the sensitivity and detection limits of several electroanalytical methods. Thus in recent years, with the emphasis placed on analyzing trace constituents by electrochemical methods, techniques had to be developed which minimized the role that the interfacial region played in the analysis and this has required an understanding of the properties of the electrical double layer.

The term "electrical double layer" refers to a region between phases in which a space charge density exists that is in excess of that found in the interiors of either pure phase. The idea of there being such a region near a phase boundary with different properties than those of the bulk phases was due first to Helmholtz and Quincke. These men were interested in the nature of interfaces formed between a solid and a solution and proposed the first model for the interfacial region. Both considered the phase boundary region to be composed of two oppositely charged layers separated from one another by some small molecular distance. Their model of the region was that of a simple electrical condenser with two parallel plates, in which one plate was located on the surface of the solid and the second plate was situated on the solution side of the interface. This model was used by them to successfully explain the observed phenomena of electroosmosis and streaming potentials.

The first refinements in this model and the application to interfacial regions formed between metal conductors and solutions were introduced independently by Gouy (36) and Chapman (13) around 1910. Both workers pointed out that Helmholtz's and Quincke's model neglected to consider the thermal energy of the charged solution particles and the effect that this energy might have on the nature of charge distribution in the interfacial region. Assuming the charged solution species to be point sources, Chapman developed a mathematical description of ionic charge distribution normal to the electrode surface considering both thermal and electrostatic interaction among solution particles. The result of Chapman's treatment was that the idea of a simple planar interface was abandoned and the idea of a more diffuse layer of charge extending hundreds of Angstroms into the solution was accepted. The charge on the electrode side of the interface, however, was still considered to be essentially a plane or sheet of electronic charge.

While the concept of a fixed plane of solution charges at the electrode-solution interface was discarded after Chapman's work, the term "double layer" region has been retained to denote this general interfacial region in which this excess space charge exists.

The new model for the electrical double layer (edl) proposed by Gouy and Chapman could still not be used to predict values for the interfacial properties of real systems. Stern (78) suggested two

refinements in the Gouy-Chapman model that eventually led to agreement between experiment and theory. He first pointed out that it was physically unrealistic to consider solution charges as point sources and thus that there should be some limiting distance within which an ion or molecule could approach the electrode surface. Secondly, Stern suggested that in addition to thermal and electrostatic energies of solution particles, the possibility of chemical interaction between ions and molecules in solution and the metal atoms of the electrode should be considered in describing particle concentrations in the interfacial region. This chemical interaction is now referred to as specific adsoprtion.

Show in Figures 1 and 2 are representations of the various electrical double layer models. The model proposed by Stern is a combination of the earlier models. The double layer region according to Stern was composed of both a rigid, compact part and a less structured, more diffuse part. The plane drawn through the primary layer of non-specifically adsorbed ions (cations in Figure 2) is called the "Outer Helmholtz Plane" (O. H. P.) and the region between it and the electrode surface is referred to as the compact part of the double layer, while that region extending from the O. H. P. into the bulk solution is referred to as the diffuse part of the double layer. The plane drawn through the centers of specifically adsorbed ions is called the "Inner Helmholtz Plane" (I. H. P.). In the absence of

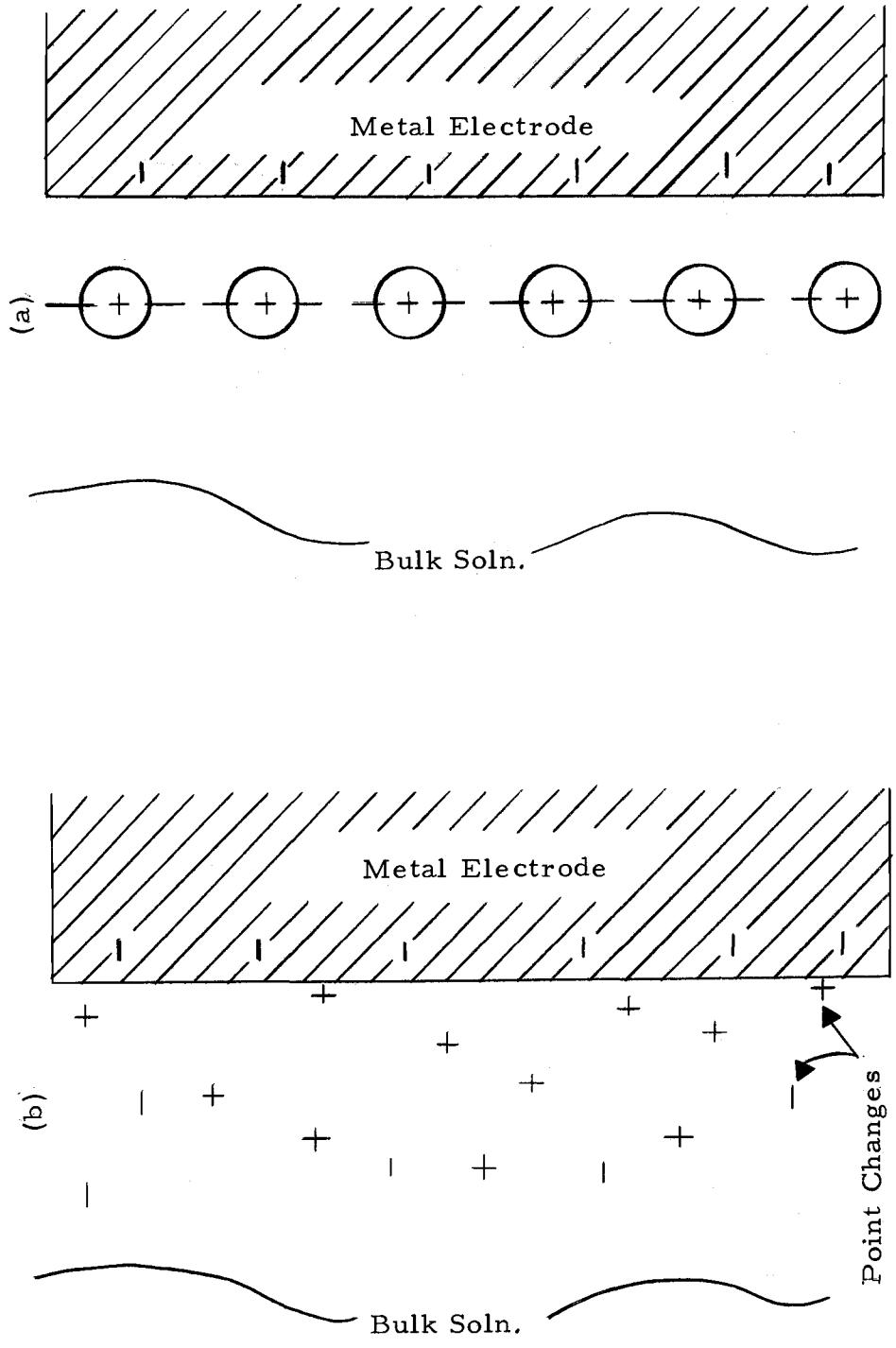

Figure 1. Models of the Double Layer: (a) Helmholtz-Quincke Model; (b) Gouy-Chapman Model.

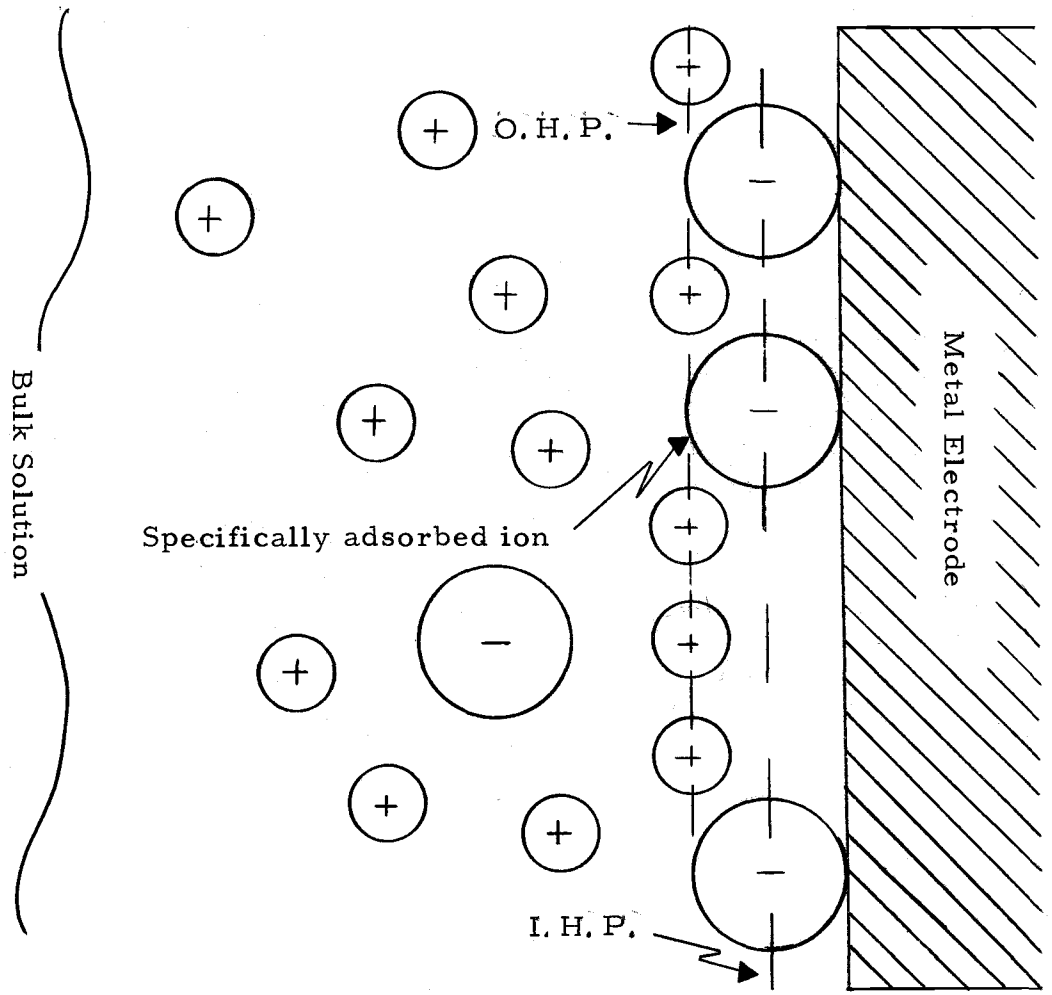

Figure 2. Stern model for the double layer.

specific adsorption, the region between the O. H. P. and the electrode surface is filled with oriented solvent molecules according to present views (16, 22).

Electrical Circuit Analogs for Double Layer Region

The presence of charged particles or oriented electrical dipoles in the region of the electrode-solution interface greatly affects the properties of the interface. Surface tension measurements furnished most of the early knowledge about double layer regions, but have recently been largely supplanted in this role by capacitance measurements. Double layer parameters, such as charge density and charge components, can be derived in different ways from both types of measurements (64); however, for a given level of precision in the final calculated parameter, surface tension measurements have to be made more accurately than capacitance measurements. While it is possible to make accurate surface tension measurements with liquid electrodes, like mercury, the procedure is very time consuming and not readily applicable to solid electrodes. Capacitance measurements, on the other hand, can be made readily with one to two percent accuracies and yield values for double layer parameters in close agreement with those derived from surface tension measurements.

In measuring capacitances of metal-solution interfaces, an electrical analog of the interface must be assumed in order to

interpret the observations. One of the simplest and most frequently employed analogs used to interpret the response of the metal-electrolyte interface to electrical signals is a parallel combination of a resistor and capacitor. The two circuit components represent the two ways in which current is conducted by the interface. Current through the resistive path is referred to as "faradaic" and that through the capacitor, "nonfaradaic." In the former, current crosses the interface by virtue of an electrochemical reaction such as an oxidation or reduction which is governed by Faraday's laws of electrolysis. In the latter (nonfaradaic) case, charged particles are not transferred across the interface, but current flows as a result of the charging and discharging of the electrical double layer. For a complete electrochemical cell consisting of two metal-solution interfaces with a bulk solution phase between them, the electrical analog is as shown in Figure 3a.

Points A and B in Figure 3a are the leads to the cell, C_{d11} and C_{d12} represent the electrical capacitances manifested by each interface, R_{f1} and R_{f2} the faradaic impedance to charge transfer across the interfaces, and R_{soln} an ohmic resistance to current flow through the bulk solution phase. If there is little electrolysis taking place in the cell, R_{f1} and R_{f2} can be considered to be very large and in the limit that zero faradaic current flows, R_{f1} and R_{f2} can be considered as open circuits and the electrical analog of the cell reduces to that

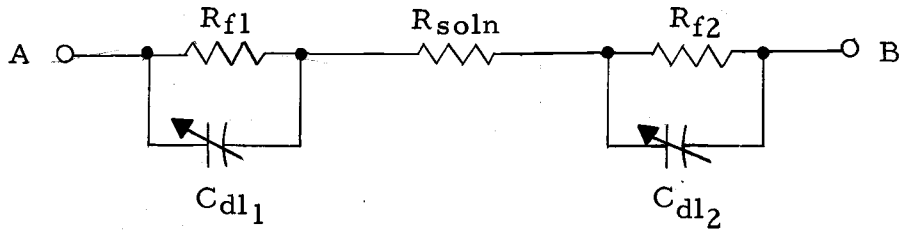

(a)

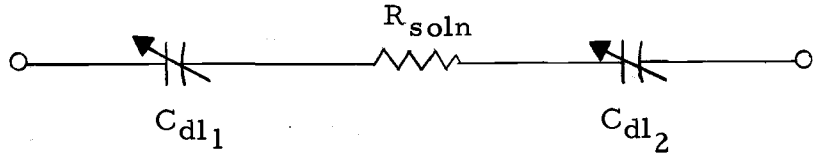

(b)

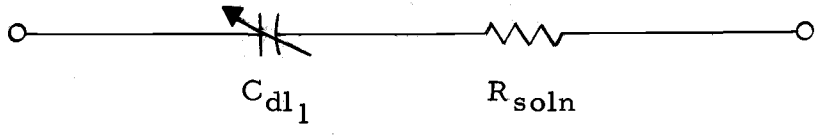

(c)

Figure 3. Electrical circuit analogs for an electrochemical cell.

shown in Figure 3b. Furthermore, if one makes the area of one phase boundary interface very large compared to the area of the second interface, the cell's response to an electrical signal will be determined by the solution resistance and the capacitative reactance of the smaller interface. This assumes that the specific capacitances (capacitance per unit area) of each interface are similar. Under these conditions, then, the equivalent circuit model of the cell can be further simplified to that shown in Figure 3c. C_{dl} is called the "differential double layer capacitance" and is represented as a variable capacitor since it can vary with the potential applied to the cell. Since the differential double layer capacitance is a function of the size of the experimental interface, it is referred to a unit area of an interface.

Pulse Technique for Measuring Interfacial Capacitance

Double layer capacitances have generally been measured by means of the AC bridge technique. The experimental setup is similar to that used in making solution conductivity measurements, except that instead of measuring solution resistance, C_{dl} is determined. AC bridge techniques have been quite suitable for measuring double layer capacitances for aqueous interfaces. The aqueous phases have typically been solutions containing moderate concentrations of strong electrolytes and hence of high conductivity. Under these conditions,

the cell's response to the AC exciting signal has been principally determined by the capacitive reactance of the double layer region and not bulk solution resistance. In working with less conducting aqueous phases and many organic solution phases, the bridge technique has not been as accurate in determining C_{dl} and hence poorer values for double layer parameters calculated from C_{dl} have generally resulted. This is the case because the signal that is detected in the bridge technique depends on the sum of the solution resistance and interfacial capacitive reactance. For poorly conducting solutions the total impedance is largely determined by the solution resistance. This is a poor situation for determining capacitance reactance.

Using the series R-C equivalent circuit as a model for the electrochemical cell, a pulse technique for measuring C_{dl} can be developed that should be capable of being used with solutions of high or low conductivities.

Consider the circuit shown in Figure 4a. Initially the switch is in the lower position and some potential, e_i, is applied to the cell. If there is no electrolysis taking place and the interfacial capacitance is charged up, there is zero electrical current flowing through R and E_{out} is observed to be zero. If the switch is now opened, the voltage applied to the combination of R and the cell is changed by some small amount, e_s. As a result of this sudden change in the applied voltage to the cell, a current flows in the circuit to charge the double layer

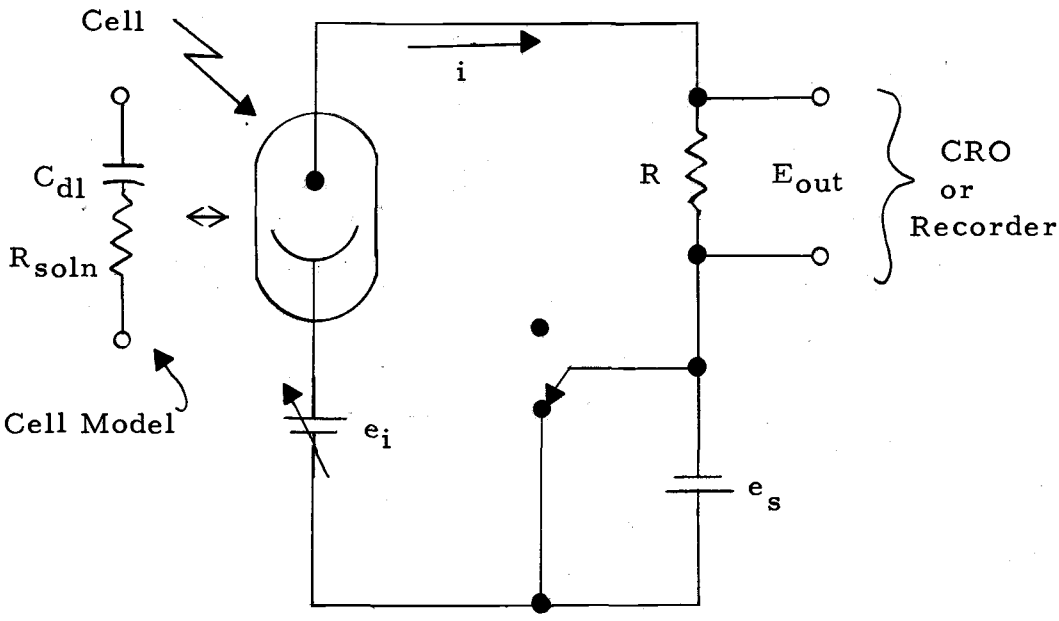

(a)

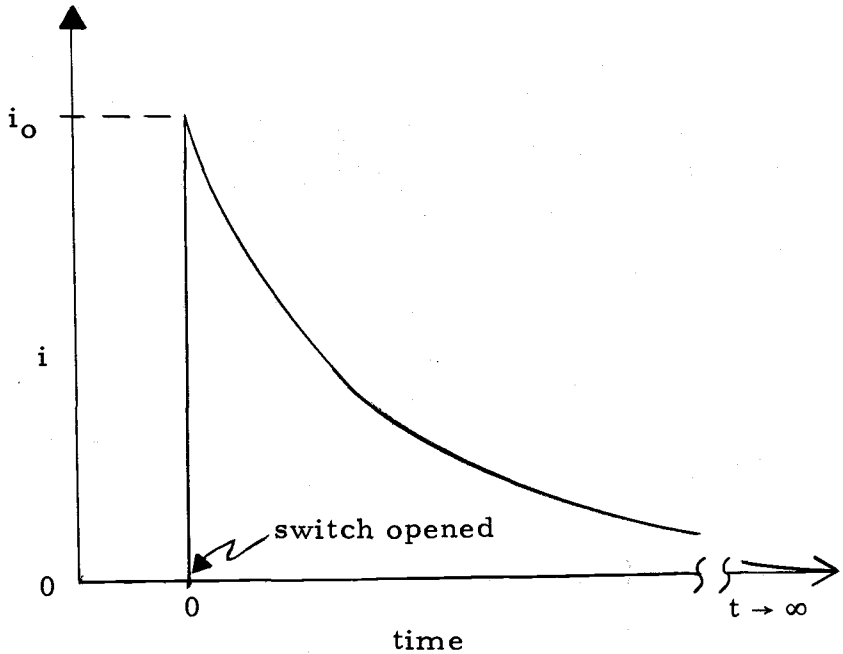

(b)

Figure 4. (a) Schematic diagram of pulse circuit for measuring double layer capacitances.
(b) Charging current waveform for pulse capacitance technique.

up to the new potential, $e_i + e_s$. The current that flows in the circuit decays exponentially with time, as expressed by Equation (1).

$$i = i_o \exp \left\{ - \frac{t}{(R+R_{soln})C_{dl}} \right\} \tag{1}$$

where i_o is the current flowing immediately after the application of the step voltage, and t is the elapsed time measured from the application of the step voltage. The current-time waveform is shown in Figure 4b.

C_{dl} can be found from Equation (1) in three ways. If the natural logarithms of each side of the expression are taken, one obtains the following equation:

$$\ln i = - \frac{t}{(R+R_{soln})C_{dl}} + \ln i_o \tag{2}$$

which on solving for C_{dl} yields:

$$C_{dl} = \frac{t}{(R+R_{soln})\ln x} \tag{3}$$

where $x = i_o/i$. Equation (3) can be used directly to determine C_{dl} if i_o, i, and t are measured during a pulse experiment. Accurate experimental measurement of i_o, however, is difficult since its value is greatly affected by the response time of the measuring instrument and the risetime of the step voltage source.

The second approach to finding C_{dl} is to make several current-time measurements later in the experiment and construct a plot of ln i versus t for the measurements. Such a plot should be linear and have a slope, according to Equation (2), of $-\frac{1}{(R+R_{soln})C_{dl}}$. If the value of the circuit resistor were known and R_{soln} determined in a separate experiment, say by means of an AC bridge, C_{dl} can be found from the slope of the semi-logarithmic plot. A better estimate of C_{dl} can be obtained if the method of least squares (86) is used to determine the slope of the best line for the ln i - time data.

The principle of measuring the time constant of a cell ($R_{soln}C_{dl}$) via a pulse experiment was proposed by Delahay, DeLevie and Guiliani (23) in 1966, and successfully used in poorly conducting solutions. The actual instrumentation used by them in their work was more complicated than indicated in Figure 4a and they did not monitor cell current, but rather measured the change in voltage of the test electrode as a function of time. The advantage of the pulse capacitance technique over the AC bridge method is that the experimentally determined parameter, the slope of the semilog plot from which C_{dl} is calculated, depends on the product of the solution resistance and double layer capacitance, and not a sum of these factors. Thus, for lower conducting solutions, or cells with a high resistance, the pulse capacitance technique can be used without a loss of accuracy in the measurement. The pulse technique is equally applicable to solutions

of medium and high conductivity.

The third method for determining C_{dl} is similar to the second approach, but makes fuller use of the information contained in the semi-logarithmic plot of the current-time data. Having determined the slope of the line in the plot of ln i versus t, the line can be extrapolated back to t = 0 to furnish a value for ln i_o and hence i_o. Since C_{dl} acts like an electrical short circuit at t = 0 as far as the external circuitry is concerned, the value of i_o is determined by the magnitude of the step voltage, e_s, and the sum of the circuit and solution resistances. The quantity $R + R_{soln}$ can be calculated from Equation (4):

$$R + R_{soln} = \frac{e_s}{i_o} \tag{4}$$

Thus by performing the extrapolation to obtain i_o, a separate measurement of R_{soln} is not required. Using the values of the slope and intercept from the least squares plot and Equation (4), C_{dl} is calculated in the following manner:

$$C_{dl} = - \frac{1}{(R+R_{soln})m} \tag{5}$$

and

$$C_{dl} = - \frac{\exp\{b\}}{e_s\, m} \tag{6}$$

where m and b are the slope and intercept values.

D. Cyclic Voltammetry

Cyclic voltammetry is a controlled potential technique similar to polarography, but different in some experimental aspects. In both techniques electrolysis of an analyte is made to occur at a relatively small polarizable electrode, referred to as the test electrode. The solution in which the test electrode is immersed is unstirred, and experimental conditions are arranged so that analyte diffusion to the electrode surface is the only important means of mass transport. As in polarography the electrolysis current observed in the cyclic voltammetric experiment is recorded as a function of the potential applied between the test and a non-polarizable reference electrode. The current-potential curve is referred to as a voltammogram. In both polarography and cyclic voltammetry the potential difference between the test and reference electrodes is varied linearly with time. The potential sweep in cyclic voltammetry differs from that in polarography in two respects. In the cyclic voltammetric experiment, at the end of one potential sweep, the sweep direction is reversed and the potential between the test and reference electrodes is scanned back to an initial potential difference that existed between these electrodes prior to the initiation of the voltage scan. The potential-time waveform for the cyclic voltammetric experiment is shown in Figure 5a. The second aspect in which the cyclic voltammetric potential sweep

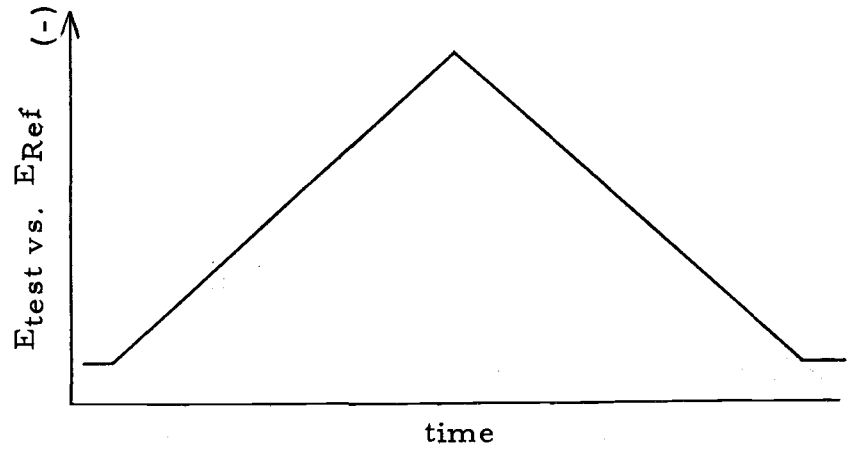

(a)

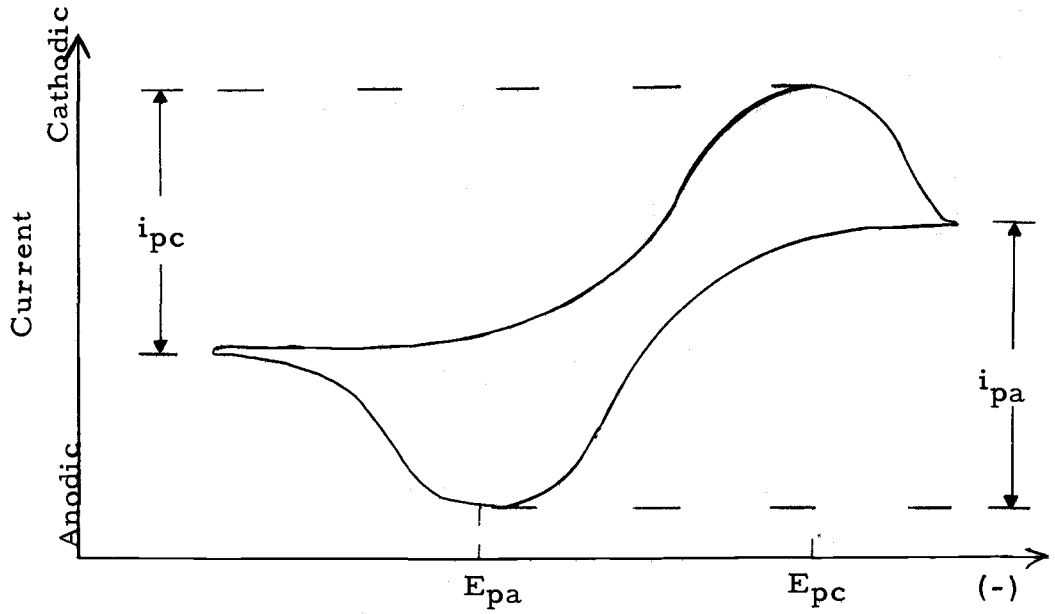

E_{test} vs. E_{Ref}

(b)

Figure 5. (a) Voltage waveform for cyclic voltammetric experiment. (b) Cyclic voltammogram.

differs from that used in polarography is the rate at which the scan is carried out. Scan rates between 0.2 and 1000 volts per second are typically used in cyclic voltammetry while scan rates generally less than 0.02 volts per second are used in polarographic work.

Current-potential curves for cyclic voltammetry are quite different in appearance from those obtained in polarography. Nicholson (68) developed the mathematical relationship between cell current and electrode potential for the cyclic voltammetric experiment. For the simple, uncomplicated electrode reaction of the form:

$$Ox + ne \rightleftharpoons R$$

the current-potential curve obtained in cyclic voltammetry looks somewhat like that illustrated in Figure 5b. If the test electrode potential is swept negatively (left-to-right in the figure), a current peak due to the reduction of the oxidized species (Ox) or analyte results. During the first part of the sweep, no current flows until the decomposition potential of the analyte is reached. Once this potential is passed, the current rises rapidly as the analyte is consumed at the electrode surface. Since the solution is unstirred, the analyte concentration in the region of the electrode is quickly depleted and the current begins to drop. On the reverse scan the current remains relatively constant until the decomposition potential of the product (R) formed in the forward scan is reached. Once this potential is reached, the rate of the electrode reaction involving the

product of the reduction step increases until the concentration of R becomes depleted and the cell current again begins to drop to zero. If the electrode reaction is fast (reversible) the cathodic and anodic peak currents are equal and the separation in the peaks is about 60/n millivolts (68). Regardless of the reversibility of the electrode reaction, the peak currents are directly proportional to the analyte concentration and are linearly related to the square root of the potential scan rate.

The current that is observed to flow in cyclic voltammetric experiments is not just due to electrolysis of the analyte. Electrolysis of residual solution impurities and double layer charging are also sources of cell current. As in polarographic work, current from these extraneous sources must be subtracted from the total observed cell current in order to obtain the true current-potential curve for the analyte.

II. DOUBLE LAYER CAPACITANCE MEASUREMENTS

A. Experimental

Chemicals

Solvent Purification. There are many published procedures for purifying sulfolane and each procedure is tailored to produce a product with a minimum of effort and which is acceptable for specific types of experiments. For the synthetic organic chemist interested in using TMS as a solvent in which to prepare a large quantity of a compound that is to be purified in a subsequent step, a single distillation at reduced pressure can be adequate. On the other hand, the solvent purity required by chemists studying medium effects in sulfolane is much higher. The procedure finally adopted in this work was a compromise between the extremes or between the methods used by Vaughan (81) and Simon (77). Clearly, if TMS is to be a general and practical solvent for electroanalytical work, the purity of the solvent must be such that impurity effects are not sigificant and the effort to produce such a solvent must not be excessive. The solvent prepared using the compromised procedure was tested for water content, ionic conductivity, and residual electroactive materials. Judging from the results of these tests, the compromise procedure was found to be suitable for producing sulfolane of a purity acceptable for use in this work.

The procedure for purifying sulfolane that was adopted after trying several others consisted of three steps: an initial vacuum distillation, a gas stripping step, and finally two more vacuum distillations. What follows is a description of the procedural steps and the equipment used to effect the purification.

Sulfolane received from Shell Chemical Co.[1] or Phillips Petroleum Co.[2] was initially distilled at reduced pressure to reduce substantially the water content and to separate the solvent from the less volatile impurities. Sulfolane furnished by Shell contains as high as 3% by weight water and varying levels of isopropyl sulfylanyl ether and 2-sulfolene (76). Another impurity expected to be present in commercial grade material by virtue of its method of manufacture is 3-sulfolene. The middle 70% fraction of the distillate from this initial distillation was collected and used in the remainder of the procedure. Each initial vacuum distillation produced approximately 300 to 400 ml of the solvent. The yield from a few of these initial distillations was pooled to obtain about a liter of material, and this was then used in the gas stripping step.

The vacuum distillation equipment used in the purification procedures was all ground glass standard taper ware. It consisted of a 1000 ml, three-neck round bottom flask fitted with a 160 mm, 75°,

---

[1] Shell Chemical Co., Downey, California.

[2] Phillips Petroleum Co., Bartlesville, Oklahoma.

three-way distilling column and a 300 mm West condenser fitted with a vacuum take-off adapter. The collecting flask was of varying capacity depending on which fraction was being collected. Both the 1000 ml flask and the 160 mm distilling tower were equipped with thermometers. The upper portions of the 1000 ml flask and the distilling column were wrapped with asbestos tape and nichrome heating wire. Power for heating the upper portions of the distilling pot and column was supplied by a Variac adjustable autotransformer[1], while power for the heating mantle used to heat the 1000 ml flask was supplied by a separate Variac. Warm water (30-40°C) was circulated through a condenser jacket to prevent the sulfolane from freezing and clogging the condenser. A cold trap (isopropanol-dry ice) was placed between the vacuum take-off adapter and the vacuum pump to freeze volatile substances and prevent them from reaching the pump. A simple mercury manometer attached to the vacuum take-off adapter was used to monitor the vacuum. While the distillation took several hours to complete, it required only an occasional check to ensure that the distillation was proceeding normally and to change collection vessels.

With pressures below 1 mm, pot temperatures were never over 120°C and the TMS distillate was collected at a column temperature

---

[1]General Radio Co., Concord, Massachusetts.

of about 100°C. The sulfolane from this distillation was a bit "whiter" than that supplied by Shell and it would crystallize if left standing at room temperature. Material supplied by Shell was liquid at room temperatures.

As mentioned earlier, sulfolane is commercially prepared by the catalytic hydrogenation of 3-sulfolene. It is not unreasonable, therefore, to expect 3-sulfolene to be present in the commercial product. The boiling point of this material is somewhat similar to that of sulfolane so that a single distillation at reduced pressure and lower temperature should not be considered adequate in eliminating this impurity. Fortunately, 3-sulfolene is thermally unstable (76) and can be decomposed rather easily, producing sulfur dioxide and butadiene. SO_2 is known to be extremely soluble in sulfolane and could thus accumulate. Both SO_2 and butadiene would be particularly objectionable impurities in electro-analytical work, since they are known to be electroactive. The second step in the purification procedure, gas stripping, is specifically aimed at eliminating the thermally unstable impurities, such as 3-sulfolene, and hopefully their decomposition products.

The gas stripping procedure consists of passing dry, clean nitrogen through heated solvent for several hours. Specifically, what was done was to add 10 to 15 grams of reagent grade sodium hydroxide pellets to a liter of initially distilled solvent. This solution was then

heated to 160 to 170°C in a 1500 ml round bottom flask for 48 to 60 hours. Pre-pure nitrogen was simultaneously passed through the solvent by means of a gas dispersion tube. The nitrogen flow rate was a few hundred ml per minute. While this seems like a long procedure, it was usually carried out over the weekend and it did not need supervision, so the step was not considered to be inconvenient or involve a great deal of effort. The product of this step was a reddish-brown solution containing some suspended matter. When commercial grade sulfolane that had not been previously distilled was subjected to this stripping procedure, the product was considerably darker in color and appeared to contain more suspended material.

The specific decomposition rates of 3-sulfolene at various temperatures have been reported (76) and it was on the basis of this information that the conditions for gas stripping were selected. Assuming an initial 3-sulfolene concentration of 0.3M in commercial sulfolane, Simon (77) has estimated that a stripping procedure carried out at 135°C for 20 hours is required to reduce the level of 3-sulfolene to less than 10^{-22}M. To insure that the sulfolene concentration in sulfolane is reduced to a very low level while the solvent does not undergo any appreciable degradation, a stripping temperature of 160°C and a reaction period of 40-60 hours were selected. Since TMS has a thermal decomposition rate of 0.002% per hour at 200°C, the conditions employed in this stripping procedure should produce less

than 0.1% decomposition of sulfolane and essentially 100% decomposition of 3-sulfolene.

The third step in the purification involves two more vacuum distillations of the material obtained from the gas stripping procedure. These distillations are similar to the initial vacuum distillation of the first step. The same equipment is used and the conditions employed are the same except only the middle 60% fraction is collected and saved. The product obtained after the first of these final two distillations is clear and "water white." It is also practically odorless. The specific conductance of the material was measured with an Industrial Instruments[1] Model RC-16B conductivity bridge using a conductivity cell with platinized electrodes. The specific conductance of the first distillate was approximately 10^{-8} mhos cm^{-1} while material collected from the second distillation in this step had a specific conductance of less than 10^{-8} mhos cm^{-1}. To measure such low specific conductances with this bridge it was necessary to parallel the cell with a 2.00 megohm resistor and calculate the specific conductances from the appropriate equations.

The water content of the first distillate was found to be about 0.01% by weight and was reduced to less than 0.005% by the last distillation. A standard Karl Fischer micro technique as described by Mitchell (63) was used for these analyses. The water content of

[1]Industrial Instruments, Inc., Cedar Grove, New Jersey.

sulfolane produced by this purification procedure is much less than the level for which Headridge (43) could observe any effect on the polarographic half-wave potential for cadmium. The water content found in solvent prepared by this procedure compares favorably with the levels reported by Simon (77) and Garnsey (35) for their solvents.

To ensure that the purified solvent remained dry, it was stored in a liter size wash bottle equipped with a drying tube and squeeze bulb and the whole assembly was kept in a dry glovebox. Solvent transfer to other flasks and containers was performed in the glovebox with the least chance of contaminating the stock solvent.

Polarographic residual currents obtained from solutions of 0.10 M tetraethylammonium perchlorate made up with the final distillate were consistently less than 0.3 microampere (the polarograph, reference electrode, and other electrochemical instrumentation are described elsewhere). These residual currents are extremely small even when allowance is made for the high viscosity of the medium and its effect on the diffusion coefficients of the impurities. These currents are so small that they are of the order of the nonfaradaic current that is expected to flow. A planar platinum electrode was used to test for electro-oxidizable impurities at anodic potentials. Residual currents obtained with this electrode (geometric electrode area 7.9×10^{-3} cm^2) were less than 2 microamperes at +1.5 v, with respect to the silver reference electrode. These results are

indicative of a solute and solvent essentially free of electroactive impurities.

It appears that the procedure for purifying sulfolane as outlined above is suitable for producing a solvent acceptable for use in electroanalytical work. While the procedure requires considerable time, it does not involve a great deal of work.

Supporting Electrolyte. Tetraethylammonium perchlorate (TEAP) was chosen as the supporting electrolyte in this work. The salt has been used as such in a few electrochemical studies (28, 43, 77) in TMS. TEAP is moderately soluble and largely dissociated in sulfolane (25) and appears to have a wide voltammetric potential range. For these reasons TEAP appears destined to be used more frequently in new work and so it seemed desirable to collect some electrical double layer measurements for this salt in TMS and to use the salt as a base electrolyte in the voltammetric work with the organosulfur compounds.

The salt used in this work was prepared from tetraethylammonium bromide (TEAB) and sodium perchlorate by a simple metathesis reaction in water. The product of the reaction was recrystallized several times and dried to insure a material of high purity.

The exact procedure consisted of the following. 1M stock solutions of TEAB and sodium perchlorate were made in water. The tetraethylammonium bromide salt was purchased from Pfaltz &

Bauer, Inc.[1] and used as received. Equal volumes of both solutions (usually about 100 ml) were added to a large evaporating dish. The resulting solution was then heated by means of a hotplate until its volume was reduced to about 50-75 ml. The evaporating dish was then removed from the hotplate and allowed to cool to room temperature. White crystals of TEAP were observed to form at the solution surface after standing a few minutes.

The crystals obtained were separated from the supernatant solution by suction filtration, washed with several portions of cold distilled water, and finally press-dried. The material was checked for bromide ion at this stage by adding a few drops of a concentrated silver nitrate solution to a solution containing a small amount of the dissolved crystal product. Bromide was always found in the product at this point. The press-dried material was then recrystallized two or more times from a 50% ethanol-water solution. Bromide was tested for in the washings from the second recrystallization and always found to be absent. The material was then recrystallized once more from the ethanol-water solvent and dried at 70°C under a vacuum for several days. The dried salt was then stored in a dessicator over phosphorus pentoxide until used.

Solutions of 0.10 M TEAP in sulfolane were prepared by placing weighed amounts of the dried salts in dry volumetric flasks and adding slightly warmed TMS. The transfer of TMS to the volumetric flasks from the stock solvent bottle was performed in a drybox and the solutions were stored there until used.

[1]Pfaltz & Bauer, Inc., Flushing, New York.

Apparatus

Microelectrodes. Several microelectrodes made of various materials were constructed and used in this electrochemical work. These electrodes include a hanging mercury drop electrode (HMDE) and microelectrodes of gold, platinum and glassy carbon. The microelectrodes discussed below were used both in the double layer capacitance measurements and in the voltammetric experiments.

The HMDE used in this work was of the non-syringe type and similar to the one described by Meites (62). It was constructed by sealing a gold wire 18 cm long and 0.055 cm in diameter into a piece of heavy-walled, soft glass tubing 13 cm long and 0.6 cm O.D. The sealed end was cut square by means of a diamond wheel saw and left unpolished. The end of the gold wire at this tip was then etched a few tenths of a millimeter by hot aqua regia, leaving a slight recess. This tip was then dipped in a pool of mercury to amalgamate the end surface of the exposed gold wire. Thereafter small mercury drops collected from a dropping mercury electrode (DME) assembly by means of a glass spoon would, when brought into contact with the electrode, attach themselves readily to the tip. Single mercury drops as large as 25 mg could easily be suspended from this electrode in air.

Mercury drops suspended from the HMDE assembly were collected from a DME (described below). The capillary tube of the DME was mounted in a horizontal position and the tip of the DME was wetted with a drop of 0.10 M TEAP in TMS. It was found that small, single, reproducible droplets could be collected with a glass spoon from this assembly. To measure the drop reproducibility, 100 drops were collected and weighed. Several of these weighings made over a period of a month agreed to within 1% of each other.

The mass of the mercury drop suspended from the HMDE assembly was found to be 10.0 mg. Knowing the mass of the drop, the density of mercury, and assuming a spherical shape for the suspended drop, an electrode area can be calculated from the equation:

$$\text{Area } (cm^2) = (4\pi)^{1/3} \left(\frac{3m}{\rho}\right)^{2/3} \qquad (7)$$

where m refers to the mass of the drop expressed in grams and ρ is the density of mercury at the proper temperature expressed in grams per cubic centimeter. At 40°C, ρ is 13.4967 g cm^{-3} (54), and thus the area of a 10 mg spherical mercury drop is calculated to be 0.0396 cm^2. This size of electrode was used throughout the voltammetric work where an HMDE was employed. In the double layer measurements an HMDE with a slightly smaller area (0.0326 cm^2) was used.

The DME assembly used to furnish mercury drops for the HMDE was also used to determine the potential of zero charge (PZC) for

mercury in 0.10 M TEAP in sulfolane. The assembly consisted of a 10 cm length of a fine bore capillary tube connected to a 150 ml capacity separatory funnel-shaped mercury reservoir by means of a piece of flexible plastic tubing. The capillary tubing, purchased from the Sargent Company[1], had a 0.005 cm diameter orifice and was not drawn to a point. The mercury used in this DME assembly was triple distilled, instrument grade material purchased from Goldsmith[2]. Maximum non-volatile residue content of the mercury was stated to be 0.004%.

The DME drop time in a deaerated solution of 0.10 M TEAP in TMS was measured at several potentials using the Heath Polarograph and a Varian F-80A recorder with its internal time base. Both pieces of equipment are described more fully in a later section. For these measurements the surface of mercury in the reservoir was adjusted to a height of 40 cm above the tip of the capillary tube when the tube was immersed in solutions. The drop time measurements reported later are the average values of two measurements made at each potential on different days. The values agreed within the experimental error for the measurement, which was 50 ms.

Solid microelectrodes of gold, platinum, and glassy carbon were all of similar construction. Glassy carbon material was

---

[1] E. H. Sargent Company, Chicago, Illinois.

[2] D. K. Goldsmith Chemical & Metal Corp., Evanston, Illinois.

furnished gratuitously by the Dow Chemical Company[1] in the form of small rods 0.3 cm in length and 0.1 cm in diameter. The physical properties of glassy carbon and its fabrication have appeared in a few articles (85, 69). The use of glassy carbon in aqueous electrochemical work has been described by Alder (1) and Zittel (87). In constructing the gold and platinum microelectrodes, short pieces of the wire 1 cm long and 0.1 cm diameter were used. These materials were soldered into brass tubes 2 cm long and 0.24 cm O.D., leaving most of the electrode material exposed. A 15 cm length of 22 gauge copper wire was soldered to the other end of the three brass tubes. These assemblies were then placed inside 7 mm I.D. glass tubes which had been plugged at one end. The tubes were filled with Clear-Lite[2] casting resin to embed the electrode assemblies. The casting resin is a methacrylate polymer and is insoluble in TMS. Other potting materials could possibly be used, but the solubility of the cured material in sulfolane should be checked. The casting resin was left to cure at room temperature for several hours.

Upon curing the polyester resin shrinks slightly from the glass tube and the rod-shaped electrodes were easily removed. The potted electrodes were free of trapped air bubbles and no visible cracks could be detected. The ends of the plastic rods were ground down

[1]Dow Chemical Company, Midland, Michigan.

[2]Taylor & Art Plastics Inc., Oakland, California.

with coarse mesh carborundum powder to expose the end of the electrode material. These planar surfaces were then polished with cotton or muslin cloth using a slurry of 600 mesh silicon carbide powder suspended in a sulfolane solution containing 0.1 M TEAP.

A completed microelectrode is shown in Figure 6b. Shown in Figure 7 are photomicrographs of the three polished electrodes.

The exposed geometric area for each microelectrode was calculated assuming a circular shape. The areas for the platinum, gold and glassy carbon electrodes were 0.0087, 0.0095 and 0.0113 cm^2, respectively. In determining electrode areas, several diameter measurements for each electrode were made with a Bausch & Lomb 7X comparator having 0.1 mm reticles, and an average value for each was computed and then used in the area calculation. Contact resistances measured for each electrode were less than an ohm.

Reference Electrode. A nonaqueous silver-silver ion electrode served as the reference electrode for all potential measurements in sulfolane. The nonaqueous reference electrode consisted of silver metal in contact with a solution of 0.10 M $AgClO_4$ in TMS. The silver-silver ion couple has been found to be reversible and stable in TMS (28) and suitable as a practical reference electrode for voltammetric work in the solvent (77). This electrode minimizes the possibility of introduction of moisture into the cell and has the advantage of simple preparation. In addition to these desirable properties for the

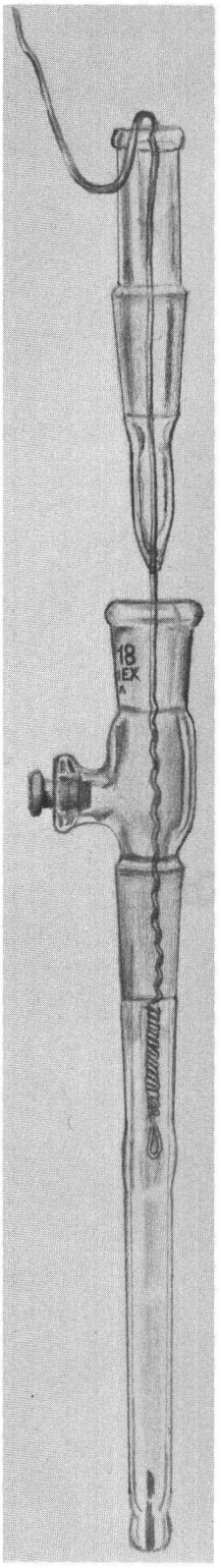

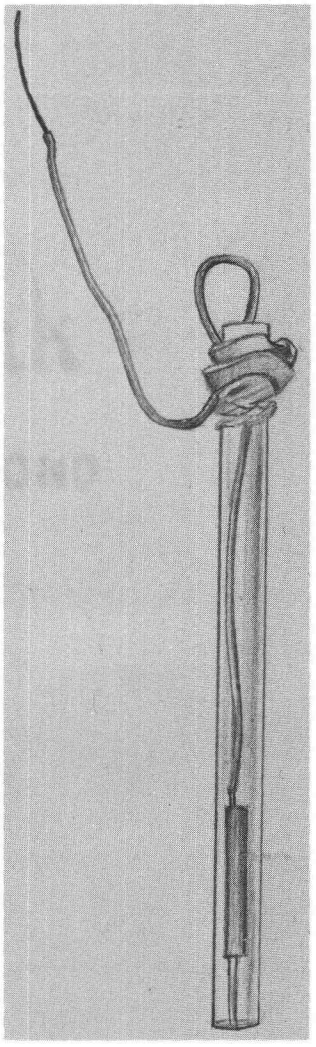

Figure 6. (a) Silver reference electrode assembly.
(b) Solid microelectrode.

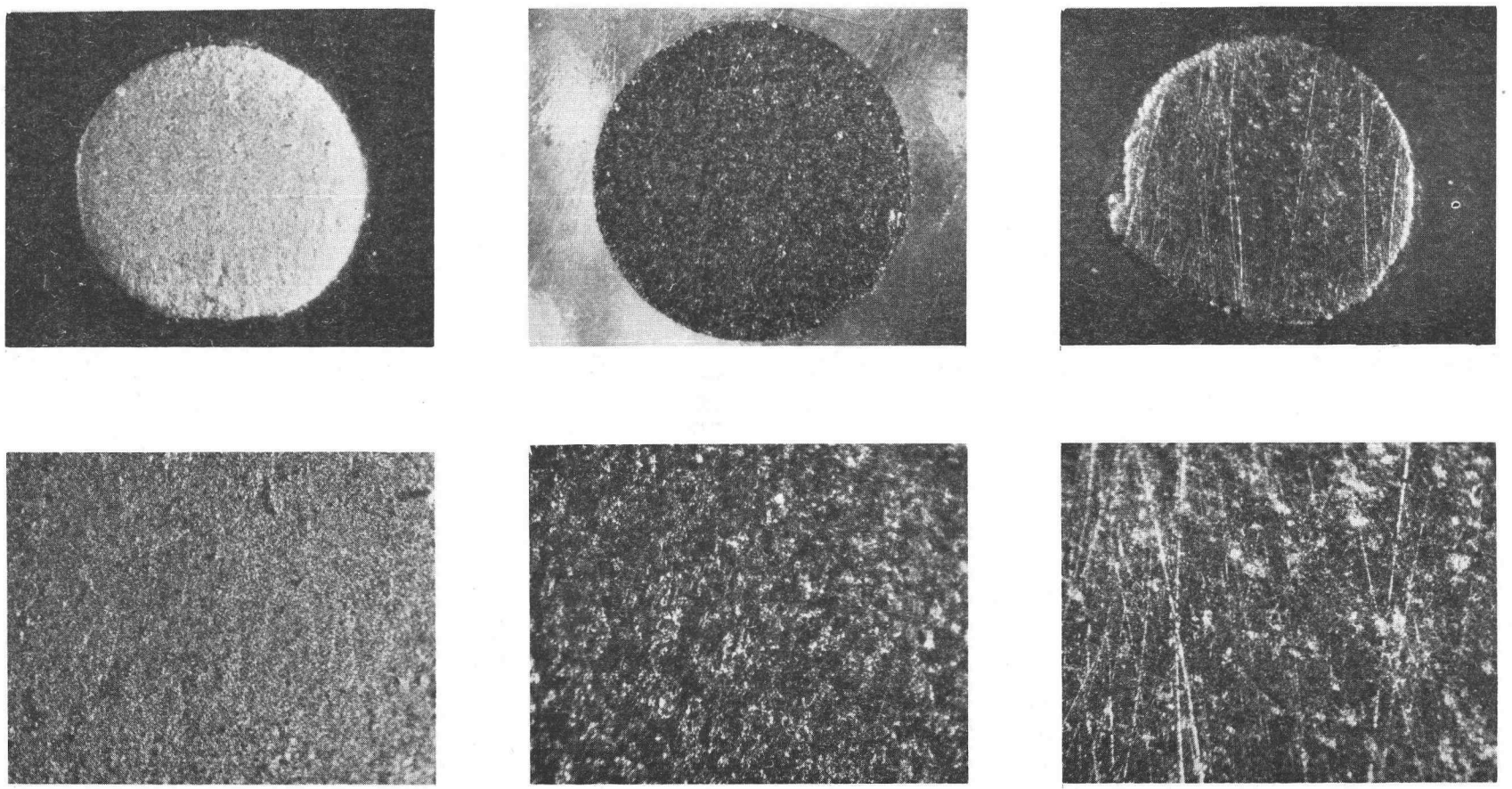

Figure 7. Photomicrographs of microelectrodes at 40x and 120x magnifications. Left to right, AUME, GCME and PTME.

reference electrode, only small liquid junction potentials should arise with its use in solutions of the supporting electrolyte.

The silver reference electrode (AgRE) used consisted of a silver wire immersed in a solution of 0.10 M silver perchlorate made up in TMS. The reference electrode used in this work is illustrated in Figure 6a. As shown in this figure, the reference electrode assembly consisted of two parts, a reference electrolyte compartment and a silver wire holder. The two-part assembly facilitated construction and made filling and maintenance of the electrode easy.

The Ag wire holder (upper portion in Figure 6a) was made by sealing a piece of glass tubing 2.5 cm long and 8 mm diameter to the smaller end of an inner member ℑ 10/18 ground joint. The overall length of the ground joint with sealed glass tube was approximately 6.5 cm. A silver wire 30 cm long and 0.069 cm diameter was sealed in the holder so that about 5 cm of the wire extended above the holder and 18 cm of wire extended below the wire-to-glass seal. The 18 cm length of Ag wire was wound into a small, tight coil 8 cm long so that it could be inserted into the reference electrolyte compartment. The area of coiled electrode in contact with the reference electrolyte was estimated to be about 1.1 cm^2.

The reference electrolyte compartment was fabricated from a 14 mm O.D. glass tube and the outer member of the upper ℑ 10/18 ground joint. The 14 mm tube was drawn so that the inner member of

a lower, second ℑ 10/18 ground joint could be sealed to the tube. An 8 mm diameter glass tube 7 cm long was sealed to the lower inner member joint. A small bundle of asbestos fibers 1 cm long was then sealed to the other end of the 8 mm tube. Assembly of the reference electrode was accomplished by inserting the electrode holder into the reference electrolyte compartment and filling the reference compartment with 0.10 M $AgClO_4$ solution by means of the small sidearm. When assembled the reference electrode assembly measured 16 cm in length.

Anhydrous $AgClO_4$ salt used to make up the reference electrolyte solution was purchased from Ventron, Inc.[1] and used as received. Minimum purity of the salt was stated to be 99%. Solutions of $AgClO_4$ were prepared and handled like the solutions of the supporting electrolyte.

The stability of the AgRE was tested and found to be quite good. A cell consisting of two identically prepared reference electrodes filled with 0.10 M $AgClO_4$ solution were immersed in a solution of supporting electrolyte at 40°C. After allowing the two reference electrodes to reach thermal equilibrium, the cell potential was measured with a Gray[2] Instrument Model 3040C Potentiometer and a

---

[1] Ventron, Inc., Beverly, Massachusetts.

[2] Gray Instrument Co., Philadelphia, Pennsylvania.

suitable galvanometer. The cell potential was found to be less than 0.001 v. The cell potential was measured again after one week and found to be about the same.

The fiber-tipped AgRE was well suited for use in this work. The flow of silver ion from the reference electrolyte compartment was so small that no silver could be detected in the working compartment of the cell after several hours of continuous use. The flow was apparently sufficient, though, to establish a stable liquid junction since no shift in the half-wave potential of a depolarizer could be observed with time. The liquid junction potential for the AgRE and the supporting electrolyte should be small anyway. Using Della Monica's equivalent conductance data (25, 27) for $AgClO_4$ and the tetraalkylammonium perchlorates, the liquid junction potential between the AgRE and a solution of a tetraalkylammonium salt can be calculated by means of the Lewis-Sargent equation (58):

$$E_J = \frac{RT}{F} \ln \frac{\Lambda'}{\Lambda''} \qquad (8)$$

where Λ' and Λ'' are the equivalent conductances of solutions I and II. The equation is applicable only to junctions formed between solutions containing univalent electrolytes at the same concentration and with one ion in common.

Listed in Table 2 are the liquid junction potentials, calculated by means of the Lewis-Sargent equation, that should arise

between the AgRE and a 0.10 M solution of a tetraalkylammonium salt in TMS at 30°C. Also included in the table are values for the equivalent conductances for these salts at infinite dilution and at 0.1 M concentration. As can be seen from the table, the combination of the AgRE with a solution of 0.10 M TEAP should produce only a small liquid junction potential.

Table 2. Liquid junction potentials expected between AgRE and 0.1 M salt solutions at 30°C in TMS.

Salt	Λ_o[a] ohm^{-1} cm^2 mol^{-1}	$\Lambda_{0.1M}$[b] ohm^{-1} cm^2 mol^{-1}	E_J[c] mv
$AgClO_4$	11.229	7.71	---
$(CH_3)_4NClO_4$	10.994	---	---
$(C_2H_5)_4NClO_4$	10.632	6.75	3.5
$(C_3H_7)_4NClO_4$	9.912	5.98	6.6
$(C_4H_9)_4NClO_4$	9.486	5.73	7.7

[a] Values taken from references (25) and (27).

[b] Obtained by extrapolation of data from references (25) and (27).

[c] Liquid junction potentials calculated by means of the Lewis-Sargent equation.

Cell. The cell used in this work is illustrated in Figure 8. It somewhat resembles a thermo-jacketed Hittorf transference cell. As can be seen from the figure, all of the electrode compartments are enclosed in a small sealed container through which water from a

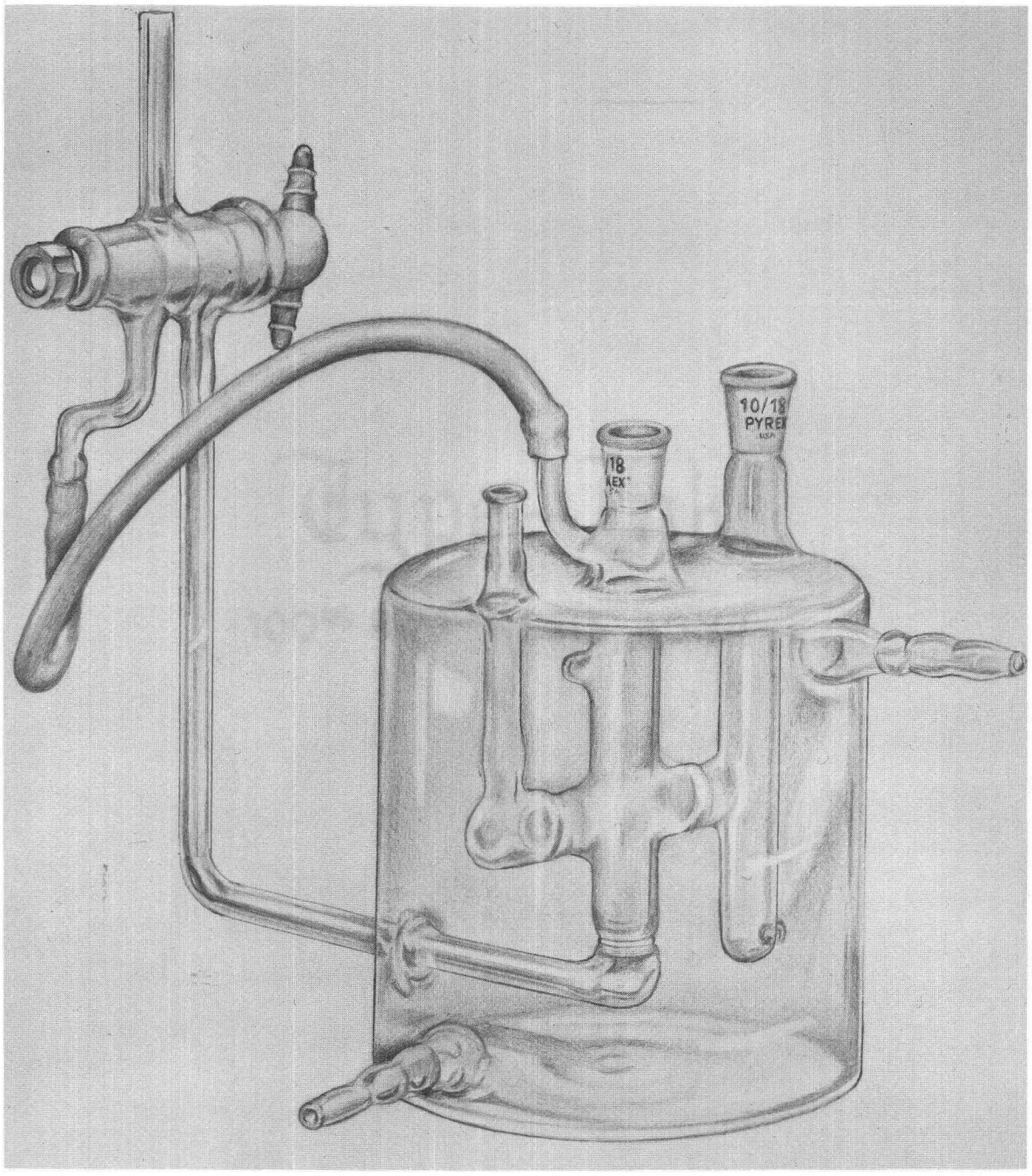

Figure 8. Electrochemical cell.

temperature-regulated bath can be circulated. Water maintained at $40^{o} \pm 0.1^{o}C$ by a Tecam Tempunit[1] was circulated through the water jacket and back into a 33 liter capacity water bath.

The working electrode compartment (center chamber) of the cell is separated from the auxiliary electrode and reference isolation compartments by fritted discs. Both fritted discs are 10 mm in diameter but of different porosities. The disc separating the auxiliary electrode compartment from the working electrode chamber is of fine porosity, while the working electrode compartment is separated from the reference isolation chamber by a disc of medium porosity. There is an additional fritted disc of fine porosity at the bottom of the working electrode compartment which is used for stirring and deaeration. Approximately 5 ml. of solution are necessary to cover the fritted discs. Samples of depolarizers could be added to this compartment by means of a calibrated micro-syringe.

The auxiliary electrode compartment has a volume of 1-2 ml. When the cell is used with a 3-electrode potentiostat, a small pool of mercury (about 1 ml.) is used as the counter or auxiliary electrode and the rest of the chamber is filled with deaerated supporting electrolyte. Contact with the mercury pool is made by means of a heavy gauge platinum wire dipping into the pool. The area of the mercury

---

[1]Cole-Parmer Instrument & Equipment Co., Chicago, Illinois.

pool auxiliary electrode in contact with supporting electrolyte is estimated to be slightly larger than 1 cm^2.

The reference electrode isolation compartment served as a means of isolating the reference electrode assembly from the working electrode chamber. Even though the fiber-tipped AgRE had a very low flow rate, it was thought best to separate the two compartments by this intermediate chamber. The reference electrode isolation chamber was filled with enough deaerated supporting electrolyte to cover the fritted disc and the AgRE assembly was inserted.

Nitrogen used to deaerate the solutions was of pre-pure grade. To insure that the gas was dry before it entered the cell, it was first passed through 60 and 40 cm long packed beds of magnesium perchlorate and barium oxide. The small sidearm near the top of the working electrode compartment was used to pass nitrogen over the top of the solution in this chamber while electrochemical measurements were being made.

Instrumentation

The instrument needed to measure double layer capacitance via the pulse technique does not have to be a special purpose instrument specifically designed for this experiment. The pulse experiment may be implemented with a controlled potential polarograph and ancillary equipment used for fast scan voltammetry. A schematic diagram of

the potentiostat used in this work is shown in Figure 9. It is similar in design to those developed by Enke and Baxter (32), and Kelley, Jones and Fisher (50), but employs integrated circuit operational amplifiers (op amps) in its construction. The integrated circuit op amps are Fairchild[1] products. Amplifiers S and C are the uA741c and F, the uA709c. Amplifier B is a Philbrick[2] P66A booster follower, which is capable of driving larger capacitive loads and has a higher current output rating than the uA741c.

Operational amplifier S is a "summer" and together with amplifier B performs as a control unit. Currents flowing from the initial potential source and pulse generator are summed and balanced by the current from amplifier F so as to keep the input to S near ground potential and functioning as a summing junction. The current from op amp F, which is wired as a voltage follower with a Field Effect Transistor (FET) input stage, is produced by the solution potential sensed by the reference electrode R. This solution potential is determined by the voltage applied to the auxiliary electrode A by means of amplifier B. The output voltage of S or P is continuously adjusted so that the potential sensed by R produces a current from amplifier F that balances the sum of currents from the other sources connected to the input of op amp S. Amplifier C functions to keep the potential

---

[1]Fairchild Semiconductor, Mountain View, California.
[2]Philbrick Researches, Boston, Massachusetts.

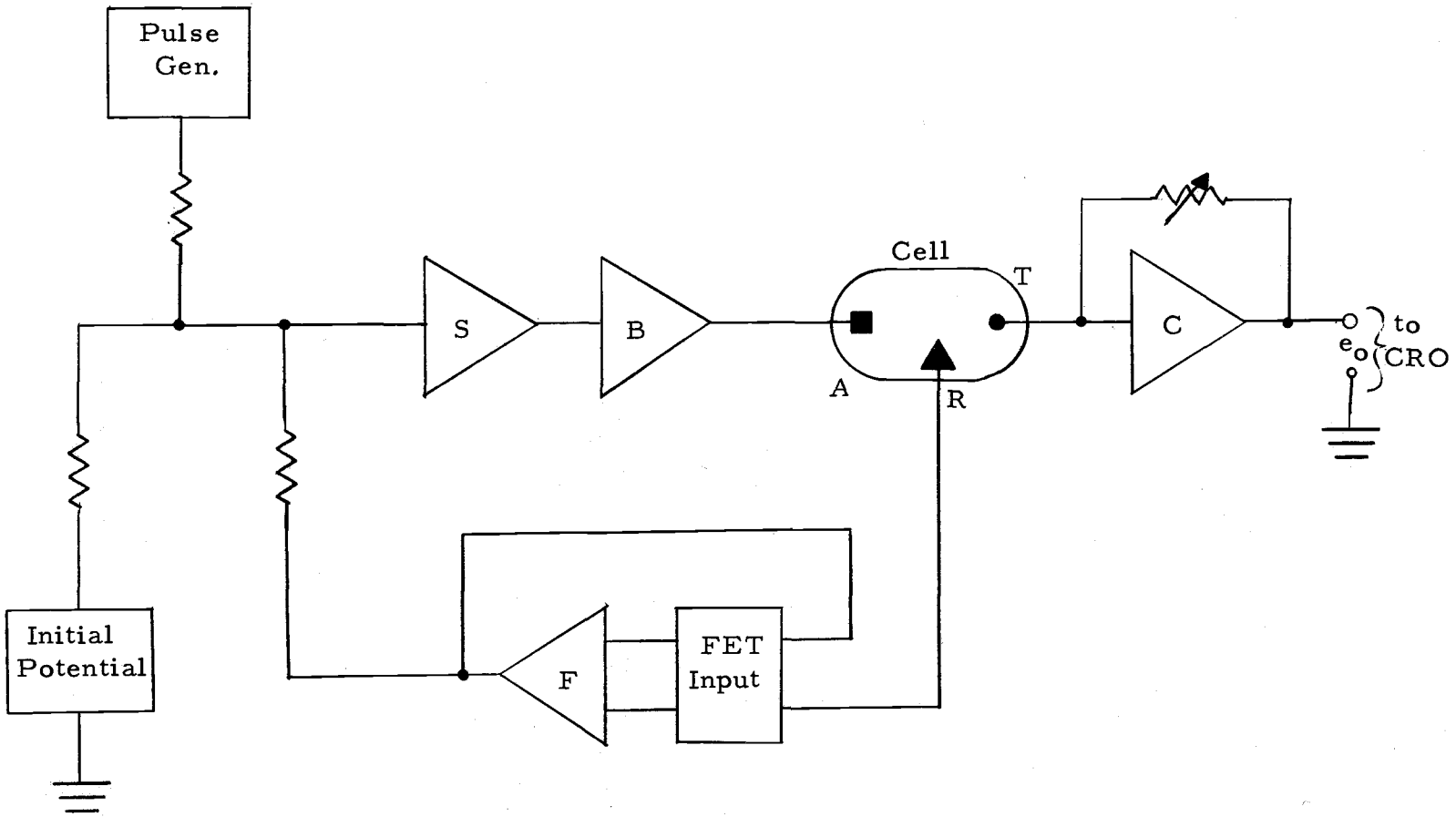

Figure 9. Controlled potential polarograph.

of the test electrode constant, near ground, and furnishes an output signal which is proportional to the current flowing through the cell between the auxiliary and test electrodes. The potential difference between the test and reference electrodes can be varied by changing the voltages applied to the input resistors of amplifier S.

Operation of the controlled potential polarograph for double layer capacitance measurements via the pulse technique is as follows. Initially the pulse or step voltage generator is in an "off" condition and some initial potential, e_i, is applied between a large massive reference electrode and a small test electrode. If the test electrode is ideally polarized (no electrochemical reaction occurring) there is no current flowing between the auxiliary and test electrodes and the output voltage of amplifier C is zero. When the step voltage generator switches on, its output voltage is summed with e_i to change the voltage applied between the reference and test electrodes by a small amount. As a result of this small change of potential, a current flows between the auxiliary and test electrodes to charge the double layer of the test electrode-solution interface. The current that flows decays exponentially as the double layer is charged. The output of amplifier C is a voltage signal proportional to the charging current and is displayed on an oscilloscope. Current-time measurements are made from the oscilloscopic trace and these data are used to construct a plot of ln i versus time. From the slope and intercept values of the plot, the

capacitance of the test electrode-solution interface can be calculated in the manner described earlier.

Further circuit details of the potentiostat and ancillary equipment are shown in Figure 10. A complete wiring schematic for the operational amplifier manifold, which includes balancing and compensation networks as well as details of the FET input stage to the reference electrode follower, can be found in reference (74). For initial potentials greater than one volt, additional potential sources similar to the unit shown in Figure 10 were used in series. The DC or initial potential difference between the test and reference electrodes was measured with a Fluke[1] Model 8200A Digital Voltmeter (DVM). The output signal of the current-to-voltage converter was displayed on a Tektronix[2] type 564 Storage Oscilloscope equipped with a 3A3 plug-in vertical amplifier anda Type 3B3 time base plug-in module. When desired, oscilloscope traces were recorded on 35 mm film (Tri-X[3]) by means of a Dumont[4] Oscillograph Record Camera Mount, Type 299, equipped with a Pentax[5] Model H1 single lens reflex camera. The pulse generator was a Tektronix Model 114 Pulse Generator.

---

[1]John Fluke Mfg. Co., Inc., Seattle, Washington.
[2]Tektronix, Inc., Beaverton, Oregon.
[3]Eastman Kodak Co., Rochester, New York.
[4]Allen B. Dumont Laboratories, Inc., Clifton, New Jersey.
[5]Honeywell Inc., Denver, Colorado.

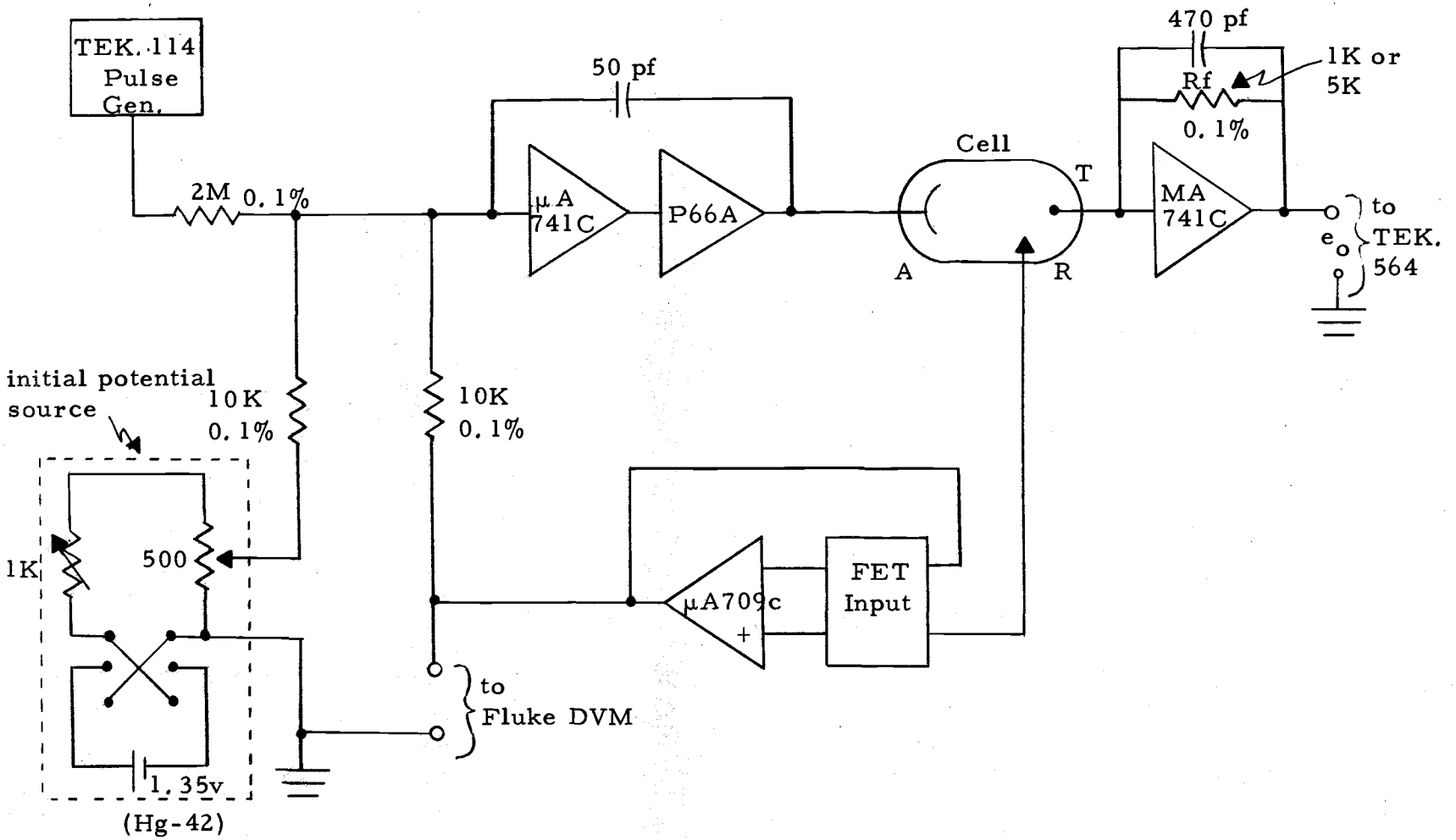

Figure 10. Wiring diagram of potentiostat.

All connections to the cell were made with shielded instrumentation cable and kept short. Noise in the output signal of the current-to-voltage converter was reduced by adding a 470 pf capacitor across the feedback resistor of the current-to-voltage converter. Noise in the system was further reduced by operating the cell in a faraday shield constructed from a 5 kilogram capacity metal solvent can and powering the potentiostat from a ±15 v battery supply (20, 1-1/2 v, Burgess[1] No. 6 telephone dry cells). By operating the system in this fashion the peak-to-peak noise in the output signal of the current-to-voltage converter was around 100-150 μv. In this work this typically corresponded to a 14-22 db signal-to-noise ratio in the current measurements used to obtain double layer capacitances.

Procedure

In operating the potentiostat for capacitance measurements, the pulse generator was adjusted to supply repetitive 5 mv step changes in the potential applied between the test and reference electrodes. The actual output of the pulse generator was a 1 v, 10 Hz square wave signal with a 10% duty cycle, as shown in Figure 11. With a pulse repetition rate of 10 Hz, there was always adequate time between pulses so that the double layer was completely discharged before it

---

[1]Clevite Corporation, Burgess Battery Div., Freeport, Illinois.

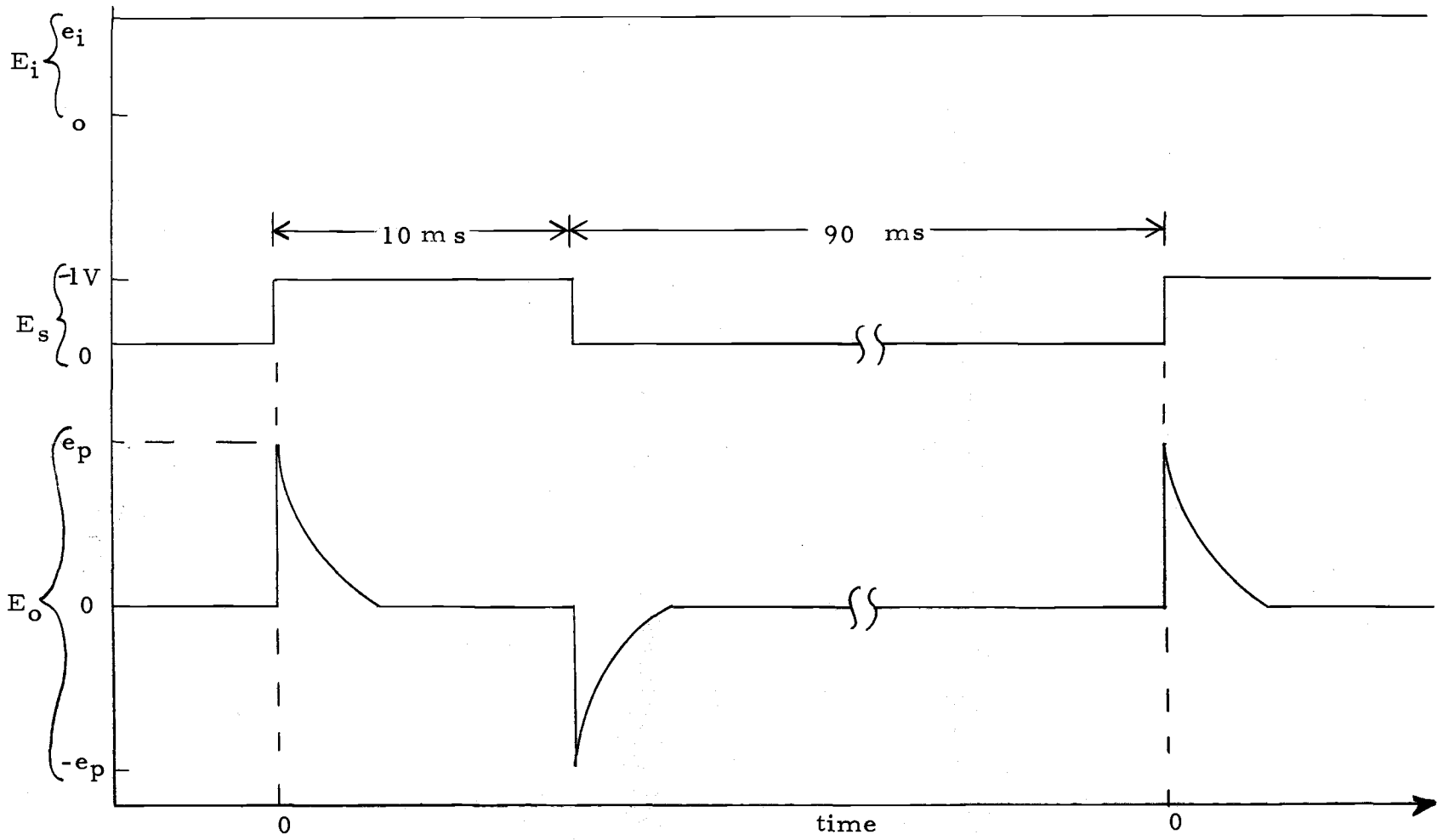

Figure 11. Voltage waveforms for electrical double layer capacitance measurement experiment. E_i=initial potential between test and reference electrode, E_s=output voltage from pulse generator, E_o=output voltage from current-to-voltage converter.

was charged again by the next pulse. The type of waveform observed with the oscilloscope at the output of the current-to-voltage converter is shown in Figure 11. For measurement purposes the time scale of the oscilloscope was expanded so that only one decay curve was displayed. Current measurements along the decay curve were always made relative to the value just prior to the application of the pulse. In this manner only current resulting from the step voltage change was measured.

For the work with electrical circuit models the simple series RC analog shown below was used.

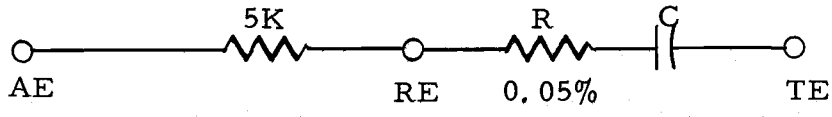

AE, RE and TE refer to points in the circuit where the auxiliary, reference and test electrode leads from the potentiostat were attached. Precision resistors of 50, 100, 200 and 1000Ω were used for R. C was either a 0.523 or 0.960 microfarad polycarbonate capacitor. The value of C was measured using a Model 1673 General Radio[1] Automatic Capacitance Bridge whose accuracy is stated to be 0.1%. With the two capacitors and four resistors there are eight possible combinations of R and C with time constants ranging from

---

[1]General Radio Company, Concord, Massachusetts.

26 to 960 microseconds. The capacitance for each combination was measured at least twice. Combinations with larger time constants were measured four or five times.

The procedure for making double layer capacitance measurements for electrode-sulfolane interfaces was as follows. The various cell compartments were thoroughly cleaned by flushing them several times with supporting electrolyte solution. Then approximately 1 ml of mercury was added by eye dropper to the auxiliary electrode compartment. Next, 5 ml of supporting electrolyte solution were delivered to the working electrode compartment by means of a pipette. This volume of solution just covered the fritted discs. The other compartments of the cell were then filled with solution to the same level. The solutions in each compartment were deaerated with pre-pure nitrogen for 10-20 minutes. The nitrogen stream was not presaturated with TMS since evaporative losses of solvent should be small due to the low vapor pressure of the solvent at this temperature. With degassing accomplished, the test electrode and reference electrode assembly were inserted in their chambers. A heavy gauge platinum wire was immersed in the mercury pool and electrical connections to the potentiostat made. Nitrogen was passed over the top of the solution in the working electrode compartment. For the capacitance measurements with the HMDE a fresh mercury drop was used at each potential.

In using the pulse technique to measure capacitance values for Hg-aqueous 1.0 M KCl interface, a cell assembly similar to the one described earlier was used in conjunction with the HMDE. The only difference between the cells was that the one used here did not have its own water jacket and consequently had to be placed in a separate water bath maintained at 25°C. All three chambers of the cell were filled with nitrogen-deoxygenated KCl solution. The reference electrode against which potentials were measured was a saturated calomel electrode connected to the cell reference electrode chamber by means of an agar salt bridge. Details of the construction of the reference electrode and salt bridge can be found in reference (82). A fresh Hg drop was used for each capacitance measurement.

A computer program written in FORTRAN IV language was used to handle the data from these experiments and calculate double layer capacitances. The program was operated on a CDC 3300 Digital Computer[1]. A listing of the program is included in Appendix I. The program basically consists of three sections: a data input and transformation section, a linear least squares curve fitting routine, and a double layer capacitance calculation and output section. In the input section of the program, experimental voltage-time measurements obtained from the oscilloscope were inputed and converted to ln

---

[1]Control Data Corporation, Minneapolis, Minnesota.

current-time data. Then these data were used by the least squares routine to determine the most reliable slope and intercept values for the ln i versus t plots. The equations used to calculate the least squares slope and intercept, as well as the standard deviations in these values, were taken from Young's book (86, pp. 145-146). Having determined the slope and intercept as well as the expected standard deviations in these parameters, the program would calculate the electrode capacitance and report capacitance values in units of microfarads per square centimeter.

B. Results and Discussion

Electrocapillarity

It has been known for a long time that the interfacial tension of an electrode in contact with an electrolytic solution varies with the potential difference applied across the interface. Curves representing this variation in interfacial tension with cell potential are called electrocapillary curves and are of importance in any theoretical or experimental study of the nature of electrode-solution double layer regions. The curves can also provide a means of checking double layer capacitance measurements made on the same interface in different experiments.

The electrocapillary curve for a mercury electrode in a solution of 0.10 M TEAP in sulfolane is shown in Figure 12. Plotted in the figure are not surface tension measurements directly, but polarographic drop times for a DME as a function of potential. The approximate relationship that is commonly used to relate surface tension to drop time for a DME is (44):

$$\lambda = \frac{mtg}{2\pi r} \qquad (9)$$

where λ is the surface tension (ergs cm^{-2}), m the Hg flow rate through the capillary (g sec^{-1}), t the drop time (sec), g the gravitational constant (cm sec^{-2}) and r the radius of the capillary orifice (cm). The data used to construct the electrocapillary curve are listed in Table 3.

The electrocapillary curve for Hg in sulfolane is parabolic and not unlike those curves obtained for mercury in aqueous solutions of simple inorganic electrolytes. The curve appears smooth and free of erratic fluctuations in surface tension, indicating that compositional changes in the double layer region occur gradually with changes in applied potential. The potential of the electrocapillary maximum (potential of zero charge, PZC) occurs around -0.80 v. While the interfacial tension or drop time appears to be a simple parabolic function of potential, in fact it is not and departs slightly from the functional relationship derived by Lippman (44).

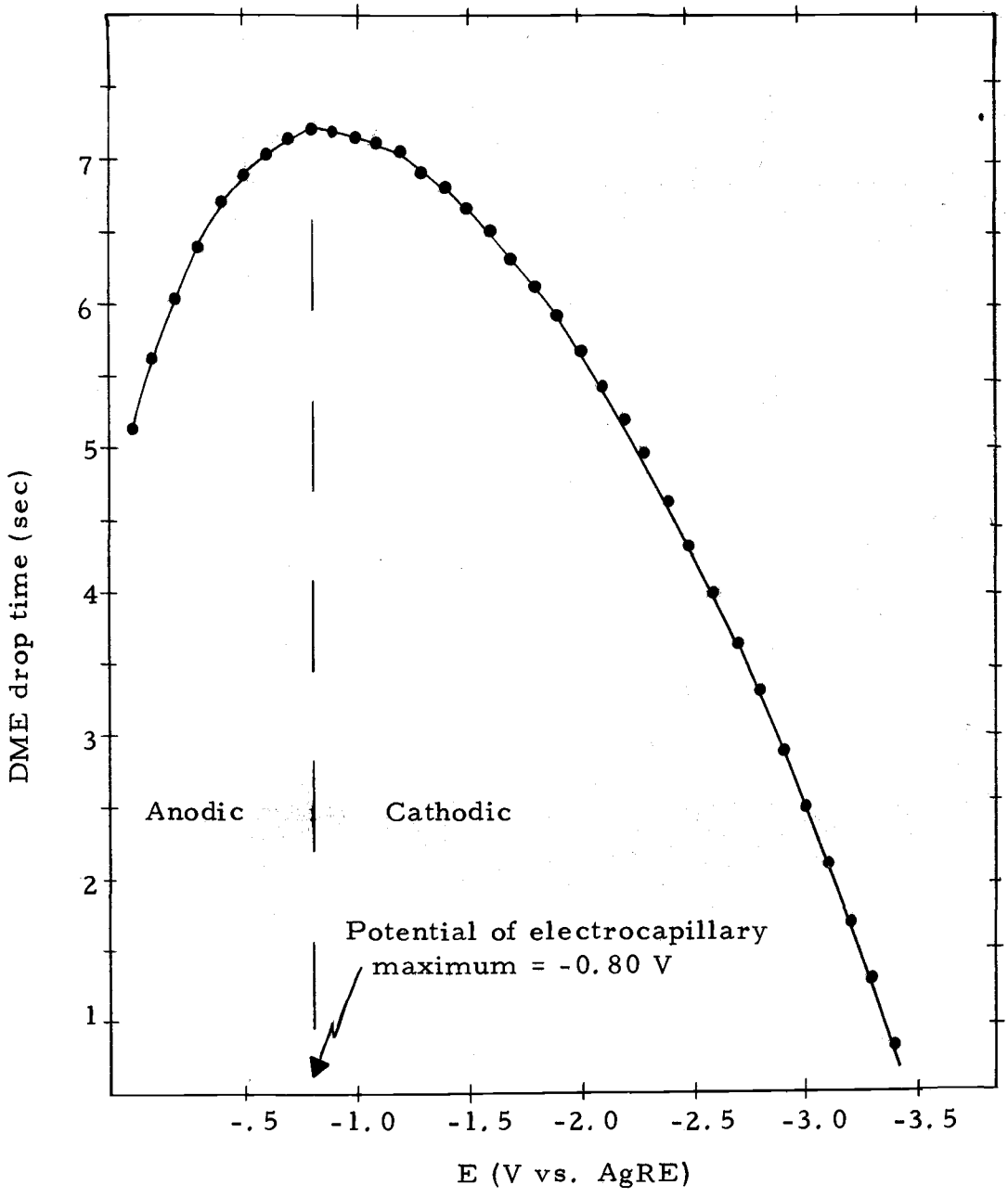

Figure 12. Electrocapillary curve for 0.1 M TEAP in sulfolane.

Table 3. DME drop time measurements in 0.1 M TEAP at 40°C.

Potential (V vs. AgRE	Drop time (sec)	Potential (V vs. AgRE)	Drop time (sec)
0.00	5.10	-1.90	5.90
-0.10	5.60	-2.00	5.65
-0.20	6.00	-2.10	5.40
-0.30	6.38	-2.20	5.18
-0.40	6.65	-2.30	5.00
-0.50	6.87	-2.40	4.60
-0.60	7.00	-2.50	4.30
-0.70	7.13	-2.60	3.98
-0.80	7.17	-2.70	3.60
-0.90	7.15	-2.80	3.27
-1.00	7.13	-2.90	2.85
-1.10	7.10	-3.00	2.45
-1.20	7.05	-3.10	2.05
-1.30	6.90	-3.20	1.65
-1.40	6.80	-3.30	1.25
-1.50	6.65	-3.40	0.80
-1.60	6.50		
-1.70	6.30	t_{PZC} = 7.17 sec	
-1.80	6.10	E_{PZC} = -0.800 V	

According to the integrated form of the Lippman equation the difference in surface tension as measured at the PZC and some other potential is related to the electrode potential in the following manner:

$$\lambda_{PZC} - \lambda = \frac{C}{2}(E-PZC)^2 \qquad (10)$$

where λ_{PZC} and λ are the values of the surface tension measured at the PZC and some other potential, E, and C is the double layer capacity of the electrode-solution interfacial region. If Equation (9) is used to substitute polarographic drop time measurements for surface tension values in Equation (10), Equation (10) can be

rearranged to:

$$(t_{PZC}-t) = \frac{\pi rC}{mg}(E-PZC)^2 \qquad (11)$$

Thus a plot of ln $(t_{PZC}-t)$ versus ln (E-PZC) should be linear with a slope of 2 and an intercept of $\frac{\pi rC}{mg}$. Shown in Figure 13 is such a plot for the electrocapillary data for mercury in the sulfolane solution. It is more clear from this plot that the electrocapillary curve shown in Figure 12 is not a simple second degree parabola. For potentials on either side of the PZC, the logarithmic plots of drop time are linear and have slopes near the theoretical value of 2. The least squares slope of the line for anodic potentials is 1.97 while for cathodic potentials the least squares slope is 1.92. While the lines have nearly the theoretical slope, each has a different intercept or value for $\frac{\pi rC}{mg}$. Since the quantity $\frac{r}{mg}$ is a characteristic of the particular capillary used and relatively constant, the variation in the intercept must be due to a change in C, the capacity of the interface reflecting a change in the nature or composition of the double layer region.

Capacitance Measurements for Cell Circuit Analogs

The potentiostat and overall method of measuring capacitances were checked using two types of systems. In the first series of tests, the capacitance of an electrical circuit analog of an electrochemical

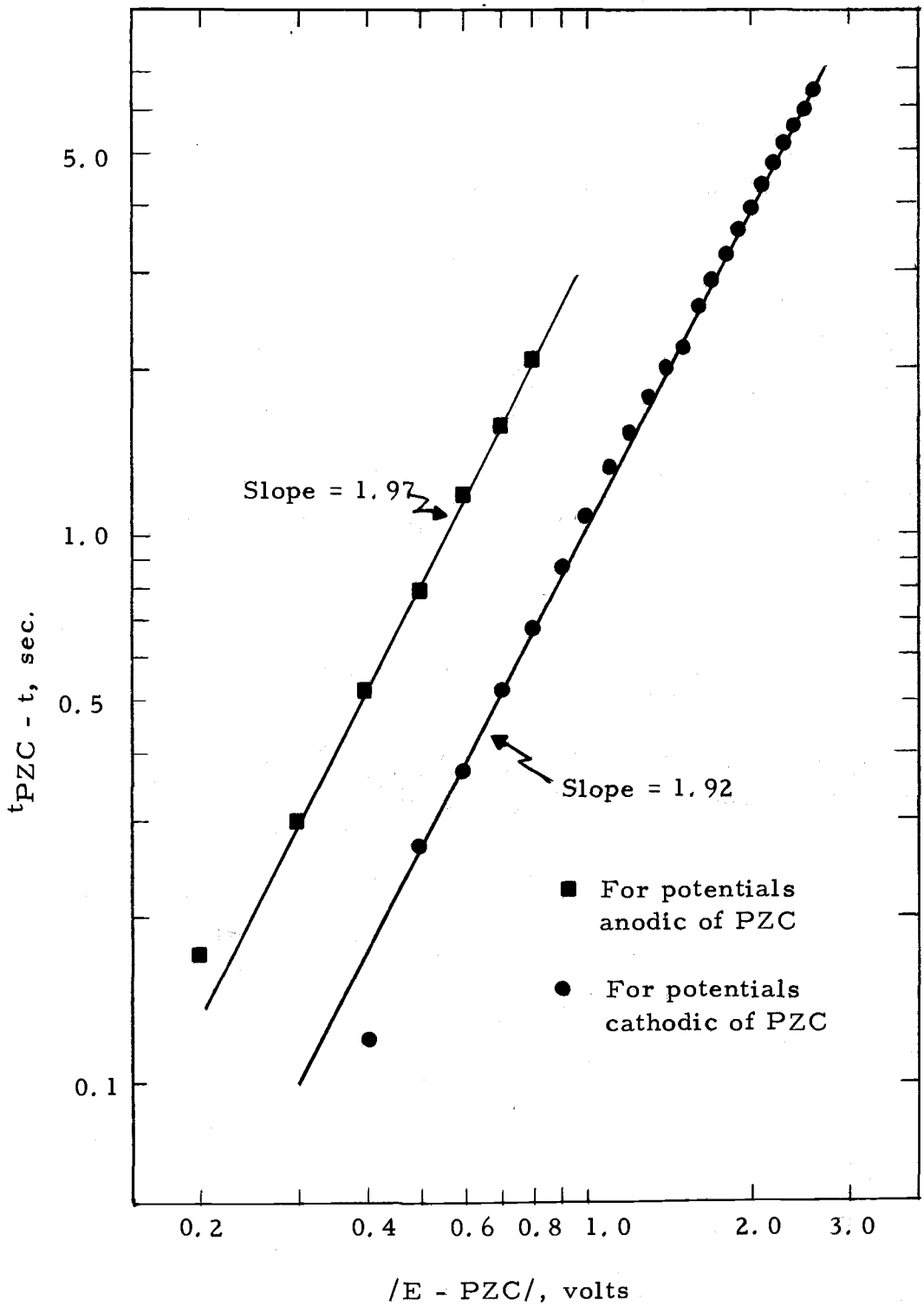

Figure 13. Logarithmic plot of polarographic drop time data for DME in 0.1 M TEAP in sulfolane.

cell was measured and the value was compared with the result obtained from a commercial capacitance bridge instrument. The second group of tests was made with a real cell whose double layer capacitances had been measured by other workers using different techniques.

The type of response observed with the instrumentation for the work with cell analogs is shown in Figure 14. The linear relationship suggested by Equation (2) between ln i and time for these types of current decay curves was verified for different combinations of resistance and capacitance by plotting the current-time measurements on semi-logarithmic graph paper. No systematic deviations in the linearities of the semilog plots were observed for measurements made over large portions of the decay curves. The only exceptions noted in these cases were for current measurements made around 50 μs or less after the application of the pulse. In these instances the observed currents tended to show a negative deviation from the semilog plot line drawn through the current measurements made for times greater than 50 μs. Fifty microseconds appeared to be approximately the response time of the instrument system and was undoubtedly responsible for the error in the current measurements in this time region. Examples of the linearity obtainable in the semilog plots are shown in Figure 15. Data used to construct the plots are listed in Table 4.

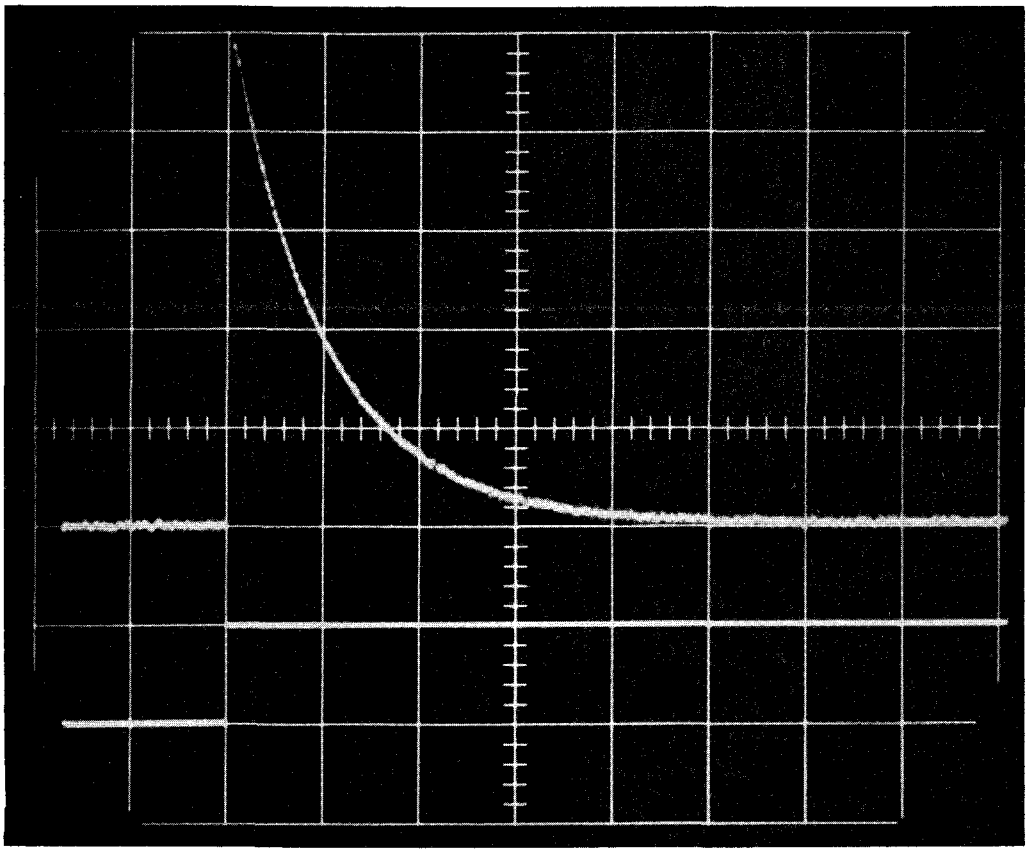

Figure 14. Response of cell analog to step voltage change. R=1K, C=0.523 μf. Upper trace: output of current-to-voltage converter, 1 mv/major vertical division and 0.5 ms/major horizontal division. Lower trace: output from pulse generator, 1 volt/major vertical division.

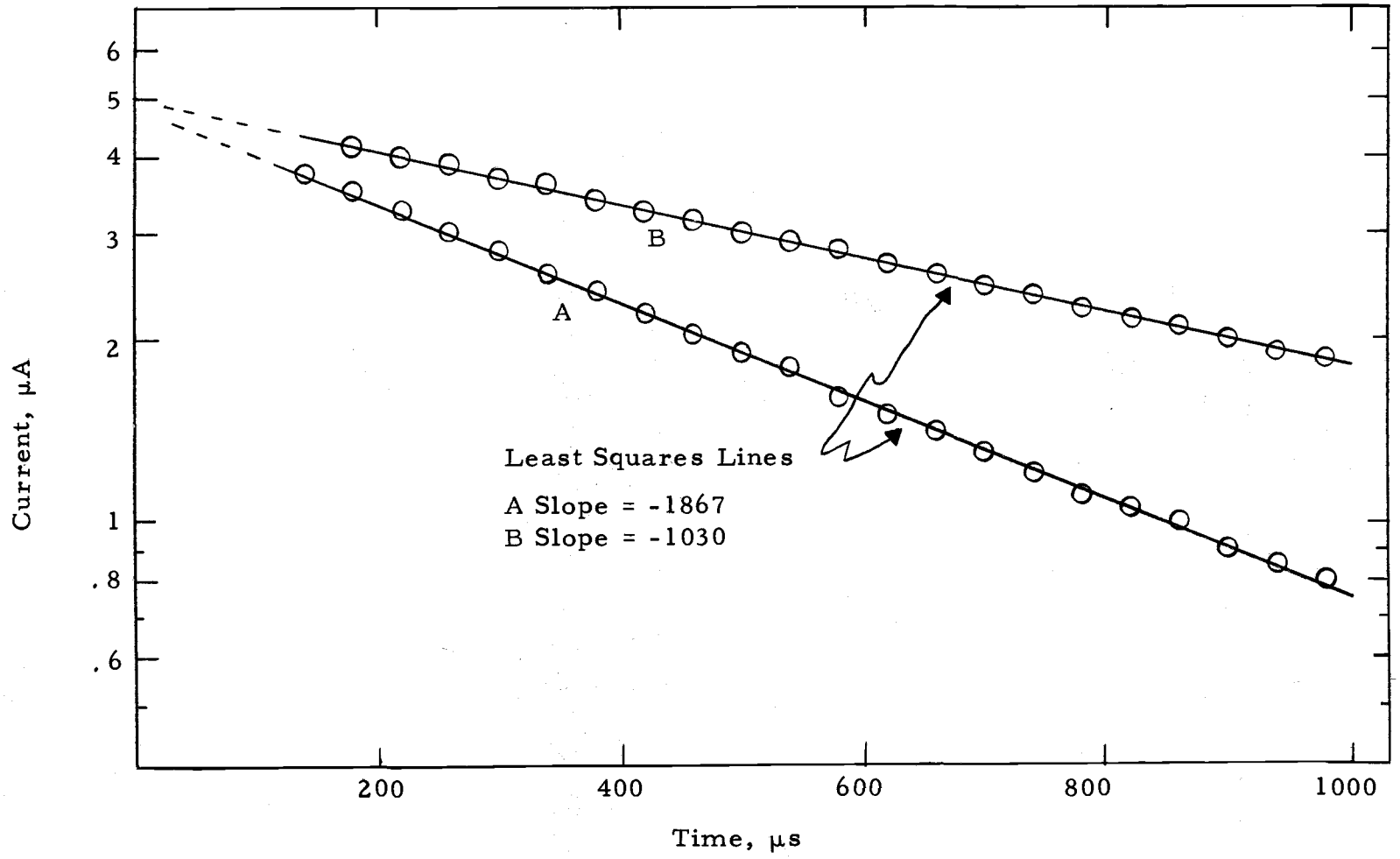

Figure 15. Semilog plot of current-time data for cell circuit analog.

Table 4. Current-time measurements for cell analog response to step voltage change.

C^a=0.523μf		C^a=0.960μf	
t(μS)	i(μA)	t(μS)	i(μA)
140	3.75	180	4.15
180	3.50	220	4.00
220	3.25	260	3.90
260	3.00	300	3.70
300	2.80	340	3.60
340	2.55	380	3.40
380	2.40	420	3.25
420	2.20	460	3.15
460	2.05	500	3.00
500	1.90	540	2.90
540	1.75	580	2.80
580	1.60	620	2.65
620	1.50	660	2.55
660	1.40	700	2.45
700	1.30	740	2.35
740	1.20	780	2.25
780	1.10	820	2.15
820	1.05	860	2.10
860	1.00	900	2.00
900	0.90	940	1.90
940	0.85	980	1.85
C^b = 0.519		C^b = 0.979	

[a]Measured with bridge.
[b]Calculated by means of Equation (6) using data from table.

Slope values determined by the least squares method for the ln i-time plots generally agreed very well with those calculated for the different combinations of R and C. For those combinations of R and C that had time constants around 100 μs or greater, the slope values determined from the least squares treatment agreed within ±2.5% of the calculated values and were usually around ±1%. Depending on how

many current-time pairs were taken and used in the least squares calculation of the slopes, the relative standard deviation in the slopes ranged from about ±0.5 to 2%. The relative standard deviations in the slope values for the lines shown in Figure 15 using all of the points for each line are 0.6%.

Capacitance values determined for the different RC combinations using Equation (6) agreed well with the values determined with the bridge instrument. The extent of agreement was generally found to be within the precision of the pulse method which, assuming only random errors, can be estimated by Equation (12) (52):

$$\left(\frac{\sigma_c}{c}\right)^2 = \sigma_b^2 + \left(\frac{\sigma_m}{m}\right)^2 + \left(\frac{\sigma_{e_s}}{e_s}\right)^2 \qquad (12)$$

where $\left(\frac{\sigma_c}{c}\right)^2$ is the relative variance in the calculated capacitance, σ_b^2 the variance in the least squares intercept from the ln i versus t plot, and $\left(\frac{\sigma_m}{m}\right)^2$ and $\left(\frac{\sigma_{e_s}}{e_s}\right)^2$ are the relative variances in the least squares slope and step voltage. The step voltage was measured with the oscilloscope and the relative variance in this measurement was estimated to be 0.0004. Equation (12) is not strictly valid for estimating the relative precision of the capacitance as calculated in the pulse experiment from Equation (6). The slope and intercept used to calculate C by means of Equation (6) are determined from the same set of ln i-time data and are not independent of one another for a particular experiment. There should therefore be a covariance term

added to Equation (12) to account for the inter-relationship between the slope and intercept values. At any rate, the capacitance values determined in the pulse experiments always agreed within $\pm 3\%$ of the values determined with the bridge instrument, provided the RC time constants were greater than about 100 μs.

An analysis of the propagation of errors for this type of experiment was made and it suggested a way in which the capacitance measurements could be improved. Equation (12) shows how the relative variance in C is related to the variances in the step voltage and least square parameters, b and m, but does not indicate how the variances in the least square parameters may be minimized in order to reduce the statistical error in C. To see how the random error in C can be reduced under the conditions of the experiment, it is first necessary to find an expression that relates the capacitance to experimentally measured quantities. By combining Equations (3) and (4) one can obtain Equation (13):

$$C = \frac{t\, i_o}{e_s \ln (i_o/i)} \tag{13}$$

which relates capacitance to directly measurable quantities. Assuming all errors in experimental parameters to be random and normally distributed, the variance in C in the above equation is given by:

$$\sigma_c^2 = \left(\frac{\partial C}{\partial t}\right)^2 \sigma_t^2 + \left(\frac{\partial C}{\partial e_s}\right)^2 \sigma_{e_s}^2 + \left(\frac{\partial C}{\partial i_o}\right)^2 \sigma_{i_o}^2 + \left(\frac{\partial C}{\partial i}\right)^2 \sigma_i^2 \tag{14}$$

where σ^2 terms represent variances in the measured or computed parameters. The partial derivative quantities can be found from Equation (13) and are:

$$\left(\frac{\partial C}{\partial t}\right)^2 = \frac{i_o^2}{e_s^2(\ln x)^2} = \frac{C^2}{t^2} \tag{15}$$

$$\left(\frac{\partial C}{\partial e_s}\right)^2 = \frac{i_o^2 t^2}{e_s^4 (\ln x)^2} = \frac{C^2}{e_s^2} \tag{16}$$

$$\left(\frac{\partial C}{\partial i_o}\right)^2 = \frac{t^2}{e_s (\ln x)^2} \left[1 - \frac{1}{\ln x}\right]^2 = \left[1 - \frac{1}{\ln x}\right] \frac{C^2}{i_o^2} \tag{17}$$

$$\left(\frac{\partial C}{\partial i}\right)^2 = \frac{t^2 i_o^2}{i_2^2 e_s^2 (\ln x)^4} = \left(\frac{1}{\ln x}\right)^2 \frac{C^2}{i^2} \tag{18}$$

where $x = i_o/i$. If the above partial derivatives are substituted into Equation (14) and the equation is rearranged slightly, the expression for the relative variance in C is found to be:

$$\left(\frac{\sigma C}{C}\right)^2 = \left(\frac{\sigma t}{t}\right)^2 + \left(\frac{\sigma e_s}{e_s}\right)^2 + \left[\frac{\ln(x)-1}{\ln x}\right]^2 \left(\frac{\sigma i_o}{i}\right)^2 + \left(\frac{1}{\ln x}\right)^2 \left(\frac{\sigma i}{i}\right) \tag{19}$$

If one can assume $\sigma i_o^2 = \sigma i^2$ Equation (19) may be simplified to:

$$\left(\frac{\sigma C}{C}\right)^2 = \left(\frac{\sigma t}{t}\right)^2 + \left(\frac{\sigma e_s}{e_s}\right)^2 + \frac{x^2 + [\ln(x)-1]^2}{(\ln x)^2} \left(\frac{\sigma i_o}{i_o}\right)^2 \tag{20}$$

The middle term on the right hand side of Equation (20) represents a time independent contribution to the statistical error in C.

The first and third terms are more interesting in that their contributions to the relative variance of C are not independent of time. If the standard deviations σ_t and σ_{i_o} are independent of the magnitude of the respective parameters being measured, one notes that the contribution of the first term diminishes with increasing t. The situation with the third term is not so obvious. The coefficient of the relative variance of i_o has been computed for various values of x and is listed in Table 5 and plotted in Figure 16. It is clear from Figure 16 that the coefficient of the relative variance for the current measurement is in a region of a minimum for a current ratio (i_o/i) value between 2 and 3.

Table 5. Current variance coefficient values.

$x(i_o/i)$	$\frac{x^2+[\ln(x)-1]^2}{(\ln x)^2}$	$x(i_o/i)$	$\frac{x^2+[\ln(x)-1]^2}{(\ln x)^2}$
1.25	43.5	4.00	8.4
1.30	32.5	4.50	9.1
1.50	15.8	5.00	9.8
1.75	10.4	5.50	10.6
2.00	8.5	6.00	11.4
2.50	7.5	7.00	13.2
2.72	7.4	8.00	15.1
3.00	7.5	10.00	19.2
3.50	7.8	20.00	45.0

The exact value of the current ratio for which the coefficient is at a minimum can be found by differentiating the coefficient with respect to x, setting the derivative equal to zero and solving for x. The value of x at the minimum was found to be "e" while the value of

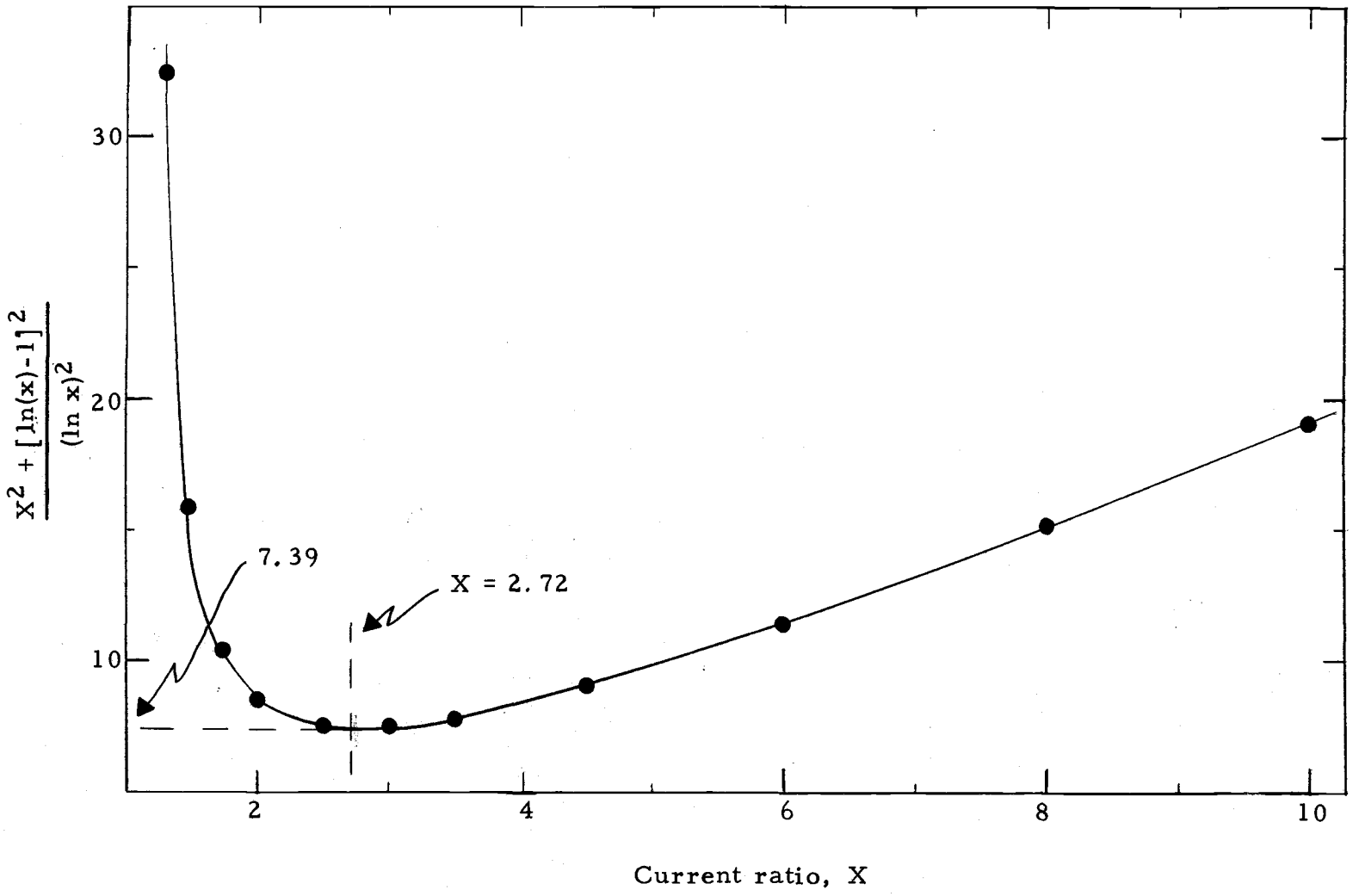

Figure 16. Current variance coefficient plotted as a function of the current ratio.

the coefficient at the minimum is 7.39. Thus for an experiment in which the relative standard deviations of all measurements are approximately the same, the relative variance in the capacitance result will be mostly determined by the last term in Equation (20).

It is clear from the minimum in Figure 16 that in collecting any current-time observations for use in a least squares technique to calculate capacitance, only those measurements for which the current ratio lies roughly between 2 and 4 should be used. By using current ratios between 2 and 4 optimal standard deviation between 2 and 4% in the capacitance determination could generally be achieved with only 6 to 10 current-time measurements.

Double Layer Capacitance Measurements for Hg-aqueous KCl Interface

Having used the instrumentation and pulse capacitance technique to measure capacitance for electrical circuit analogs, it was desirable to test the method and equipment on a well studied chemical system before attempting to measure differential double layer capacitance for electrode-sulfolane interfaces. The system selected was the Hg-aqueous 1M potassium chloride interface. It is one of the interfaces whose properties have been extensively measured and discussed and for which accurate double layer capacitance measurements have been reported in tabular form.

Listed in Table 6 are the double layer capacitance values measured at five potentials for the Hg-1 M KCl interface as determined by the pulse technique along with Grahame's accurate results obtained with his AC bridge technique. The values from the pulse technique are taken from one experiment at each potential and are generally reported to one more significant figure than justified from the statistical error in the measurement as calculated from Equation (12).

Table 6. Double layer capacitances for Hg-1M KCl interface.

-E (V vs. N.C.E.)	C^a μf /cm^2	C^b μf /cm^2
0.22	44.9	42.7
0.56	40.3	39.6
0.85	19.6	18.7
1.08	17.0	16.4
1.43	18.4	18.0

[a]This work
[b]Reference (29).

The agreement between results is very good, certainly within the precision of each technique. There appears, however, to be some systematic error between the results. The values obtained in this work are consistently higher than those determined by the AC bridge technique. Some of this error may be attributable to the existence of a small liquid junction potential in the pulse work which would have the effect of shifting the potentials of the capacitance measurements. A second probable source of a small systematic error in the capacitance measurements would be the presence of a small faradaic current

flowing as a result of the application of the step voltage change. A small faradaic current in addition to the charging current would make it appear as if the interfacial capacity were larger than it really were. A more detailed examination of this effect is discussed below.

Double Layer Capacitance Measurements in Sulfolane

The work with cell circuit analogs and the agreement in the double layer capacities as determined by the two methods was encouragement enough to apply the pulse technique to the measurement of interfacial capacities formed between various electrode materials and 0.1 M TEAP in sulfolane.

The differential double layer capacities for the HMDE, GCME, PTME and AUME in sulfolane are shown as a function of potential in Figures 17 and 18. For each electrode there are two curves. One was calculated using Equation (6), which assumes no faradaic current due to the pulse ($\gamma = 0$). The second curve ($\gamma \neq 0$) was calculated by means of a slightly different equation which was derived assuming a faradaic current contribution to the observed cell current. A discussion of the faradaic effect is presented later along with the equation used to calculate the double layer capacitance with the complication. Data used to construct the curves are listed in Tables 7 and 8. The values presented in these tables are the results of a single experiment at each potential. To check the reproducibility of these values, five

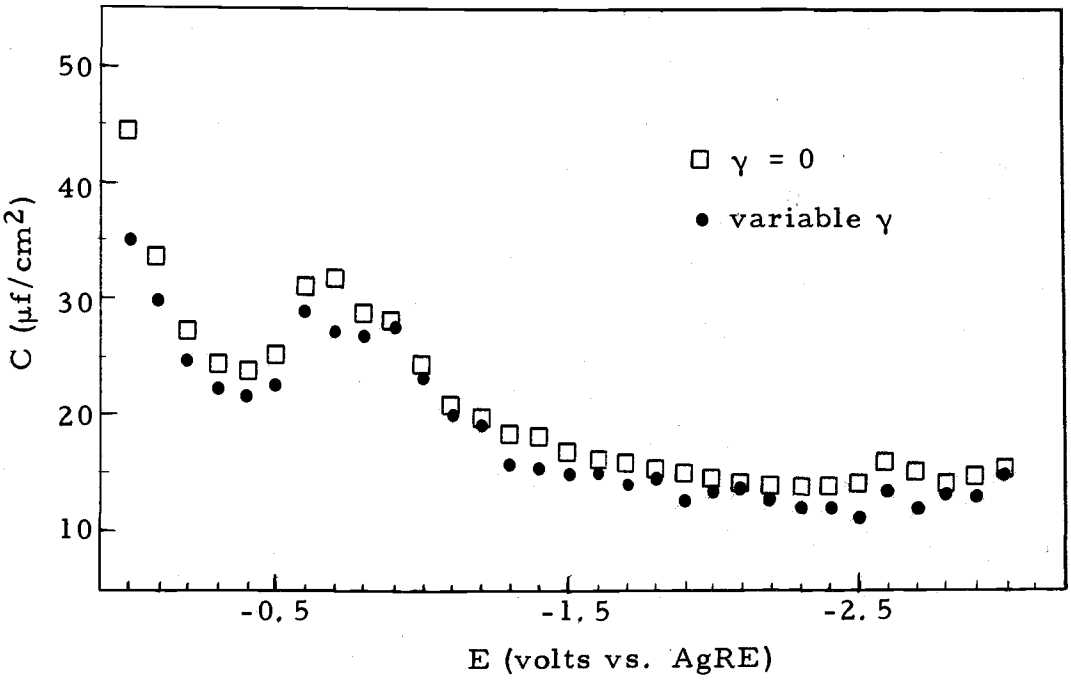

A

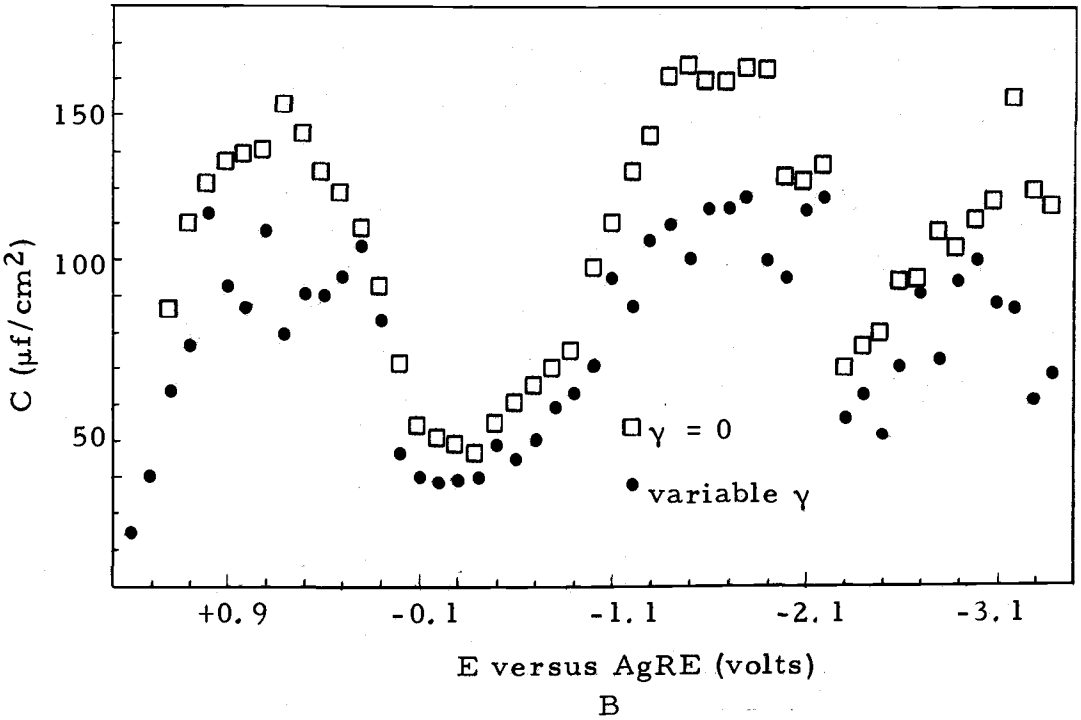

B

Figure 17. Differential double layer capacitances of HMDE (A) and GCME (B) in 0.10 M TEAP in sulfolane at 40°C.

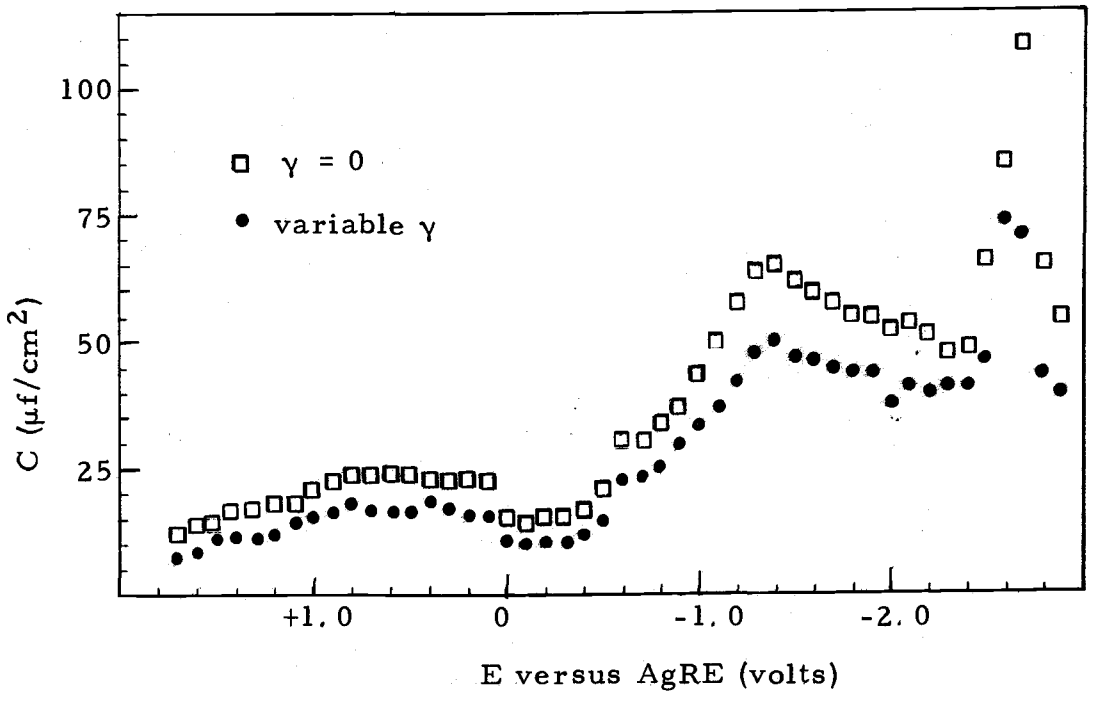

A

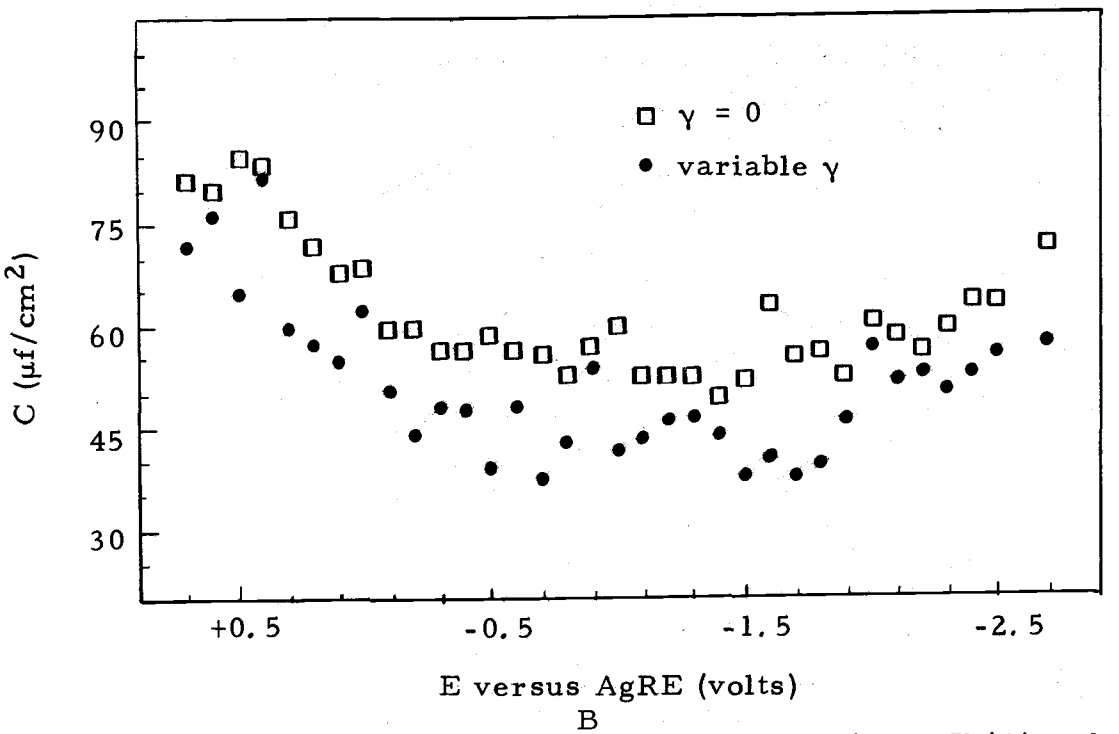

B

Figure 18. Differential double layer capacitances of PTME (A) and AUME (B) in 0.10 M TEAP in sulfolane at 40°C.

Table 7. Differential double layer capacitance values for solid microelectrodes.

Potential volts vs. AgRE	PTME $C\mu$ f/cm^2 $\gamma=0$	PTME $C\mu$ f/cm^2 $\gamma\neq0$	AUME $C\mu$ f/cm^2 $\gamma=0$	AUME $C\mu$ f/cm^2 $\gamma\neq0$	GCME $C\mu$ f/cm^2 $\gamma=0$	GCME $C\mu$ f/cm^2 $\gamma\neq0$
1.70	11.8	8.22				
1.60	12.9	8.65				
1.50	14.5	11.7				
1.40	16.7	11.8			48.5	35.4
1.30	17.3	11.5			70.8	50.5
1.20	18.0	12.4			96.4	75.2
1.10	18.2	14.4			120	87.4
1.00	20.8	15.8			131	124
0.90	22.1	16.5			137	103
0.80	23.8	18.4			139	97.2
0.70	23.6	16.8	76.8	66.8	140	119
0.60	23.6	16.8	74.4	71.5	154	90.1
0.50	23.7	16.9	79.3	60.0	145	101
0.40	22.7	19.0	78.5	77.3	134	101
0.30	22.8	17.6	70.6	55.1	129	106
0.20	22.9	16.2	66.5	52.7	119	114
0.10	22.6	16.0	62.5	50.4	103	94.3
0.00	14.5	11.3	63.5	57.9	82.0	57.6
-0.10	14.3	10.3	54.8	45.9	64.9	49.8
-0.20	15.4	10.8	54.8	39.7	61.7	48.9
-0.30	15.5	10.8	51.2	43.7	59.6	49.7
-0.40	16.3	12.1	51.2	43.7	57.2	50.5
-0.50	20.6	15.1	53.9	34.6	65.5	59.6
-0.60	30.8	23.5	51.2	43.7	70.6	55.2
-0.70	30.3	24.1	50.3	33.2	75.8	61.5
-0.80	33.7	25.5	47.5	38.4	81.0	70.3
-0.90	37.1	30.7	51.8	49.4	85.7	73.7
-1.00	43.8	34.3	54.7	36.8	108	81.2
-1.10	49.5	37.1	47.5	38.4	121	106
-1.20	57.5	42.9	47.7	41.6	134	97.5
-1.30	63.1	48.5	47.7	41.6	144	116
-1.40	65.1	50.8	44.4	39.5	160	120
-1.50	61.4	47.6	47.3	33.5	164	110
-1.60	59.8	46.7	57.7	36.0	159	125
-1.70	57.9	44.7	50.3	33.2	159	125
-1.80	54.7	44.6	50.9	35.1	163	128
-1.90	54.7	44.6	47.7	41.7	163	110
-2.00	52.3	38.0	55.6	52.1	133	104
-2.10	53.1	41.3	53.3	47.4	132	124
-2.20	51.5	39.8	51.4	48.5	136	128
-2.30	47.3	40.8	54.8	45.9	80.8	66.7
-2.40	48.8	41.2	58.6	48.1	86.4	73.5
-2.50	65.7	46.8	58.3	50.6	90.0	62.1
-2.60	85.5	74.8	65.5	52.7	104	81.4
-2.70	109	71.3			105	101
-2.80	65.0	44.4			118	82.7
-2.90	54.2	40.1			113	104
-3.00					121	110
-3.10					126	98.3
-3.20					154	97.2
-3.30					128	71.8
-3.40					115	77.9

Table 8. Effect of γ value on electrical double layer capacitance measurements for the HMDE.

Potential (V vs AgRE	γ =0 (μ A)	C (μ f/cm^2)	γ * (μ A)	C (μ f/cm^2)	γ ** (μA)	C (μ f/cm^2)
0.000	44		0.68	35.2	0.65	35.8
-0.100	34		0.32	30.0	0.35	29.6
-0.200	27		0.22	24.9	0.22	24.9
-0.300	24		0.21	22.3	0.17	22.7
-0.400	24		0.21	21.6	0.25	21.2
-0.500	25		0.25	22.7	0.20	23.2
-0.600	31		0.19	29.0	0.13	29.6
-0.700	32		0.39	27.2	0.38	27.4
-0.800	29		0.19	26.8	0.15	27.3
-0.900	28		0.01	27.9	0.03	28.0
-1.000	24		0.12	23.1	0.10	23.3
-1.100	21		0.08	20.1	0.10	20.0
-1.200	19		0.13	19.4	0.25	19.9
-1.300	18		0.50	15.8	0.50	15.8
-1.400	18		0.50	15.6	0.55	15.3
-1.500	17		0.40	15.0	0.40	15.0
-1.600	16		0.20	15.2	0.10	15.6
-1.700	16		0.35	14.1	0.32	14.2
-1.800	15		0.08	14.8	0.15	14.5
-1.900	15		0.45	12.7	0.40	13.0
-2.000	14		0.20	13.5	0.20	13.5
-2.100	14		0.10	13.6	0.15	13.4
-2.200	14		0.20	12.9	0.20	12.9
-2.300	14		0.35	12.1	0.27	12.5
-2.400	14		0.35	12.2	0.25	12.7
-2.500	14		0.52	11.4	0.50	11.6
-2.600	16		0.49	13.5	0.53	13.2
-2.700	15		0.59	12.1	0.57	12.1
-2.800	14		0.29	13.2	0.28	13.2
-2.900	14		0.32	13.0	0.32	13.0
-3.000	16		0.20	15.0	0.22	14.9

* calculated by means of equation (22).

** γ value selected which minimized the relative std. dev. of C. as calculated from equation (12).

potentials for each electrode were selected and the value of the double layer capacitances at these potentials were measured again on a different day. The reproducibility of the HMDE capacitance values (with faradaic correction) was within the expected precision of the experiment, which was generally around 3 to 4%.

The reproducibility in the capacitance values of the solid electrodes was not as good. The PTME values measured at the five potentials were generally within 10% of the values measured earlier and showed no trend in their deviations. The precision of the GCME and AUME capacities ranged from 5 to 40% and also displayed no trend in their deviations. The lack of reproducibility in double layer capacities for the same electrode is indicative of changes in surface properties. The changes could be associated with reorientation of the microscopic crystals that comprise the surface and hence alter the electronic properties of the surface and there could be changes in exposed electrode areas brought about with reorientation at the surface. The capacitance value one measures for a solid electrode is a gross value which is some sort of average for all the microscopic surfaces and that these may change with time affecting the gross capacitance value is not unreasonable. Repolishing the surfaces and remeasuring capacitance values produced results that differed from the original measurements by tens to hundreds of percent. Other workers have noted the same lack of reproducibility in capacitance measurements

made on solid electrodes using different measuring techniques (73). The problem was anticipated, but the capacity-potential curves for the solid electrodes were measured anyway to furnish a rough estimate of the magnitude of the capacities expected for these electrodes in TMS.

The differential capacity-potential curves for the HMDE in sulfolane are similar in shape to those obtained for mercury in aqueous solutions (37, 39) and to curves obtained for the electrode in several nonaqueous systems (72). The double layer capacitance values for the HMDE-0.1 M TEAP interface ranged from about 12 to 36 $\mu f/cm^2$ over the potential range studied. This range of capacitance values for the tetraalkylammonium salt is similar to the range of values reported by Lawrence and Parsons (56) for potassium hexafluorophosphate and sodium perchlorate in the same solvent. A capacity maximum or "hump" is observed for TEAP on the anodic side of the electrocapillary maximum potential. Similar observations were reported for $NaClO_4$ and KPF_6. The existence of the hump in the capacity curve may be an intrinsic property of the solvent and independent of the particular salt. The value of the capacity maximum for TEAP is about 30 $\mu f/cm^2$, which is intermediate to the reported values for $NaClO_4$ and KPF_6. The final rise in double layer capacity for large anodic potentials parallels that for $NaClO_4$ and is probably a pseudo-capacitance (38) associated with the electrochemical

oxidation of mercury. A similarly expected steep rise in capacitance at high cathodic potentials where electrochemical reduction of solvent or solute takes place could not be observed owing to drop detachment at these extreme potentials. The start of such a rise in capacitance is evident, though.

A broad minimum in the capacity-potential curve for the HMDE occurs around -2.5 v. The value of this minimum capacity is 11.6 $\mu f/cm^2$ and is comparable to values obtained for various other salts in dimethylsulfoxide and other solvents. From an analytical standpoint, the potential range around -2.5 v should be a good region in which to observe fast scan voltammetric waves owing to the relatively low charging currents expected in this range. Sulfolane, however, would not appear to offer any significant reduction in charging current interference in voltammetric analysis over other nonaqueous solvents.

Effect of Faradaic Correction

Plots of the natural logarithm of decay current versus time were not always linear for experiments performed with real cells. The non-linearity in the log plots is illustrated in Figure 19 for some measurements made with the PTME. The curvature in each line in the figure is apparent and quite unlike the results obtained using the series RC circuit model of the cell.

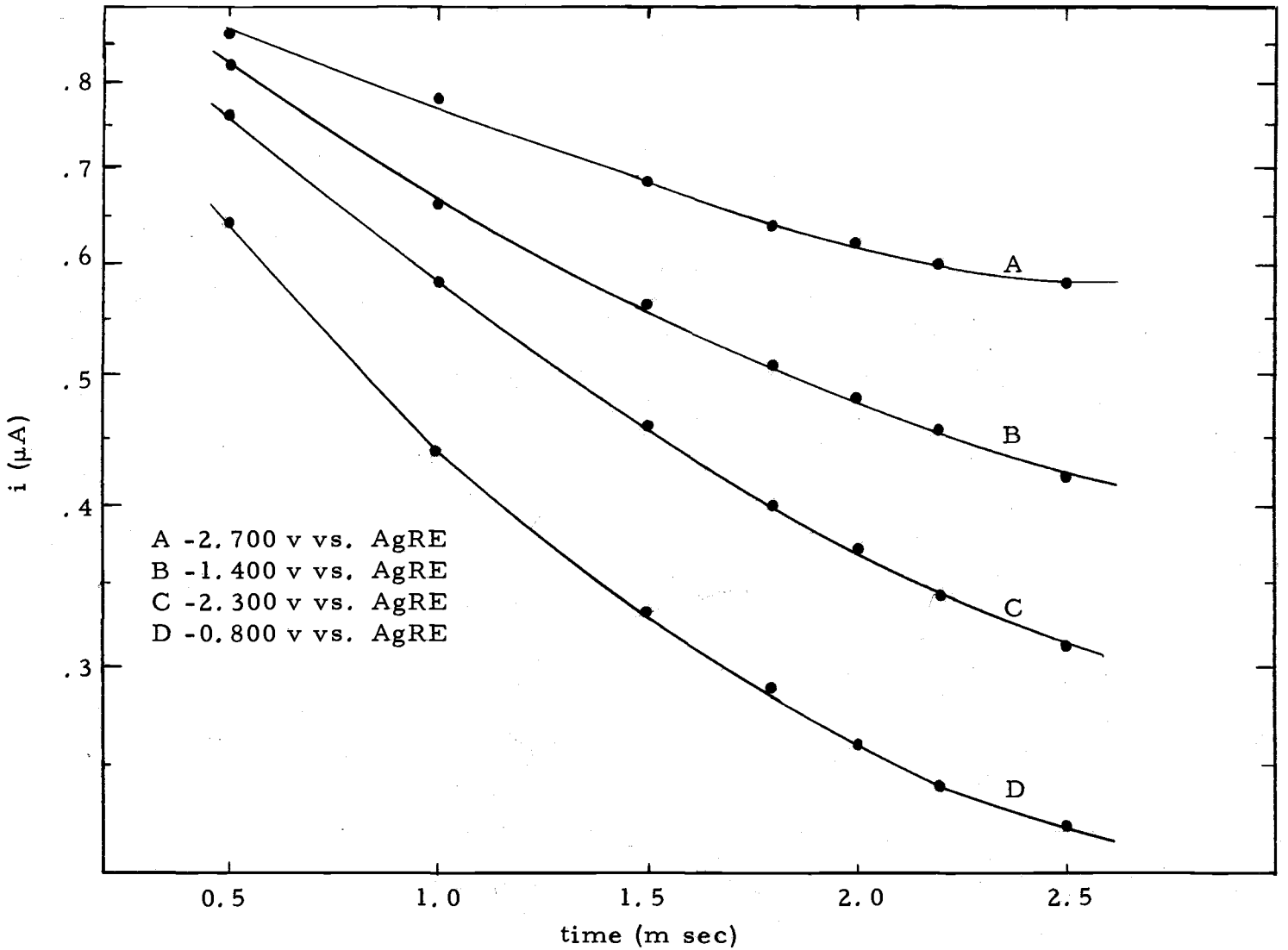

Figure 19. Ln(i) vs. time plots for PTME at various potentials in 0.10 M TEAP.

Qualitative differences in the decay curves observed for the real cell and electrical model were made very obvious when the real cell was operated near potentials where electrode or solvent decomposition occurred. In these instances the observed current would not decay to the current level just prior to the application of the pulse. In work with a simple series RC circuit analog, the current always returned to its value before the step voltage change.

The most obvious and reasonable explanation for these observations is that the test electrode-solution interface is not ideally polarized and that the application of a step voltage produces both a faradaic current and charging current and it is the sum of these that is measured in an experiment. In terms of an electrical analog this means abandoning the simple series RC model of Figure 3c for the work in sulfolane and returning to a more general, or experimentally more realistic model of the test-solution interface as shown in Figure 3a.

The faradaic complication in measuring double layer capacitance via the pulse technique is a serious one, as it is for the AC bridge method. Fortunately there exists a means of getting around the complication in the pulse technique without changing the experiment significantly if two assumptions about the nature of the faradaic process are made. If the faradaic and double layer charging processes are independent of one another and if the rate of the

electrochemical reaction resulting from the pulse can be considered constant on the time scale of double layer charging, a constant current proportional to the rate of the electrode reaction can be subtracted from the observed current to yield the real charging current and hence the true interfacial capacity. The current decay waveform for the pulse experiment under these conditions should look something like that shown in Figure 20, where i_r refers to the cell current flowing before application of the step voltage, and γ the magnitude of the faradaic current resulting from the pulse. A plot then of ln $(i - \gamma)$ versus time should be linear and the double layer capacitance can be calculated from the least squares slope and intercept of this plot according to Equation (21) (see Appendix II for derivation), where e_s is the step voltage and m' and b' are the least squares slope and intercept values of the ln $(i - \gamma)$ versus time plot. Equation (21) is a slightly more complicated expression for calculating double layer capacitance with the faradaic complication. It is clear that if there were no faradaic complication due to the pulse ($\gamma = 0$) then Equation (21) reduces to Equation (6).

$$C_{dl} = \frac{[\gamma + \exp(b')]^2}{e_s\, m' \exp(b')} \qquad (21)$$

It would seem that because of the manner in which the pulse capacitance technique is carried out, setting at a fixed initial potential

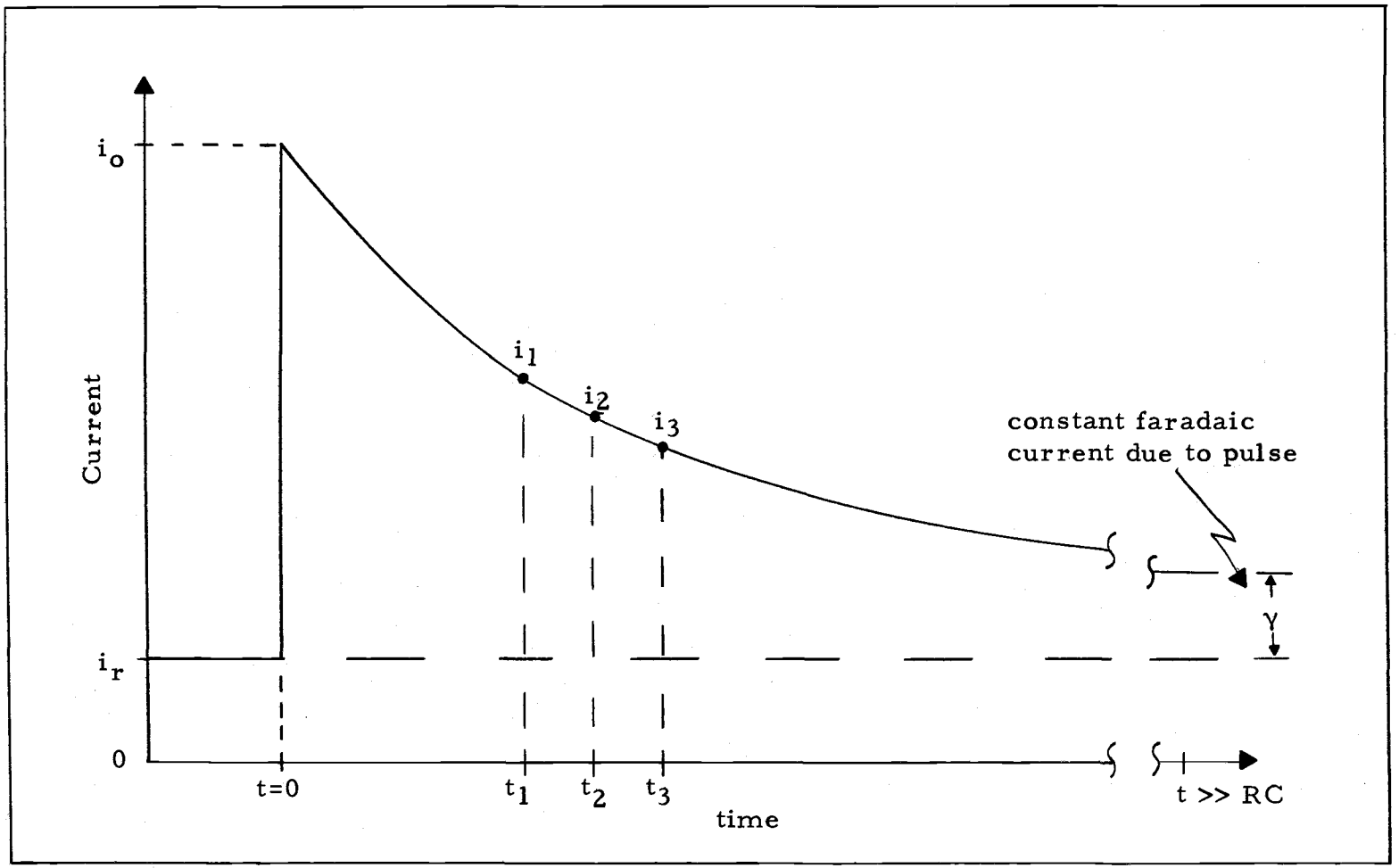

Figure 20. Current decay waveform for pulse capacitance technique with faradaic complication.

for a few minutes, and observing the charging current decay curves for several hundred voltage pulses, γ would itself decay to zero owing to electrolysis and depletion of the electroactive material. This situation would arise if the pulse faradaic current were due to an electrochemical reaction involving trace amounts of electroactive materials. Indeed, if sufficient time were allowed to pass, a depletion layer around the electrode would be established, and the faradaic current would drop to near zero. On the other hand, if the pulse faradaic current were due to an electrochemical reaction involving the solvent or an electroactive material that was chemically regenerated at the electrode surface, γ would not appear to decay with the passage of time.

γ can be found in various ways. The most direct method would be to measure it on the decay curve near the end of the pulse interval. In most cases, though, γ will be buried in noise and thus hard to measure. A second method is to calculate γ from current measurements made earlier along the decay curve. If three current measurements are made at regular time intervals, γ can be calculated from Equation (22), see Appendix III for derivation (idea suggested by Davis,(19)):

$$\gamma = \frac{i_1 i_3 - i_2^2}{i_1 + i_3 - 2 i_2} \qquad (22)$$

where i_1, i_2 and i_3 are currents measured from i_r as shown in Figure 20. Obviously, if more than three current measurements are made, more than one value for γ can be calculated and these values may be used or averaged to obtain a better estimate of γ.

The third way of determining γ is more or less a trial and error method. In this approach several intelligent guesses for the value of γ are made and used to construct several ln $(i - \gamma)$ versus time plots. The value of γ that leads to the smallest statistical error in the calculated capacitance is the value to be used. The statistical error in C that is minimized can be determined from Equation (11), though this is only an approximation since this error equation was derived for the case in which C is calculated from Equation (6). If γ and the error in γ are small, Equation (12) should provide a good estimate for the statistical error in C, even though C is calculated from Equation (21). This may seem like a very difficult approach, but when using a computer to perform the least squares routine and capacitance calculations, the selection of γ by the minimization of the statistical error in C is a feasible approach.

The effect that faradaic correction has on the linearity of the semilog plots and the statistical error in C can be seen in Figures 21 and 22. The experimental measurements used to construct the plots in Figure 21 are the same that were used in Figure 19. The improvement in the linearity of the semilog plots for these measurements on

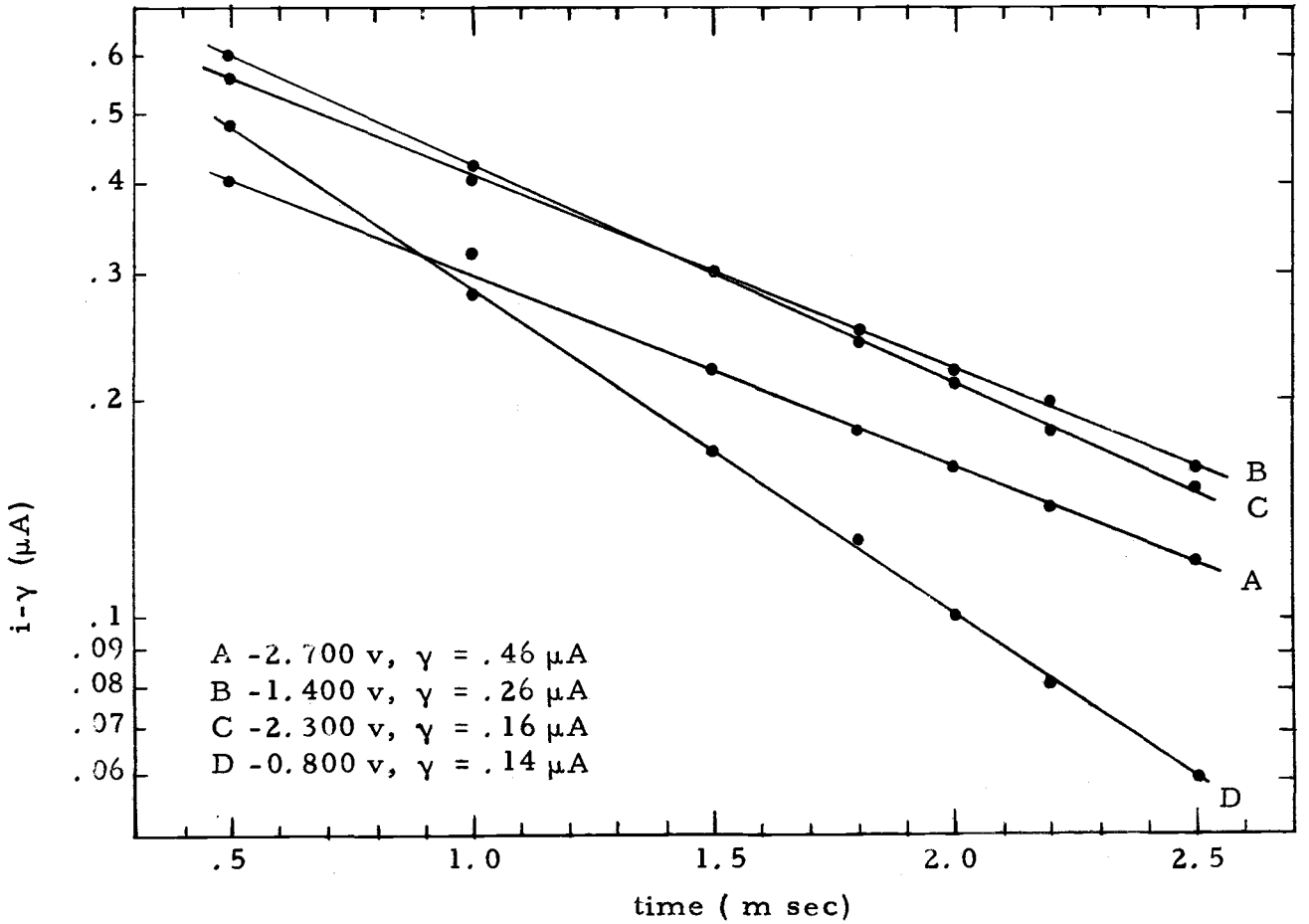

Figure 21. Ln (i-γ) vs. time plots for PTME at various potentials in 0.10 M TEAP.

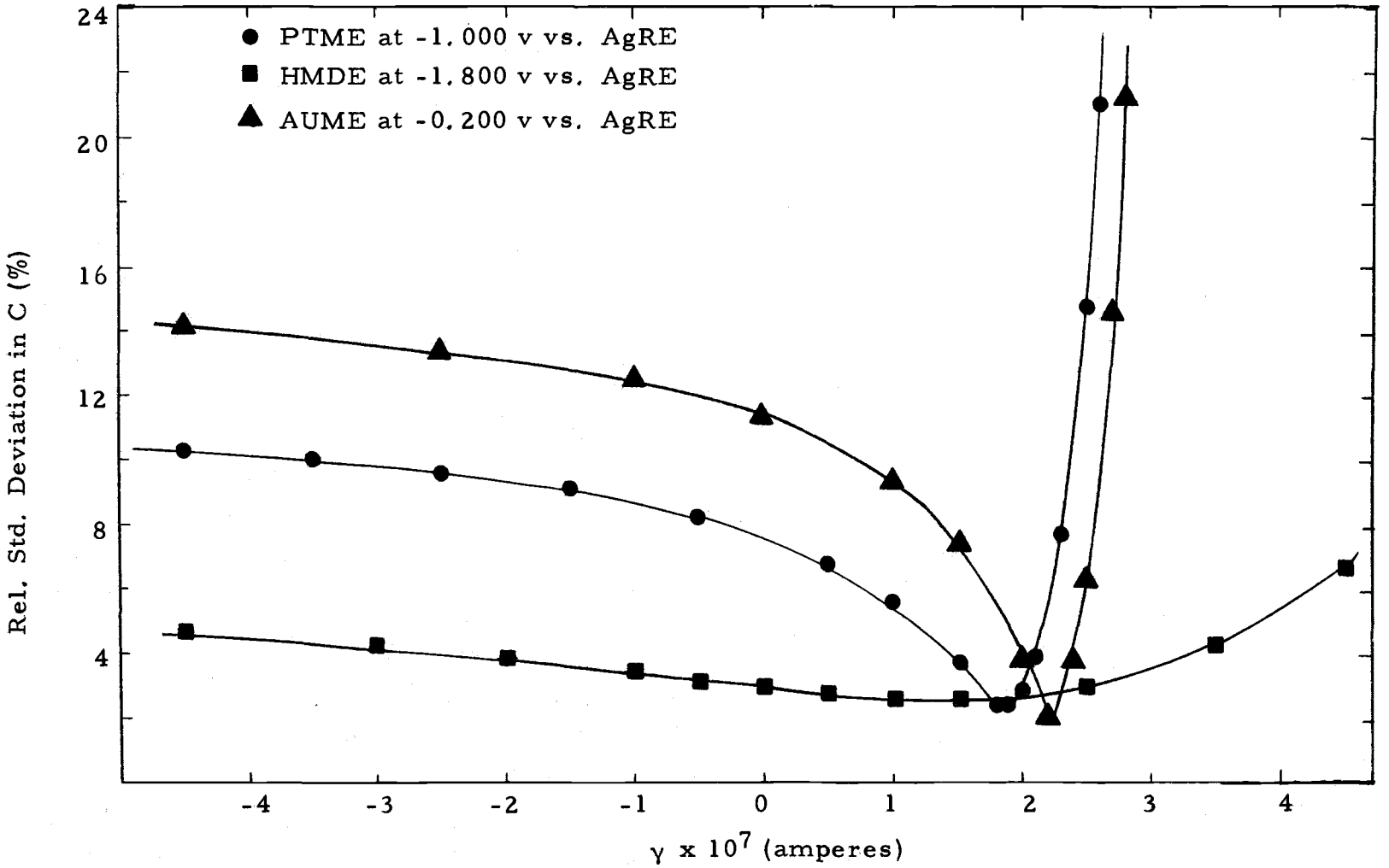

Figure 22. Effect of faradaic correction on statistical error in capacitance calculation.

platinum is significant, and was so for the gold and glassy carbon electrodes also. Improvement in the linearity of the semilog plots for the HMDE were not usually as dramatic, since the average faradaic current density correction for the HMDE was much smaller than that for the other electrodes. Over the potential range studied with each electrode, the HMDE had an average faradaic current density correction of 5 $\mu A/cm^2$, while the values for the AUME, GCME and PTME were 17, 19, and 29 $\mu A/cm^2$, respectively. The lower faradaic correction required for mercury is most likely due to a smaller electrochemical kinetic rate constant for an electrode reaction involving the solvent.

Plotted in Figure 22 is the square root of the relative variance in C, calculated from Equation (12) as a function of γ. The parameters used in Equation (12) were obtained in the following manner. For a given set of current-time measurements, several values for γ were assumed and used to construct plots of ln $(i - \gamma)$ versus time. The least squares intercepts and slopes of these plots, as well as the standard deviations in these quantities, were then appropriately substituted into Equation (12) to find the relative standard deviation in C and plotted as a function of γ.

The shapes of the curves shown in Figure 22 are interesting and demonstrate the effect that faradaic correction has on the statistical error in the calculated capacitance. As expected when γ is not

a significant fraction of the current measurements being used to construct the ln (i - γ) versus time plots, little effect in the statistical error of C as computed by means of Equation (12) should be observed. For the platinum and gold electrodes, γ is a much larger fraction of i and thus affects the statistical error in C more. All of the curves shown in Figure 22 have a minimum in the relative standard deviation of C around 0.1 to 0.2 μA. The value of the minimum is about 2%, which is essentially the estimated standard deviation in the step voltage. This was not typical for all capacitance measurements for which this type of plot was constructed. The value of the minimum ranged from 2 to 5% and was generally around 3 to 4%.

The values of γ used to calculate the double layer capacitances plotted in Figures 17 and 18 and listed in Tables 7 and 8 were determined by means of Equation (22). To check that these values were producing capacitances with near minimum statistical errors, a second set of γ values were determined for all of the HMDE data which did minimize the statistical error in the computed capacitance result. These γ values and the calculated double layer capacities are listed in Table 8 along with the capacitance results obtained by using γ values calculated from Equation (22). As can be seen from the table, the γ values determined by each method are in good agreement and the differences in the calculated capacitances using either value are small and within the error expected for the overall

experiment. This supports, at least for the HMDE, the use of Equation (22) to estimate the appropriate faradaic correction needed in the pulse capacitance technique.

Calculation of Interfacial Tension Values and Check of Parabolic Relationship with Potential

If the pulse capacitance technique is providing reliable double layer capacitance measurements for the mercury-sulfolane interface, the interfacial tension values derived from the measurements should be related to electrode potentials by Equation (10) and should be consistent with the electrocapillary measurements made for the same interface.

Conversion of double layer capacitance measurements for an electrode-solution interface to interfacial tension values requires a double integration of the capacity-potential curve (22, 64). The result of the first integration is an electrode charge density-potential curve and a subsequent integration of this curve yields the surface tension-potential curve, or the electrocapillary curve, as it is called.

The double layer capacity-potential curve for the HMDE in sulfolane (γ corrected curve, Figure 17a) was integrated by numerical summation using the trapezoidal rule approximation. The integration was started at the potential of the electrocapillary maximum or potential of zero charge (PZC) and continued in cathodic and anodic

directions using 100 mv wide potential steps. A short computer program was written and used to perform the calculations. The results of the first integration of the capacity-potential curve for the HMDE are listed in Table 9 and the electrode charge density is plotted as a function of electrode potential in Figure 23. The plot is a smooth concave curve not unlike those obtained for mercury electrodes in aqueous media (37, 64).

Integration of the charge density-potential curve in Figure 22 was performed in the same manner as was the first integration. The results of the second integration are also listed in Table 9. The units of the second integration results are ergs cm^{-2} and numerically equivalent to the units of dynes cm^{-1}. It should be pointed out that the interfacial tension values listed in Table 9 are actually differences in interfacial tension. The value listed in the table for each potential is the difference between the surface tension measured at the PZC (-0.80 v versus AgRE in this case) and the surface tension at the potential stated.

According to Equation (10), a plot of ln $(\lambda_{pzc}-\lambda)$ versus ln (E-PZC) should be linear and have a slope of 2. Such a logarithmic plot for the surface tension values listed in Table 9 was made and is shown in Figure 24. For potentials on either side of the PZC, the plots are linear and have least square slopes of 1.97 and 1.83, which are in fair agreement with the theoretical value of 2 considering the

Table 9. Electrode charge densities and interfacial tension values for the HMDE in sulfolane.

-E V vs AgRE	C μ f/cm^2	$\int$CdE μ coul/cm^2	$\iint Cd^2E$ λ PZC$^-$ λ ergs/cm^2
0.000	35.8	-21.02	82.90
0.100	29.6	-17.74	63.52
0.200	24.9	-15.02	47.14
0.300	22.7	-12.64	33.31
0.400	21.2	-10.44	21.77
0.500	23.2	- 8.23	12.43
0.600	29.6	- 6.53	5.53
0.700	27.4	- 2.74	1.37
0.800	27.3	0	0
0.900	28.0	2.76	1.38
1.000	23.3	5.33	5.43
1.100	20.0	7.50	11.84
1.200	19.9	9.49	20.34
1.300	15.8	11.28	30.72
1.400	15.3	12.83	42.77
1.500	15.0	14.34	56.36
1.600	15.6	15.88	71.47
1.700	14.2	17.36	88.09
1.800	14.5	18.80	106.2
1.900	13.0	20.18	125.6
2.000	13.5	21.50	146.5
2.100	13.4	22.84	168.7
2.200	12.9	24.16	192.2
2.300	12.5	25.43	216.9
2.400	12.7	26.69	243.0
2.500	11.6	27.90	270.3
2.600	13.2	29.14	298.8
2.700	12.1	30.41	328.6
2.800	13.2	31.68	359.7
2.900	13.0	32.98	392.0
3.000	14.9	34.38	425.7

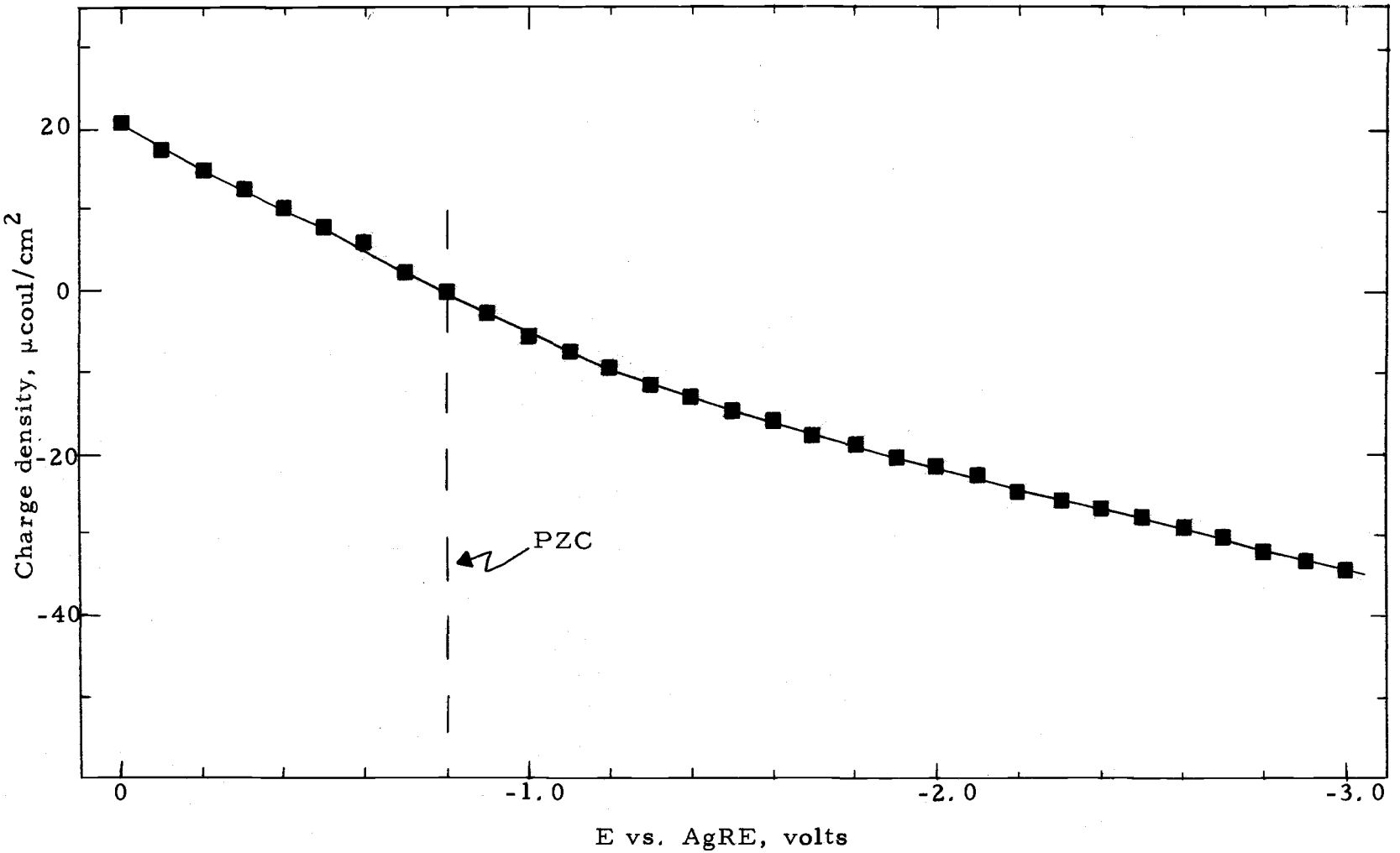

Figure 23. Electrode charge density versus electrode potential for HMDE in 0.1 M TEAP in sulfolane.

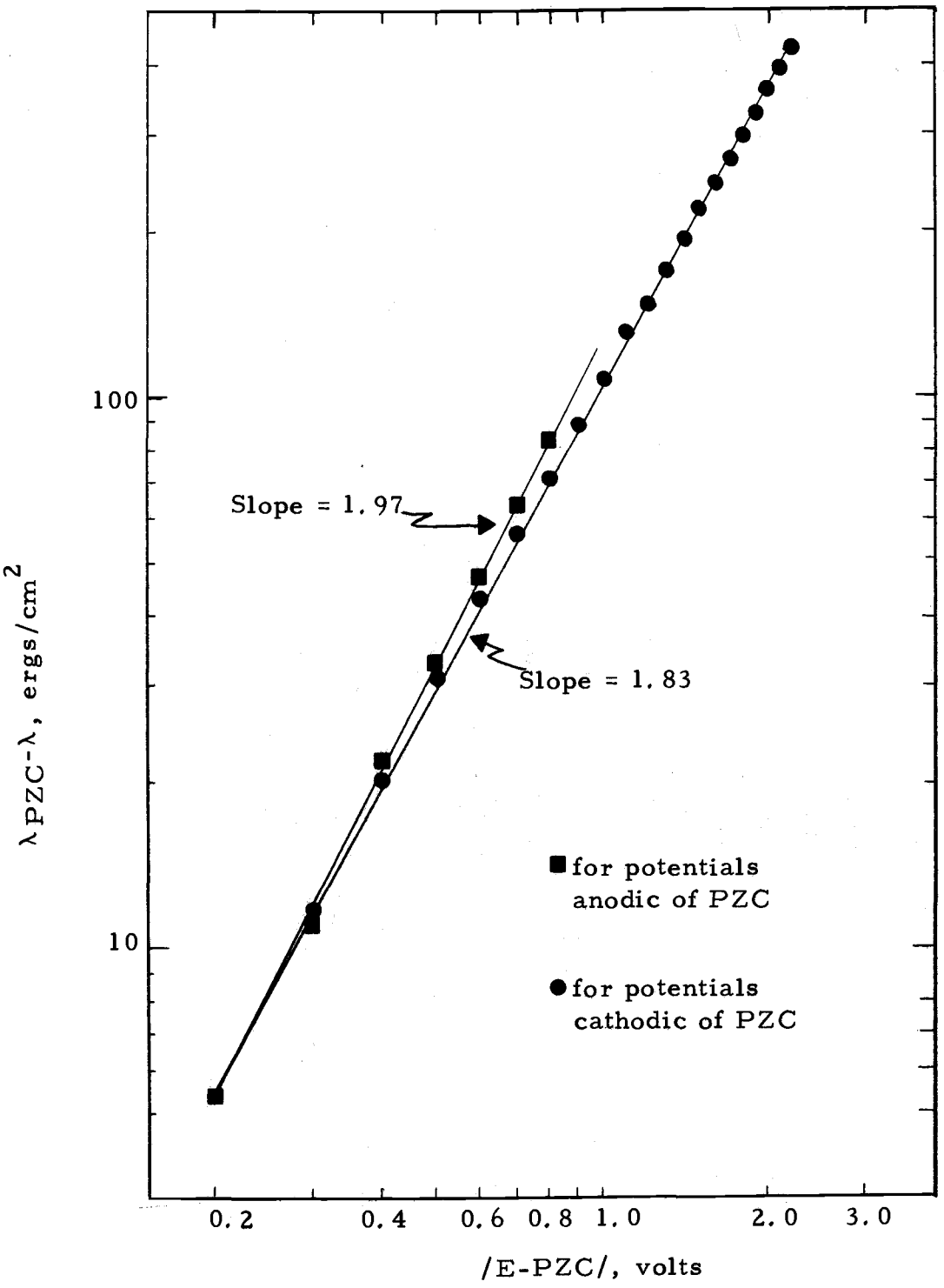

Figure 24. Interfacial tension values between an HMDE and a solution of 0.1 M TEAP in sulfolane as a function of electrode potential.

rather simple model of the double layer upon which Equation (10) is based. The 1.97 and 1.83 slope values also agree very well with the slope values determined from electrocapillary measurements considering the wide potential steps used in the numerical situations.

III. VOLTAMMETRY IN SULFOLANE

A. Experimental

Chemicals and Solutions

Sulfolane and supporting electrolyte, tetraethylammonium perchlorate, were the same materials as used in the double layer capacitance work. Details of solvent purification and electrolyte preparation and purification can be found in the earlier capacitance experimental section. Solutions of the 0.1 M TEAP in sulfolane used in the voltammetric work were also prepared using procedures discussed earlier. Stock solutions of 0.10 M TEAP were always stored in a drybox until used.

The organosulfur compounds used in this voltammetric work were purchased from commercial suppliers and generally used without further purification. N-butyl mercaptan (B.P. 96-98°C) and n-butyl sulfide (B.P. 182-186°C) were purchased from Matheson[1], while n-butyl disulfide (B.P. 110-112°C/13 mm) was obtained from Eastman[2]. Diphenyl disulfide was purchased from Chemicals Procurement Laboratories[3]. The diphenyl disulfide was of practical grade

---

[1]Matheson, Coleman, and Bell, Div. of Matheson Company, Inc., Norward, Ohio.

[2]Eastman Kodak Co., Organic Chemicals Div., Rochester, New York.

[3]Chemical Procurement Laboratories, Inc., College Point, New York.

purity and was recrystallized several times from ethanol until white crystals with a melting point of 61°C were obtained. Stock solutions (0.25 M) of these organosulfur compounds were prepared by dissolving weighed amounts of the materials in 0.10 M TEAP solutions in sulfolane.

Apparatus

The apparatus used in performing the voltammetric experiments in TMS was the same as that used in making double layer capacitance measurements in sulfolane. The same cell as shown in Figure 8 was used in conjunction with the silver reference electrode to obtain voltammograms for the organosulfur compounds and the same microtest electrodes, including the DME, that had been used in the capacitance measurements were also used here.

Instrumentation

All voltammetric experiments were performed with 3-electrode potentiostatic equipment designed to reduce electrode potential control inaccuracies. Some conventional polarographic work was carried out using a Heath[1] Model EUW-401 Polarographic System, while a Chemtrix[2] Model SS-2 Polarographic Analyzer was used for fast scan

[1]Heath Company, Benton Harbor, Michigan.
[2]Chemtrix, Inc., Beaverton, Oregon.

and cyclic voltammetric experiments. Both instruments are similar in design, but differ considerably in implementation of design and construction.

The Heath Polarographic unit consists of three modules assembled so as to function as a versatile, controlled potential instrument. The three modules that comprise the unit are the EUA-19-2 Polarography Module, the EUW-19B Operational Amplifier manifold and the EUA-19-4 Chopper Stabilizer module. Enke and Baxter (32) have discussed the basic Heath 3-electrode polarograph and its operation in some detail and so it will not be discussed here. With this system, initial potentials may be set with an accuracy of $\pm$ 0.5% at any value in the range of $\pm$ 3 v. The potential of the test electrode can be linearly varied over a potential range of $\pm$ 5 v at rates of 0.05 to 2.0 v per minute. The sensitivity of cell current measurements could be varied from 0.5 to 1000 μA per 10 v output signal at the recorder jacks.

A Varian[1] Model F-80A X-Y plotter was used in conjunction with the Heath unit to record polarograms. The X-axis of the recorder was driven by the potential difference between the test and reference electrodes. This signal is available as an output signal from the polarograph. The Y-axis was driven by a voltage signal from the polarograph which is proportional to cell current. This recorder is

[1]Varian Aerograph, Walnut Creek, California.

also equipped with an internal time base so that the plotter can be used as a Y-time recorder. This feature of the recorder was used to measure DME drop times in supporting electrolyte as a function of cell potential for constructing the electrocapillary curve for Hg in TMS. The stated accuracy of the recorder for monitoring voltage signals is 0.3% of full scale, while the accuracy of the internal time base is 3% of the stated range. Slew velocity of the recorder is 17 in/sec for each axis.

The Chemtrix Polarographic Analyzer System consisted of a Tektronix Type 564 Storage Oscilloscope equipped with a Chemtrix Polarographic Amplifier Type 300 and a Type 205 Polarographic Time Base. The polarographic amplifier used with the 564 oscilloscope has a current sensitivity range of 800 to 0.08 μA per full scale deflection with an accuracy of ± 3% of the full scale reading. The Type 205 Polarographic Time Base has potential sweep ranges of 0.5, 1.0 and 2 v with sweep periods ranging between 0.1 to 10 seconds. With these potential ranges and sweep periods, potential scan rates of 0.05 to 20 v per second are available with an accuracy between 5 and 6%. Initial cell potentials can be set with this instrument anywhere between ± 2 v. The Chemtrix instrument is capable of supplying ramp type and triangular or cyclic voltage scans in a single or repetitive fashion. Voltammetric measurements, such as peak currents or peak voltages, can be read directly from the voltammogram stored on the

oscilloscope screen or from a photograph taken of the display. The photographic recording equipment used to record cyclic voltammograms displayed on the oscilloscope was described in the double layer instrumentation section.

Although the Heath and Chemtrix polarographic units were 3-electrode instruments designed to compensate for iR potential drop in voltammetric experiments, a large uncorrected iR drop was observed in this work. Consequently, all potential measurements, such as voltammetric peak potentials, solvent breakdown potentials, etc., had to be corrected for iR drop. The magnitude of the cell ohmic solution resistance, left uncompensated for by the potentiostat, was determined by a method similar to one suggested by Meites (62). For the HMDE voltammetric peak potentials and peak currents were measured for a series of 0.1 M TEAP solutions containing small, but different amounts of dissolved oxygen. A plot of the peak potential as a function of the peak current was linear. The slope of the line in the plot gave the value of the uncompensated resistance of the cell. The uncompensated resistance found for the HMDE was 1.7 KΩ. The values of the uncompensated resistances for the GCME, PTME and AUME were determined from the double layer capacitance experiments via Equation (A27) (see Appendix II). The average values for the uncompensated resistance for each of these electrodes were:

GCME 4.8 KΩ, PTME 5.4 KΩ, and AUME 5.7 KΩ.

Procedure

The cell was operated at 40°C for all voltammetric experiments by circulating water maintained at this temperature through the cell jacket. Cyclic voltammograms were collected for the various organosulfur compounds at various concentrations using different potential scan rates.

The procedure for collecting the voltammograms was as follows. The various cell compartments were thoroughly cleaned by flushing them several times with supporting electrolyte solution. Then approximately 1 ml of mercury was added by eye dropper to the auxiliary electrode compartment. Next, 5 ml of supporting electrolyte solution were delivered to the working electrode compartment by means of a pipette. This volume of solution just covered the fritted discs. The other compartments of the cell were then filled with solution to the same level. The solutions in each compartment were deaerated with pre-pure nitrogen for 10-20 minutes. The nitrogen stream was not presaturated with TMS since evaporative losses of solvent should be small due to the low vapor pressure of the solvent at this temperature. With degassing accomplished, the test electrode and reference electrode assembly were inserted in their chambers. A heavy gauge platinum wire was immersed in the mercury pool and electrical connections to the potentiostat made. Nitrogen was passed

over the top of the solution in the working electrode compartment. Residual curves were collected at various potential scan rates for all of the microelectrodes. Having obtained the residual or background current-potentials curves, an aliquot of a stock solution of an organosulfur compound was added to the working electrode compartment, stirred, and voltammograms recorded using the different microelectrodes. Once all of the scans were made, another aliquot of the organosulfur compound was added and a new series of scans collected. This procedure was carried out for several aliquot additions. The volume of the organosulfur stock solution added to the cell ranged from 10 to 200 μl and was added by means of a microsyringe[1] (accurate to ± 1 μl). Thus for these additions, analyte concentrations in the working electrode compartment could be varied between approximately 0.5 to 10 mM.

Prior to every voltammetric scan carried out with each of the solid microelectrodes, the electrode surface was repolished with a slurry of 600 grit silicon carbide powder in a solution of 0.10 M TEAP in sulfolane. After polishing, the electrode was rinsed with supporting electrolyte, wiped dry and inserted into the working electrode compartment, and a voltammetric scan made. Only with this repolishing treatment could reproducible voltammetric peak potentials

---

[1]Hamilton Company, Inc., Whittier, California.

be obtained with these electrodes.

B. Results and Discussion

Although little voltammetric work has been performed in sulfolane, initial observations (28, 43) indicate that the solvent may have a very wide potential range in which to effect electrochemical reactions. There was interest in this work to measure the potential ranges accessible in TMS for various electrodes and determine whether electrode reactions for some hard to reduce or oxidize organosulfur compounds could be observed. These compounds, particularly mercaptans, sulfides and disulfides, were of interest since they represent a class of organic pollutants for which it is necessary to have new, more sensitive methods for their analysis. It was thought that if electrode reactions involving these compounds could be effected in sulfolane, new electroanalytical techniques could be developed.

Accessible Potential Ranges in TMS

The potential range accessible in a voltammetric experiment is generally determined by decomposition reactions involving solvent, background electrolyte or the test electrode. The electrode potentials at which these decomposition reactions occur with appreciable rates determine the potential range that can be used to observe electrode reactions involving an analyte. The potential ranges available for

various electrodes in sulfolane with 0.1 M TEAP as supporting electrolyte are listed in Table 10. The values were obtained from voltammetric experiments using cathodic and anodic potential scans with a sweep rate of 1 v/sec. The potentials reported are those for which a 20 μA cell current was observed to flow. The value of 20 μA may seem to be a bit arbitrary, and it is, but since the final rise in current is very steep, its actual value is not critical in determining the limiting potential. For the PTME, GCME, and AUME the 20 μA currents correspond to current density values of 2.30, 1.77 and 2.11 mA/cm^2. The nonfaradaic current component of the total 20 μA is small and hence slower voltammetric scan rates should have little effect on the limiting potentials. For example, the charging currents estimated for the GCME at the limiting potentials of + 1.3 and - 3.3 v are only 0.6 and 0.8 μA, respectively. The potential range for mercury listed in Table 10 is actually larger than that stated. Owing to drop detachment, -3 v was the most cathodic potential that could be reached with the HMDE. Polarographic experiments with a dropping mercury electrode, however, indicate that potentials as negative as -3.3 to -3.4 v are accessible with mercury electrodes.

Table 10. Accessible potential range in sulfolane with 0.1 M TEAP.

Test Electrode	Potential Range (v vs. AgRE)
HMDE	+ 0.1 < -3 (-3.3)
PTME	+ 1.6 to -3.0
GCME	+ 1.3 to -3.3
AUME	+ 1.2 to -3.2

The large overall 3.4 and 4.6 v potential ranges measured for mercury and platinum agree with those determined by Desbarres et al. (23) in TMS under similar experimental conditions and compare generally with those reported (59) for acetonitrile and dimthylformamide. The potentail ranges determined for the glassy carbon and gold electrodes in TMS are similar and close to the 4.5 v value for platinum.

The nature of the cathodic and anodic limiting reactions were not investigated, but one can speculate about them. The cathodic limiting potentials for all of the electrodes are nearly equal, possibly indicating a similar decomposition reaction for each electrode. Possible limiting reactions for the system include reduction of the tetraethylammonium cation, the perchlorate anion, or reduction of TMS. There has been no report of a direct reduction of perchlorate ion in a nonaqueous solvent, thus leaving the other two named reactions more likely. Of these, a reasonable reaction involving the tetraethylammonium ion would be:

$$(C_2H_5)_4\,N^+ + e^- \longrightarrow (C_2H_5)_3\,\dot{N} + H\text{-}\underset{H\ H}{\overset{H\ H}{C\text{-}C}}\cdot$$

However, no triethylamine odor could be detected in the cell after an hour or so of electrolysis was carried out using the PTME at a current density of 5 mA/cm^2. If the limiting reaction did involve reduction of the tetraalkylammonium ion to triethylamine, electrolysis

under these conditions would lead to a concentration of the amine in the cell of around 10^{-4} M, which should be detectable. This seems to point to the reduction of TMS as the reaction responsible for the limiting cathodic potential. Sulfones are electrochemically reducible in other solvents (60). The reaction involves breaking the carbon-sulfur bond and the formation of sulfinates. In the case of TMS, reduction would lead to the formation of butane sulfinate. Butane sulfinate has been observed to be the product of the reaction between sodium metal and sulfolane (83).

The anodic limiting potentials vary more. In the case of mercury, the anodic limiting reaction is probably the oxidation of the electrode. This may also be the case for the gold and platinum electrodes; these materials being more noble than mercury, the oxidation reaction simply occurs at more anodic potentials. Another possibility for the anodic limiting reaction in TMS is the oxidation of the perchlorate ion to the neutral free radical:

$$ClO_4^- \longrightarrow ClO_4^{\cdot} + e^-$$

This reaction has been proposed as the anodic limiting one in acetonitrile, with subsequent reaction with the solvent to form other products.

Voltammetric Waves for Organosulfur Compounds

Voltammetric scans were made on a number of solutions containing n-butyl mercaptan, n-butyl sulfide and n-butyl disulfide to determine whether the potential range accessible in sulfolane was large enough to effect any analytically useful electrode reactions involving these compounds. These compounds have been reported (60) to be difficult to oxidize or reduce in other solvents and would thus serve as model compounds to test the useful potential range available in TMS.

It was found that voltammetric waves could be observed for all of the butyl sulfur compounds in sulfolane. Electrooxidation reactions for the mercaptan and sulfide could be effected on the microelectrodes of gold, glassy carbon and platinum and electroreduction reactions for butyl disulfide could be observed on the same electrodes. Cyclic voltammograms obtained for n-butyl mercaptan and n-butyl sulfide showed only one anodic wave and displayed no cathodic peaks on reverse scan. Cyclic voltammograms observed for n-butyl disulfide showed only one cathodic wave and no anodic peak on reverse scan. This behavior of showing either a cathodic or an anodic wave on the forward scan and no wave on the reverse scan indicates that the electrode reaction responsible for the voltammetric wave on the forward scan is not reversible. These observations about the

irreversibility of the electrode reactions involving butyl mercaptan, sulfide and disulfide agree with those of Mann (60) for the electrode reactions in acetonitrile. Aliphatic mercaptans in this solvent have been shown to undergo oxidation to the disulfide. The suggested reaction scheme is outlined in Equations (23) and (24) with the aliphatic mercaptan represented by RSH and the disulfide by RSSR.

$$RSH \longrightarrow RS\cdot + H^+ + e^- \qquad (23)$$

$$2\ RS\cdot \longrightarrow RSSR \qquad (24)$$

If this reaction scheme applies in TMS, the product of the oxidation of butyl mercaptan should be butyl disulfide. Electrooxidation of butyl sulfide in TMS may involve the formation of a sulfonium ion, as it apparently does in acetonitrile.

As mentioned above voltammetric reduction waves could be observed on the gold, platinum and glassy carbon microelectrodes, but not on the HMDE. It is felt that the disulfide can be reduced on mercury, but that it occurs very near solvent decomposition. These potentials could not be reached with the HMDE owing to drop detachment. Attempts to observe a conventional DC polarographic wave with a DME for the disulfide, also failed because of irregular behavior of the capillary electrode. At extreme negative potentials, and in the presence of the disulfide, extremely short drop times were noted. In fact, the dropping mercury electrode was more of a streaming

electrode and had a high background noise current due to double layer charging.

Cyclic voltammetric scans were also made on solutions of phenyl disulfide and reduction waves were observed using the HMDE and AUME, but no waves were observed on the GCME and PTME. Cyclic voltammograms obtained for phenyl disulfide on mercury showed one cathodic wave and displayed an anodic wave on the reverse scan corresponding to the reoxidation of the product formed on the forward or cathodic scan. The separation in the cathodic and anodic peak potentials for the waves is consistent with a reversible two electron transfer reaction that probably involves the cleavage of the sulfur-sulfur bond. Cyclic voltammograms obtained for phenyl disulfide using the AUME showed only a cathodic wave on the forward and no anodic wave on the reverse sweep, indicating an irreversible reduction taking place on this electrode.

Shown in Figures 25a-25k are some representative cyclic voltammograms obtained for n-butyl mercaptan, -sulfide, -disulfide, and phenyl disulfide using various electrodes. Voltammetric data for these waves are given in Table 11. The general qualitative shape of the voltammetric waves did not change significantly over the narrow scan rate and concentration ranges used in these experiments. There was some initial trouble encountered in obtaining reproducible peak potentials for these waves, as well as for waves obtained at other

Figure 25. Cyclic voltammograms obtained for some organosulfur compounds using various electrodes.

(A) n-butyl mercaptan, initial anodic scan 0 to +2v, using AUME, 20 μA/major vertical division.

(B) n-butyl mercaptan, initial anodic scan 0 to +2v, using GCME, 50 μA/major vertical division.

(C) n-butyl mercaptan, initial anodic scan 0 to +2v, using PTME, 20 μA/major vertical division.

(D) n-butyl sulfide, initial anodic scan -0.50 to +1.5 v using AUME, 10 μA/major vertical division.

(E) n-butyl sulfide, initial anodic scan +0.30 to +1.30 v using GCME, 10 μA/major vertical division.

(F) n-butyl sulfide, initial anodic scan -0.55 to +1.45 v using PTME, 10 μA/major vertical division.

(G) n-butyl disulfide, initial cathodic scan -2 to -4 v using AUME, 20 μA/major vertical division.

(H) n-butyl disulfide, initial cathodic scan -2 to -4 v using GCME, 20 μA/major vertical division.

(I) n-butyl disulfide, initial cathodic scan -2 to -4 v using PTME, 20 μA/major vertical division.

(J) Phenyl disulfide, initial cathodic scan -1.4 to +3.4 v using AUME, 10 μA/major vertical division.

(K) Phenyl disulfide, initial cathodic scan -1 to -2 using HMDE, 20 μA/major vertical division.

(L) Dissolved oxygen, initial cathodic scan -0.7 to -2.7 v using HMDE, 2 μA/major vertical division.

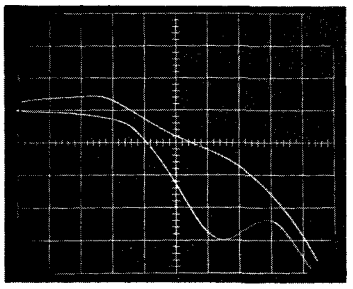

A

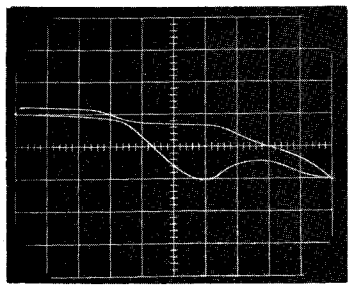

B

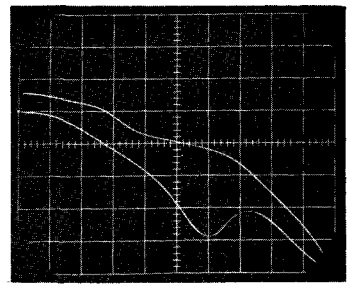

C

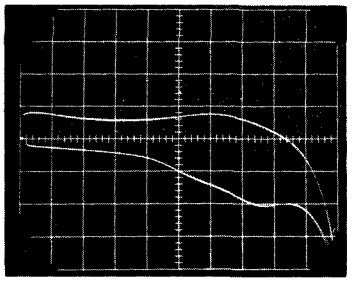

D

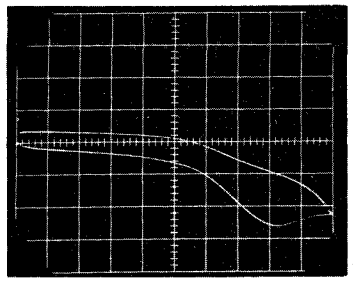

E

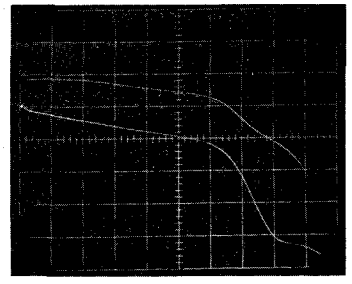

F

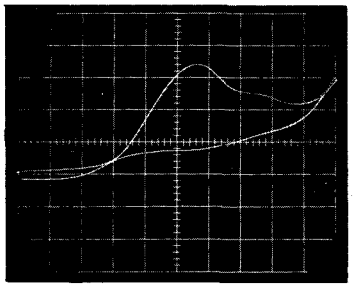

G

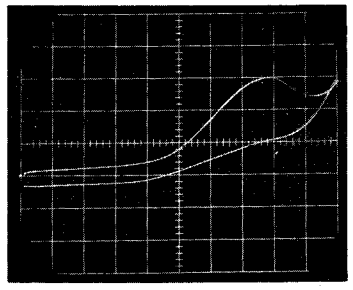

H

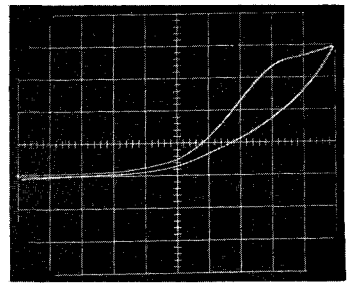

I

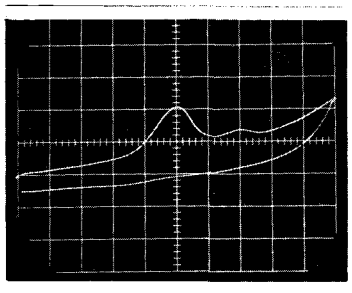

J

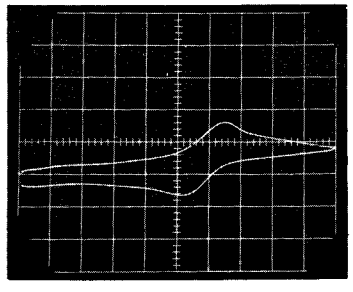

K

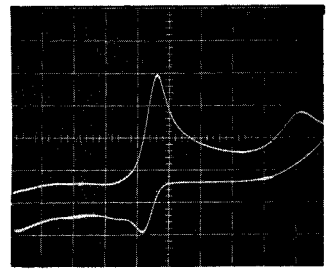

L

concentrations and different scan rates. It was found, however, that by simply repolishing the electrodes prior to each voltammetric scan, peak potential measurements could be reproduced to around 50 mv from run to run as well as from day to day. Cathodic and anodic peak potentials observed for phenyl disulfide and oxygen using the HMDE were more reproducible. For successive scans made on the same mercury drop, peak potentials were generally reproducible to about 10 to 20 mv and agreed with results obtained on other days using different drops. The better precision in peak potentials obtained using the HMDE may in part be due to a better signal-to-noise ratio for measurements with this electrode. In obtaining peak potentials from experimental voltammograms, the current-potential curves have to be corrected for background or noise currents arising from the electrolysis of residual impurities, solvent, and double layer charging. It was observed that waves obtained with the HMDE had smaller background current corrections than did waves obtained with the solid electrodes. This is consistent with the results from the double layer capacitance experiments which indicate that the mercury electrode should have a lower capacitive to faradaic current ratio than the other electrodes and that the HMDE had a smaller γ current density than the solid electrodes.

Table 11. Cyclic voltammetric data for some organosulfur compounds.

Compounds[a]	HMDE Peak Potential[c]	GCME Peak Potential[c]	PTME Peak Potential[c]	AUME Peak Potential[c]
Oxygen	-1.61, -2.5 -1.58[b]			
n-Butyl mercaptan		+0.71[b]	+0.78[b]	+0.84[b]
n-Butyl sulfide		+0.98[b]	+0.87[b]	+0.94[b]
n-Butyl disulfide		-3.2	-3.3	-2.7
diphenyl disulfide	-1.64 -1.61[b]			-2.3

[a]Voltammetry at various electrodes for 1 v/sec sweep rate, reactant concentration 1-10 mM in 0.1 M TEAP sulfolane;

[b]Oxidation peaks, all those unmarked are reduction peaks.

[c]Volts vs. AgRE

Voltammetric peak currents observed for the reactions at the various electrodes did tend generally to increase with increasing analyte concentrations. Peak currents, though, were too irreproducible to determine whether a satisfactory linear relationship existed between concentration and peak current. For successive scans carried out on the same solution, peak currents would vary by as much as 20%. The fluctuation in peak currents was believed to be due to changes in electrode area as a result of repolishing since peak currents measured for the reduction of diphenyl disulfide at the HMDE were reproducible to within a few percent. A plot of peak current versus concentration for this reduction wave was not found to be linear over the entire concentration of 0.5 mM to 20 mM. At low

concentrations and consequently low peak currents, peak current appeared to be a linear function of concentration. At higher concentrations there was a negative deviation from the extrapolated line obtained at lower concentrations. This effect was probably due to a non-linear scan rate created by the large uncompensated resistance of the cell.

IV. SUMMARY

A new pulse method for measuring differential double layer capacitances has been developed in this work. The method, while similar in principle to an existing pulse technique, is implemented experimentally in a different manner, that permits double layer capacitances to be determined without having to measure the cell's solution resistance in a separate experiment.

The technique is based on the determination of the cell time constant which, for an ideally polarized test electrode-solution interface, is composed of the double layer capacitance and solution resistance. By applying small step voltage changes to a cell, an exponentially decaying current due to the charging of the double layer is observed. A plot of the logarithm of current against time is linear with a slope whose magnitude is equal to the reciprocal of the cell's time constant, the product of the double layer capacitance and solution resistance. Extrapolation of the line obtained in the semilog plot back to the moment that the pulse was applied yields a value for the intercept. The intercept is the logarithm of a current which is related by means of Ohm's law to the pulse voltage and solution resistance. The slope and intercept values of the semilog plot can be combined with the value of the step voltage to calculate the double layer capacitance by a simple equation. The method of least squares can be used to

determine the best slope and intercept values for a set of current-time measurements.

An analysis of the propagation of errors was made for the experiment. It revealed that there is a region along the decay curve in which current measurements should be made in order to obtain the best relative precision in the capacitance value. This portion of the current decay curve corresponds approximately to a region in which the charging current has decayed to around 50 to 25% of its peak value.

The pulse capacitance technique was implemented using a three-electrode potentiostat built with integrated circuit operational amplifiers. The instrumentation and technique were tested on cell circuit RC analogs to determine the accuracy with which capacitance could be measured and the limitations of the equipment. A computer program was written to facilitate data handling. It incorporated a least squares routine for obtaining the best slope and intercept values for the semi-log plot of current versus time data. The program calculated capacitance values as well as the estimated precision in the capacitance. It was found that the accuracy of the capacitance measurements was within the precision of the measurements themselves, which was around $\pm$ 3%. The method was next tested using a real cell. Double layer capacitance measurements were made for a Hg-1.0 M KCl interface. The values determined were compared with ones reported in the literature and found to agree within experimental error.

After the successful testing of the pulse technique on the Hg-aqueous KCl interface, the method was used to determine the double layer capacitance-potential curves for interfaces formed between electrodes of various materials and solutions of 0.10 M tetraethylammonium perchlorate in sulfolane. It was observed that the simple RC model of the double layer was not applicable for these interfaces. A more complex model for the double layer was assumed which allowed for a faradaic current to follow due to the voltage pulse, i.e., that the test electrode-solution interfaces were not ideally polarized. A method was found for estimating the faradaic current due to the pulse and used to correct the current measurements. A new equation was derived for calculating capacitances using the slope and intercept values of the semilog plot of the corrected current versus time measurements.

Some of the advantages of the capacitance technique over the AC bridge technique are that the method is applicable to solutions of both high and low conductivities and that correction in the capacitance determination can be made for a non-ideally polarized interface. The technique can be implemented using instrumentation commonly used for fast scan voltammetry, thus not requiring a special instrument useful only for double layer capacitances. The experiment could also be easily interfaced with a small digital laboratory computer for automated measurements. Two advantages that this method has over the

time constant technique proposed by Delahay are that no separate measurements of the solution resistance and no differential voltage measurements involving two test electrode-solution interfaces are required. A disadvantage of the pulse technique proposed here is that much data handling is involved, making a computer almost a necessity.

Except for a capacity hump anodic of the potential of zero charge, the capacitance-potential curve for mercury is similar in shape to those obtained for the electrode in nonaqueous solvents. The value of the capacity maximum is about 30 $\mu f/cm^2$. The capacity-potential curve was integrated by numerical summation to give the surface charge density and interfacial tension relative to the maximum value as a function of electrode potential. The parabolic relationship between interfacial tension and electrode potential was checked and found to agree closely with results obtained from polarographic drop time measurements. Capacitance-potential curves were measured for gold, glassy carbon, and platinum. The double layer capacitances for these electrodes were usually higher than for mercury and had larger faradaic current corrections.

The voltammetric potential ranges accessible in sulfolane with tetraethylammonium perchlorate supporting electrolyte are very large. The range available with mercury is +0.1 to -3.3 v, while for gold, glassy carbon, and platinum the ranges are +1.2 to -3.2, +1.3 to -3.3 and +1.6 to -3.0 v as measured with respect to a silver-silver ion

reference electrode in the solvent.

Voltammetric waves were observed for n-butyl mercaptan, -sulfide, -disulfide and phenyl disulfide. The substances gave reasonably well-defined peaks with characteristic peak potentials. Anodic waves were observed for the mercaptan and sulfide on gold, glassy carbon and platinum electrodes. Cathodic waves were observed for butyl disulfide. All electrode reactions involving the aliphatic sulfur compounds appeared irreversible. Phenyl disulfide could be reversibly reduced on mercury.

BIBLIOGRAPHY

1. Alder, J. F. Evaluation of a range of electrode materials for solid electrode voltammetry. Journal of Electroanalytical Chemistry and Interfacial Electrochemistry 30:427. 1971.

2. Arnett, E. M. and C. F. Douty. Solvent effects in organic chemistry. II. Sulfolane--a weakly basic aprotic solvent of high dielectric constant. Journal of the American Chemical Society 86:409-412. 1964.

3. Benoit, R. L., A. L. Beauchamp, and M. Deneux. Equilibria between silver, chloride and bromide ions in sulfolane. Journal of Physical Chemistry 73:3268-3273. 1969.

4. Benoit, R. L., M. Guay, and J. Desbarres. Reactions in sulfolane. Part II. Electrochemical oxidation-reductions of halogens. Canadian Journal of Chemistry 46:1261-1266. 1968.

5. Benoit, R. L. and G. Choux. Reactions in sulfolane. Part III. Water-sulfolane interactions. Canadian Journal of Chemistry 46:3215-3219. 1968.

6. Bordwell, F. G. and W. H. McKellin. The reduction of sulfones to sulfides. Journal of the American Chemical Society 73:2251-2253. 1951.

7. Bordwell, F. G., R. H. Ives, and E. C. Steiner. Acidities of sulfones. Journal of the American Chemical Society 89:3905-3906. 1967.

8. Born, M. Volumen und Hydratationswarme der Ionen. Zeitschrift fur Physik 1, 45 (1920).

9. Brown, V. K., L. W. Ferrigon, and D. E. Stevenson. Acute toxicity and skin-irritant properties of sulfolane. British Journal of Industrial Medicine 23:302-306. 1966.

10. Burwell, R. L. and C. H. Langford. Solvent characteristics of tetramethylene sulfone. Journal of the American Chemical Society 81:3799-3800. 1959.

11. Butler, J. N. Solubility and complex formation equilibria of silver chloride in propylene carbonate. Analytical Chemistry 39, 1799 (1967).

12. _____ Ionic equilibrium. Addison-Wesley Inc., Reading, Mass. 1964. pp. 281-283.

13. Chapman, D. L. A contribution to the theory of electrocapillarity. Philosophical Magazine 25:475-481. 1913.

14. Coetzee, J. F. and R. J. Bertozzi. A recommended titrant: Anhydrous perchloric acid in sulfolane. Analytical Chemistry 41:860-862. 1969.

15. Coetzee, J. F., J. M. Simon, and R. J. Bertozzi. Polarography in sulfolane and reference of potentials in sulfolane and other nonaqueous solvents to water scale. Analytical Chemistry 41:766-772. 1969.

16. Conway, B. E. Theory and principles of electrode processes. New York, Ronald Press, 1965. pp. 25-169.

17. Criss, C. M. and E. Luksha. Thermodynamic properties of non aqueous solutions. IV. Journal of Physical Chemistry 72, 2966 (1968).

18. Cumper, C. N. and A. I. Vogel. Physical properties and chemical constitution. Part XXVII. Dipole moments of some cyclic ethers, sulfides, sulfoxides, and sulfones. Journal of the Chemical Society 3521-3526. 1959.

19. Davis, D. S. Nomography and empirical equations. New York, Reinhold, 1962. pp. 19-20.

20. Day, M. C. and J. Selbin. Theoretical inorganic chemistry, 2nd edition. New York, Reinhold Publishing Co., 1969. pp. 533-540.

21. Deal, C. H., H. Evans, E. Oliver, and M. Papadopoulos. A better way to extract aromatics. Petroleum Refiner 38(9):185-192. 1959.

22. Delahay, P. Double layer and electrode kinetics. New York, Interscience, 1966. pp. 1-149.

23. Delahay, P., R. DeLevie, and A. M. Guiliani. Experimental study of the electrical double layer in very dilute aqueous solutions. Electrochimica Acta 11:1141-1146. 1966.

24. Della Monica, M., U. Lamanna, and L. Jannelli. Chemical properties of sulfolane. Gazzetta Chemica Italiana 97:367-370. 1967.

25. Della Monica, M. and U. Lamanna. Solvation numbers of some ions in sulfolane by conductance measurements. Journal of Physical Chemistry 72:4329-4331. 1968.

26. Della Monica, M., U. Lamanna, and L. Senatore. Silver complexes with I^-, Br^-, and SCN^- in sulfolane. Inorganica Chimica Acta 2:363-366. 1968.

27. _____ Transport numbers and ionic conductances in sulfolane at 30°C. Journal of Physical Chemistry 72:2124-2126. 1968.

28. Desbarres, J., P. Pichet, and R. L. Benoit. Reactions in sulfolane. Part I. Preliminary electrochemistry. Electrochimica Acta 13:1899-1904. 1968.

29. Devanathan, M. A. V. Theory of the electrical double layer and the interpretation of differential capacity curves. Transactions of the Faraday Society 50:373-385. 1954.

30. Drago, R. S. and K. F. Purcell. Coordinating solvents. In: Nonaqueous solvent systems, edited by T. C. Waddington. New York, Academic Press, 1965. p. 246.

31. Dunn, C. L. et al. Sulfinol process bids for acid-gas removal jobs. Oil and Gas Journal 62:95-99. 1964.

32. Enke, G. G. and R. A. Baxter. A versatile and inexpensive controlled-potential polarographic analyzer. Journal of Chemical Education 4:202-209. 1964.

33. Fernandez-Prini, R. and J. E. Prue. Conductance measurements on solutions of salts in sulfolane and their interpretation. Transactions of the Faraday Society 62:1257-1264. 1966.

34. Filippova, Z. Toxicity of sulfolane and sulfolene. Khimiya Seraoganicheskikh Soedinenii Soderzhashchikhsya v Neftyakh i Nefteproduktakh 8:701-705. 1968.

35. Garnsey, R. and J. E. Prue. Precise cryoscopic determination of osmotic coefficients for solutions of some alkali salts in dimethylsulfoxide and in sulfolane. Transactions of the Faraday Society 64:1206-1218. 1968.

36. Gouy, G. Constitution of the electric charge at the surface of an electrolyte. Journal de Physique 9:457-467. 1910.

37. Grahame, D. C. The electrical double layer and the theory of electrocapillarity. Chemical Reviews 41:441-501. 1947.

38. _____ Properties of the electrical double layer at a mercury surface. Part I. Methods of measurement and interpretation of results. Journal of the American Chemical Society 63:1207-1215. 1941.

39. _____ Measurement of the capacity of the electrical double layer at a mercury electrode. Journal of the American Chemical Society 71:2975-2978. 1949.

40. Grischkevich-Trokhimovski, E. Sulfides with a five-membered nucleus. Journal of the Russian Physical-Chemical Society 48:901-928. 1916.

41. Hall, S. K. and E. A. Robinson. The sulfuric acid solvent system. Part VI. The basicities of compounds containing sulfur-oxygen bonds. Canadian Journal of Chemistry 42:1113-1122. 1964.

42. Hanley, J. L. and R. T. Iwamoto. Electrochemical study of copper ions in a series of sulfone solvents. Journal of Electroanalytical Chemistry and Interfacial Electrochemistry 24:271-277. 1970.

43. Headridge, J. B., D. Pletcher, and M. Callingham. Polarography of inorganic substances in anhydrous sulpholan. Journal of the Chemical Society A:684-685. 1967.

44. Heyrovsky, J. and J. Kuta. Principles of polarography. New York, Academic Press, 1966. pp. 17-19.

45. Jannelli, L., M. Della Monica, and A. Della Monica. Proprieta chimico fisiche del solfolano. Gazzetta Chemica Italiana 94:552-577. 1964.

46. Jeffery, G. H., R. Parker, and A. I. Vogel. Physical properties and chemical constitution. Part XXXII. Thiophen compounds. Journal of the Chemical Society 570-575. 1961.

47. Johnson, D. A. Some thermodynamic aspects of inorganic chemistry. London, Cambridge University Press, 1968. pp. 97-114.

48. Jones, J. G. Contrasting behavior of boron trifluoride and phosphorus pentafluoride toward sulfolane. Inorganic Chemistry 5:1229-1232. 1966.

49. Jordon, T. E. and F. Kipnis. Solubility characteristics of sulfones. Industrial and Engineering Chemistry 41:2635-2637. 1949.

50. Kelley, M., H. Jones, and D. Fisher. Controlled-potential and derivative polarograph. Analytical Chemistry 31:1475-1485. 1959.

51. Kolthoff, I. M. and T. B. Reddy. Polarography and voltammetry in dimethylsulfoxide. Journal of the Electrochemical Society 108, 980 (1961).

52. Laitinen, H. A. Chemical analyses. New York, McGraw-Hill, 1960. pp. 544-545.

53. Lamanna, U. and M. Della Monica. Transport numbers and ionic conductivity in sulfolane at 30°C. Corsi e Seminari di Chimica 13:37-38. 1968.

54. Lange, N. A. Handbook of chemistry, 10th ed. New York, McGraw-Hill, 1967. p. 1200.

55. Langford, C. H. and P. O. Langford. Sulfone ligands in cobalt (II) complexes. Inorganic Chemistry 1:184-185. 1962.

56. Lawrence, J. and R. Parson. Specific adsorption at the mercury/sulfolane interface. Transactions of the Faraday Society 64:751-770. 1968.

57. _____ Adsorption isotherms in mixed solvent systems. Journal of Physical Chemistry 73:3577-3581. 1969.

58. MacInnes, D. A. The principles of electrochemistry. New York, Dover, 1961. p. 233.

59. Mann, C. K. Nonaqueous solvents for electrochemical use. In: A. J. Bard (ed.), Electroanalytical chemistry, Vol. 3. New York, Dekker, 1969. pp. 117-134.

60. Mann, C. K. and K. K. Barnes. Electrochemical reactions in nonaqueous systems. New York, Marcel Dekker, 1970. pp. 381-402.

61. Martinmaa, J. Studies on sulfolane. Part I. Sulfolane as solvent in polarography, electrochemical reductions, and ESR spectroscopy. Suomen Kemistilehti B42:33-36. 1969.

62. Meites, L. Polarographic techniques. 2nd ed. New York, Interscience, 1965. p. 70.

63. Mitchell, J. and D. M. Smith. Aquametry. New York, Interscience, 1948. pp. 65-78.

64. Mohilner, D. M. The electrical double layer. In: A. J. Bard (ed.). Electroanalytical chemistry, Vol. 1, New York, Dekker, 1966. pp. 241-409.

65. Moore, R. J. and R. A. Trimble. Tetrahydrothiophene. U.S. Patent 2,471,077. May, 1949. (Abstracted in Chemical Abstracts 43:7512. 1949.)

66. Morman, D. H. and G. A. Harlow. Sulfolanes as solvents for potentiometric titrations. Analytical Chemistry 39:1869-1872. 1967.

67. Morrow, G. S. Sulfolane. Kirk-Othmer encyclopedia of chemical technology, 2nd ed., New York Interscience Publishers 19:250-254. 1969.

68. Nicholson, R. S. Theory of stationary electrode polarography: single scan and cyclic methods applied to reversible, irreversible, and kinetic systems. Doctoral dissertation. Madison, University of Wisconsin, 1964. 162 numb. leaves.

69. Noda, T., M. Inagaki, and S. Yamada. Glass-like carbons. Journal of Non-Crystalline Solids 1:285-302. 1969.

70. Padova, J. Nonaqueous electrolyte solutions. In: Water and aqueous solutions. Edited by R. A. Horne. New York, Wiley-Interscience, 1972. pp. 113-117.

71. Parker, A. J. and R. Alexander. Solvation of ions, XIII. Journal of the American Chemical Society 90:3313. 1968.

72. Payne, R. The electrical double layer in nonaqueous solutions. In: P. Delahay and C. Tobias (ed.), Advances in electrochemistry and electrochemical engineering. New York, Wiley, 1970. pp. 1-76.

73. Perkins, R. S. and T. N. Anderson. Potentials of zero charge. In: J. Bockris and B. E. Conway (ed.), Modern aspects of electrochemistry, Vol. 5. New York, Plenum, 1969. pp. 203-279.

74. Petcoff, D. Stationary electrode voltammetry and chronoamperometry in an alkali metal carbonate-borate melt. Doctoral dissertation. Corvallis, Oregon State University, 1970. 255 numb. leaves.

75. Roberts, J. J. and G. P. Warwick. Formation of 3-hydroxytetrathiophene 1,1-dioxide from myleron, S-(β-L-alanyl) tetrahydrothiophenium mesylate, tetrahydrothiophene and tetrahydrothiophene 1,1-dioxide in the rat, rabbit and mouse. Biochemical Pharmacology 6:205-208. 1961.

76. Shell Chemical Company, New York. Technical Bulletin (Sulfolane) IC:68-71, 1968. 15 p.

77. Simon, J. M. Polarography and medium effects in sulfolane. Doctoral dissertation. Pittsburgh, University of Pittsburgh, 1969. 162 numb. leaves.

78. Stern, O. The theory of the electrolytic double-layer. Zeitschrift fur Elektrochemie 30:508-516. 1924.

79. Tommila, E., E. Lindell, M. Virtalaine, and R. Laakso. Densities, viscosities, surface tensions, dielectric constants, vapour pressures, activities, and heats of mixing of sulfolane-water, sulfolane-methanol, and sulfolane-ethanol mixtures. Suomen Kemistilehti 42:95-104. 1969.

80. U.S. National Bureau of Standards Circular 500, U.S. Government Printing Office, Washington, D.C. 1952.

81. Vaughn, J. W. and C. F. Hawkins. Physical properties of tetrahydrothiophene-1,1-dioxide and 3-methyltetrahydrothiophene-1,1-dioxide. Journal of Chemical and Engineering Data 9:140-142. 1964.

82. Warden, B. E. The electrochemical oxidation of aqueous, sulfur dioxide solutions at a glassy carbon electrode. Master's thesis, Corvallis, Oregon State University, 1973. 74 numb. leaves.

83. Wellisch, E., E. Gipstein, and O. J. Sweeting. Cleavage and dimerization of sulfolane. Journal of Polymer Science 2:39-42. 1964.

84. Wisniak, J., C. Eicholz, and A. Fertilio. Solubility of fatty acids and their methyl esters in furfural and commercial grade sulfolane. British Chemical Engineering 15, 76 (1970).

85. Yamada, S. and H. Sato. Some physical properties of glassy carbon. Nature 193:261-262. 1962.

86. Young, H. D. Statistical treatment of experimental data. New York, McGraw-Hill, 1962. pp. 96-132.

87. Zittel, H. E. and F. J. Miller. A glassy carbon electrode for voltammetry. Analytical Chemistry 37: 200-203. 1965.

APPENDICES

```
      PROGRAM STAT
C     THIS PROGRAM CALCULATES DOUBLE LAYER CAPACITANCES FROM LEAST
C      SQUARE PARAMETERS OBTAINED FROM SEMILOG PLOT OF CHARGING CURRENT
C      VERSUS TIME.
      DIMENSION Y(20)
      DIMENSION  GAM(200), BP(200), SBP(200), RERSIM(200)
      DIMENSION RSBP(200),XMP(200), SMP(200), RSMP(200)
      DIMENSION RX(1000),RY(1000),RXY(1000)
  995 FORMAT(' ','**************************************************
     1***************'/)
  998 FORMAT('    RX(',I3,') = ',E10.3,'   RY(',I3,') = ',E10.3,'   RXY(
     1',I3,') = ',E10.3)
  999 FORMAT(//,
     1'     SUMRX  =  ',E10.3,'   SUMRY  =  ',E10.3,'   SUMRXY  = ',E10.3
     1       ,/,'     XBAR   =  ',E10.3,'   YBAR   =  ',E10.3,'   XYBAR
     1 = ',E10.3,/,'     STDEVX =  ',E10.3,'   STDEVY =  ',E10.3,'   STDE
     1VXY = ',E10.3,/,'     RSTDVX =  ',E10.3,'   RSTDVY =  ',E10.3,'   R
     1STDVXY = ',E10.3,/,'     SSDX   =  ',E10.3,'   SSDY   =  ',E10.3,
     1'   SSDPXY  = ',E10.3,/,                                          '
     1  SUMSX  =  ',E10.3,'   SUMSY  =  ',E10.3,'   SUMSPXY = ',E10.3,/,
     1'     POINTS =  ',E10.3,'   SSRES  =  ',E10.3,/,'     LSQSLOPE  ',E1
     10.3,'   LSQYCEPT  ',E10.3,/,'     STDB   =  ',E10.3,'   STDA   =  '
     1,E10.3,/,'     BCONFACT  ',E10.3,'   ACONFACT  ',E10.3,/,'     CORLC
     10E = ',E10.4,/)
      NN = 0
 1006 CONTINUE
      MM=1
      G4 = FFIN(60)
      GO TO (1009,1008),EOFCKF(60)
 1008 RX(MM)=FFIN(60)
      GO TO(1009,1007),EOFCKF(60)
 1007 CONTINUE
      RY(MM) = FFIN(60)
      GO TO (1009,1010),EOFCKF(60)
 1010 RX(MM) = RX(MM)*.000001
      Y(MM) = RY(MM)*1.E-6
      MM=MM+1
      GO TO 1008
 1009 CONTINUE
      LLMAX=MM-1
      IF(LLMAX-2)99,996,996
  996 CONTINUE
      G4 = G4*1.E-06
      DO 3 IG = 1,LLMAX
    3 RY(IG) = ALOG(Y(IG) - G4)
      NN = NN + 1
      GAM(NN) = G4
      XLMAX = LLMAX
      SSX = 0.
      SSY = 0.
      SSDY = 0.
      SSDX = 0.
      SUMRY = 0.
      SUMRX = 0.
      SSPXY = 0.
      SSDPXY = 0.
      SUMRXY = 0.
      DO 1003  MM=1,LLMAX
      SUMRX=SUMRX+RX(MM)
      SUMRY=SUMRY+RY(MM)
      RXY(MM) = RX(MM)*RY(MM)
      SUMRXY = SUMRXY + RXY(MM)
      WRITE(61,998)MM,RX(MM),MM,RY(MM),MM,RXY(MM)
 1003 CONTINUE
```

```
      XBAR=SUMRX/XLMAX
      YBAR=SUMRY/XLMAX
      XYBAR=SUMRXY/XLMAX
      DO 1004 MM=1,LLMAX
      SSDX=SSDX+(RX(MM)-XBAR)*(RX(MM)-XBAR)
      SSDY=SSDY+(RY(MM)-YBAR)*(RY(MM)-YBAR)
      SSDPXY = SSDPXY + (RXY(MM)-XYBAR)*(RXY(MM)-XYBAR)
      SSX=SSX+RX(MM)*RX(MM)
      SSY=SSY+RY(MM)*RY(MM)
      SSPXY=RX(MM)*RY(MM)*RX(MM)*RY(MM)+SSPXY
 1004 CONTINUE
      STDEVX=SQRT(SSDX/(XLMAX-1.))
      STDEVY=SQRT(SSDY/(XLMAX-1.))
      STDEVXY = SQRT(SSDPXY/(XLMAX-1.))
      RSTDVX = STDEVX*100./XBAR
      RSTDVY = STDEVY*100./YBAR
      RSTDVXY = STDEVXY*100./XYBAR
      B=(SUMRXY-XLMAX*XBAR*YBAR)/(SSX-XLMAX*XBAR*XBAR)
      CORLCOE = B*STDEVX/STDEVY
      A=YBAR-B*XBAR
      SSRES = SSDY - B*B*SSDX
      S2 =(( SSY-SUMRY*SUMRY/XLMAX-(B/XLMAX)*(XLMAX*SUMRXY-SUMRX*SUMRY)
     1)/(XLMAX-2.))
      STDB = SQRT(S2/( SSX-XLMAX*XBAR*XBAR))
      STDA = SQRT(S2)*SQRT( SSX/(XLMAX* SSX-SUMRX*SUMRX))
      ACONFAC=SQRT(SSRES/(XLMAX-2.))*SQRT(1./XLMAX+XBAR*XBAR/SSDX)
      BCONFAC=SQRT(SSRES/((XLMAX-2.)*SSDX))
      WRITE(61,999)SUMRX,SUMRY,SUMRXY,XBAR,YBAR,XYBAR,STDEVX,STDEVY,STDE
     1VXY,RSTDVX,RSTDVY,RSTDVXY,
     1    SSDX,SSDY,SSDPXY,SSX,SSY,SSPXY,XLMAX,SSRES,B,A,STDB,STDA,BCONF
     1AC,ACONFAC,CORLCOE
      D = EXP(A)
      UF = -1.*(G4 + D)*(G4 + D)/.005/D/B
      UFPCM2 = UF/.0326
      R1 = .005/(G4 + D)
      R2 = R1*D/G4
      RERUF = 100*((STDA*STDA + .0004 + STDB*STDB/B/B)**.5)
      RERDLC = 100.*((RERUF*RERUF*1E-04 + .0016)**.5)
      WRITE(61,11) R1,R2,G4
      WRITE(61,10) UF,RERUF,UFPCM2,RERDLC
   10 FORMAT(' UF = 'E9.2' RERUF ='F7.2' UFPCM2 = 'E9.2' RERDLC = 'F
     16.2/)
   11 FORMAT(/' R1 = 'E9.2' R2 = 'E9.2,' GAMMA = 'E9.2/)
      IF(UF*UF .GE. 0)1,99
    1 CONTINUE
      WRITE(61,995)
      BP(NN) = A
      SBP(NN) = STDA
      RSBP(NN) = 100.*STDA/A
      XMP(NN) = B
      SMP(NN) = STDB
      RERSIM(NN) = RERUF
      RSMP(NN) = 100.*STDB/B
      GO TO 1006
   99 CONTINUE
      WRITE(61,667)
  667 FORMAT(//////////)
      DO 666 LJ=1,NN
   12 FORMAT(' ' E9.2'     '7(E10.3'     '))
  666 WRITE(61,12) GAM(LJ),BP(LJ), SBP(LJ), RSBP(LJ),XMP(LJ), SMP(LJ),
     1 RSMP(LJ), RERSIM(LJ)
      CALL EXIT
      END
```

1

APPENDIX II

Derivation of Capacitance Equation for Potential Step Experiment Using More General Model for Test Electrode-Solution Interface

Consider the response of an electrochemical cell to an electrical signal to be determined by the test electrode-solution interface and bulk solution properties and that the following model is applicable:

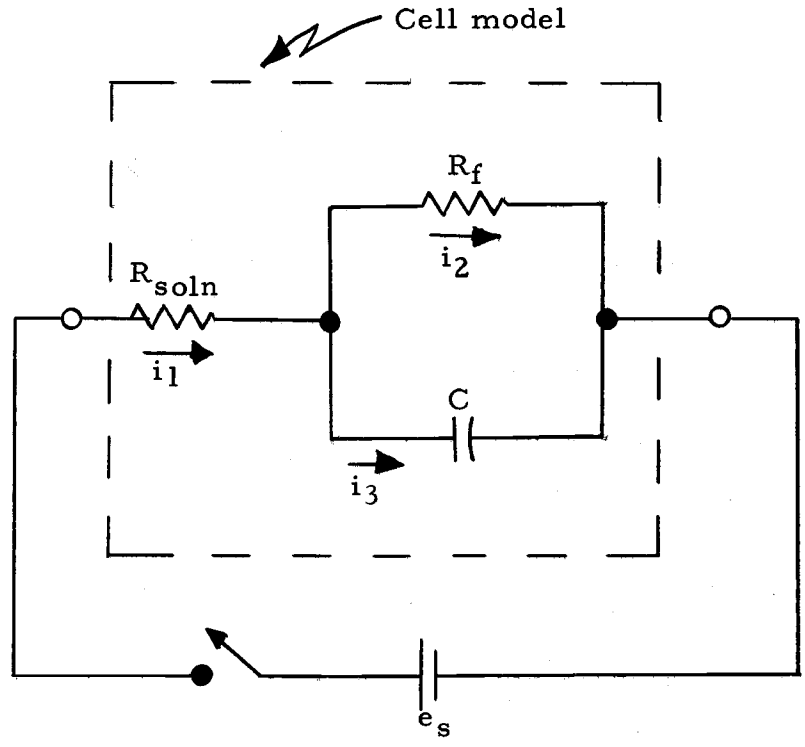

e_s step voltage
i_1 cell current observed from application of step voltage
i_2 faradaic current due to step voltage
i_3 double layer charging current due to step voltage
R_{soln} bulk phase solution resistance
R_f faradaic resistance
C double layer capacity

When the switch is closed:

$$e_s - i_1 R_{soln} - i_2 R_f = 0 \qquad (A1)$$

$$e_s - i R_{soln} - e_c = 0 \qquad (A2)$$

where e_c = potential difference across double layer capacitor.

Subtracting Equation (A2) from Equation (A1):

$$e_c = i_2 R_f \qquad (A3)$$

or

$$\frac{Qc}{C} = i_2 R_f \qquad (A4)$$

where Qc is the charge on the double layer capacitor. Assuming C and R_f to be independent of time in the experiment, Equation (A4) can be differentiated with respect to time to yield:

$$\frac{dQc}{dt} \cdot \frac{1}{C} = \frac{di_2}{dt} \cdot R_f \qquad (A5)$$

or

$$\frac{di_2}{dt} = \frac{i_3}{R_f C} \qquad (A6)$$

Differentiating Equation (A1) with respect to time, and assuming R_{soln} to be time independent yields:

$$\frac{de_s}{dt} - \frac{di_1}{dt} R_{soln} - \frac{di_2}{dt} R_f = 0 \qquad (A7)$$

but after the switch is closed ($t>0$) $\frac{de_s}{dt} = 0$ so that

$$\frac{d\,i_2}{dt} = \left(\frac{R_{soln}}{R_f}\right) \frac{d\,i_1}{dt} \tag{A8}$$

Substituting Equation (A6) into Equation (A8) and rearranging, one obtains:

$$\frac{d\,i_1}{dt} = - \frac{i_3}{R_{soln}\,C} \tag{A9}$$

Since we know that $i_1 = i_2 + i_3$ then

$$\frac{d\,i_1}{dt} = \frac{d\,i_2}{dt} + \frac{d\,i_3}{dt} \tag{A10}$$

Using Equation (A9) and Equation (A6), Equation (A10) can be rewritten to yield:

$$\frac{d\,i_3}{dt} = - i_3 \left[\frac{1}{R_{soln}\,C} + \frac{1}{R_f\,C}\right] = \frac{- i_3}{C} \cdot \left[\frac{R_{soln} + R_f}{R_{soln}\,R_f}\right] \tag{A11}$$

Let

$$\frac{1}{C} \left[\frac{R_{soln} + R_f}{R_{soln}\,R_f}\right] = k$$

Then

$$\frac{d\,i_3}{i_3} = - k\,dt \tag{A12}$$

which can be integrated to yield:

$$\ln i_3 = - kt + \text{integration constant} \tag{A13}$$

At the moment the switch is closed ($t = 0$), R_f is short circuited by C so that i_3 is limited by e_s/R_{soln} so that i_3 is given by:

$$i_3 = \frac{e_s}{R_1} e^{-kt} \tag{A14}$$

The current that is measured in the experiment is i_1 and one must therefore obtain an expression for i_1 as a function of time. By combining Equation (A9) with Equation (A14) one obtains:

$$\frac{d\, i_1}{dt} = - \frac{e_s}{R^2_{soln}\, C} e^{-kt} \tag{A15}$$

or

$$d\, i_1 = - \frac{e_s\, e^{-kt}}{R^2_{soln} C} dt \tag{A16}$$

which can be integrated to yield

$$i_1 = \left(\frac{e_s}{R^2_{soln}\, C} \right) \cdot \left(\frac{1}{k} \right) e^{-kt} + \gamma \tag{A17}$$

where γ is a constant of integration. Replacing k with $\left[\frac{R_{soln} + R_f}{R_{soln} R_f}\right] \frac{1}{C}$ Equation (A17):

$$i_l = \left(\frac{e_s}{R_{soln}}\right)\left(\frac{R_f}{R_{soln} + R_f}\right) \exp\left\{-\left(\frac{R_{soln} + R_f}{R_{soln} R_f}\right)\frac{t}{C}\right\} + \gamma \qquad \text{(A18)}$$

Subtracting γ from each side and taking the natural logarithm of each side of Equation (A18) yields:

$$\ln (i_l - \gamma) = \ln\left[\left(\frac{e_s}{R_{soln}}\right)\left(\frac{R_f}{R_f + R_{soln}}\right)\right] - \left(\frac{R_{soln} + R_f}{R_f}\right)\frac{t}{R_{soln} C} \qquad \text{(A19)}$$

Thus a plot of $\ln(i_l - \gamma)$ versus t is linear with a slope, m', of $-\left(\frac{R_{soln} + R_f}{R_f}\right)\left(\frac{1}{R_{soln} C}\right)$ and an intercept, b', of $\ln\left[\left(\frac{e_s}{R_{soln}}\right)\frac{R_f}{R_f + R_{soln}}\right]$. Note that if the test electrode-solution interface were ideally polarized, $R_f = \infty$, $\gamma = 0$, Equation (A19) reduces to:

$$\ln (i_l) = \ln\left(\frac{e_s}{R_{soln}}\right) - \frac{t}{R_{soln} C} \qquad \text{(A20)}$$

What is γ and how do you use it to obtain an expression for the double layer capacitance? When the double layer is finally charged at $t = \infty$,

$$i_1 = \gamma = \frac{e_s}{R_{soln} + R_f} \tag{A21}$$

Thus γ is a constant since R_{soln} and R_f have been assumed time invariant.

Remembering that $-m' = \left(\frac{R_{soln} + R_f}{R_{soln} R_f}\right) \frac{1}{C}$ then C is given by:

$$C = -\left(\frac{R_{soln} + R_f}{R_{soln} R_f}\right)\left(\frac{1}{m'}\right) \tag{A22}$$

One must obtain an expression for $\frac{R_{soln} R_f}{R_{soln} + R_f}$ from experimentally determinable quantities e_s, b' and γ. Let $D = e^{b'}$ then:

$$D = \left(\frac{e_s}{R_{soln}}\right)\left(\frac{R_f}{R_{soln} + R_f}\right) = \left(\frac{R_f}{R_{soln}}\right)\left(\frac{e_s}{R_{soln} + R_f}\right) \tag{A23}$$

but $\frac{e_s}{R_{soln} + R_f}$ equals γ from Equation (A21), thus

$$D = \gamma \frac{R_f}{R_{soln}} \tag{A24}$$

or

$$R_f = \frac{D R_{soln}}{\gamma} \tag{A25}$$

From Equation (A21)

$$R_{soln} + R_f = \frac{e_s}{\gamma} \tag{A26}$$

replacing R_f with $\frac{D\,R_{soln}}{\gamma}$ in Equation (A26) and rearranging, one obtains:

$$R_{soln} = \frac{e_s}{\gamma + D} \tag{A27}$$

Substituting $\frac{e_s}{\gamma + D}$ for R_{soln} in Equation (A25):

$$R_f = \left(\frac{D}{\gamma}\right)\left(\frac{e_s}{\gamma + D}\right) \tag{A28}$$

and the product of $R_{soln}\,R_f$ is given by:

$$R_f\,R_{soln} = \frac{D}{\gamma}\left(\frac{e_s}{\gamma + D}\right)^2 \tag{A29}$$

From Equations (A26) and (A29) the ratio of the sum of R_{soln} and R_f to their product is:

$$\frac{R_{soln} + R_f}{R_f\,R_{soln}} = \frac{e_s}{D\left(\frac{e_s}{\gamma + D}\right)^2} = \frac{(\gamma + D)^2}{D\,e_s} \tag{A30}$$

and substituting this $\frac{(\gamma + D)^2}{D\,e_s}$ for $\frac{R_{soln} + R_f}{R_f\,R_{soln}}$ in Equation (A22) the double layer capacitance is given by:

$$C = -\frac{(\gamma + D)^2}{D\,e_s\,m'} = -\frac{[\gamma + \exp(b')]^2}{e_s\,m'\,\exp(b')} \tag{A31}$$

APPENDIX III

Derivation of an Equation for γ

For a set of three pairs of current-time measurements along a decay curve in which the current is related to time in the following manner:

$$i = A \exp (Bt) + \gamma$$

where A, B and γ are constants independent of t, the three following separate equations can be written:

$$i_1 = A \exp (Bt_1) + \gamma$$

$$i_2 = A \exp (Bt_2) + \gamma$$

$$i_3 = A \exp (Bt_3) + \gamma$$

On rearranging and taking the natural logarithm for each equation, the following three expressions are obtained:

$$\ln (i_1 - \gamma) = \ln A + Bt_1 \qquad (A32)$$

$$\ln (i_2 - \gamma) = \ln A + Bt_2 \qquad (A33)$$

$$\ln (i_3 - \gamma) = \ln A + Bt_3 \qquad (A34)$$

Subtracting Equation (A33) from Equation (A32) and by suitable rearrangement, the following expression can be obtained:

$$\ln \frac{i_2 - \gamma}{i_1 - \gamma} = B(t_2 - t_1) \qquad (A35)$$

Similar manipulations involving Equations (A33) and (A34) result in Equation (A36):

$$\ln \frac{i_3-\gamma}{i_2-\gamma} = B(t_3-t_2) \tag{A36}$$

If $(t_2-t_1) = (t_3-t_2)$, then it can be shown that

$$\frac{(i_2-\gamma)}{(i_1-\gamma)} = \frac{(i_3-\gamma)}{(i_2-\gamma)} \tag{A37}$$

$$(i_2-\gamma)^2 = (i_3-\gamma)(i_1-\gamma)$$

$$(i_2-\gamma)^2 = i_2^2 - 2\,i_2\gamma + \gamma^2$$

$$(i_3-\gamma)(i_1-\gamma) = i_1 i_3 - i_1\gamma - i_3\gamma + \gamma^2$$

Thus: $$i_2^2 - 2\,i_2\gamma = i_1 i_3 - i_1\gamma - i_3\gamma$$

and therefore:

$$\gamma = \frac{i_1 i_3 - i_2^2}{i_1 + i_3 - 2i_2} \tag{A38}$$

APPENDIX IV

Salt Solubilities in TMS

Compound solubilities are useful measurements. They can be combined with other physical measurements for a solvent to deduce important thermodynamic properties concerning various solution processes. Solubility information is also of great importance to people interested in effecting chemical or electrochemical reactions, perhaps more advantageously, in new solvents. Thus in light of the great interest shown in sulfolane as a solvent, it was surprising to find so few solubility measurements. Outside of Jordan's qualitative solubility information (49) and the reported solubilities of several fatty acids and their methyl esters in commercial grade sulfolane (84), no extensive quantitative solubility data could be found. Solubility products in TMS, as expected, are even more scarce, with only K_{so} values for AgCl (71, 3), AgBr (3, 26), AgI (26) and AgSCN (26) having been reported.

To remedy partially the above situation and to provide another means of comparing the solvent properties of TMS with those of other solvents, the solubilities of 26 chloride and perchlorate salts were determined by instrumental neutron activation analysis (INAA).

Experimental

Chemicals

Sulfolane (Shell Chemical Co.) was twice distilled below 100°C in vacuo. The solvent prepared in this fashion was found to contain less than 0.02% by weight water as determined by a Fisher titration (63). All salts used in this work with the exception of tetramethylammonium chloride and tetraethylammonium perchlorate were of reagent grade quality or purified according to published procedures. In the cases of tetramethylammonium chloride and tetraethylammonium perchlorate, the salts were used as received from the suppliers, K & K Laboratories[1] and Pfaltz and Bauer, Inc.[2]

Sample Preparation

A small amount of each salt sufficient to saturate 3 ml of the solvent was placed in 5 ml glass ampules and the sulfolane was added. The ampules were sealed and placed in a water bath maintained at 40.0° ± 0.5°C. The solutions were allowed to equilibrate for some 250-300 hr with periodic shaking. At the end of the equilibration period, the ampules were opened and a 1 ml aliquot of each supernatant solution was transferred in the open atmosphere to a clean 1/2

[1] K & K Laboratories, Plainview, New York.

[2] Pfaltz & Bauer, Inc., Flushing, New York.

dram polyethylene vial (polyvial). The 1/2 dram polyvials containing the samples were sealed and placed inside 2 dram polyvials for activation.

Activation and Counting

Determination of the salt solubilities in sulfolane was accomplished by subjecting the chloride sample to neutron irradiation and subsequently measuring the amount of induced ^{38}Cl activity. On the basis of a preliminary activation, the 26 samples were divided into two groups. Those with low solubilities (less than 20 m-moles per L.) are referred to as group A and those with higher solubilities, group B. Samples in group A were then reactivated for 30 minutes at a thermal neutron flux of 7.0×10^{10} neutrons cm^{-2} sec^{-1} in the Oregon State University Triga reactor. A second activation on the samples of this group was carried out at a flux of 1.4×10^{11} neutrons cm^{-2} sec^{-1}. Group B samples were also activated twice for 30 minutes each time, but at thermal neutron fluxes of 2.8×10^{10} and 5.6×10^{9} neutrons cm^{-2} sec^{-1}. Included in each group was a set of three ammonium chloride standards so that a calibration plot of ^{38}Cl activity vs. Cl concentration could be used for analysis.

After each activation the 1/2 dram polyvials were placed in new 2 dram polyvials and counted with a 3 in. x 3 in. NaI (Tl) well detector coupled to a 400 channel analyzer. The 1.64 and 2.16 MeV photopeak

areas of 37-min ^{38}Cl were corrected for Compton scattering and decay and both peaks were used generally for analysis. Where interferences were noted, only one γ-ray was used. The number of chloride ions per formula unit was taken into consideration in calculating the salt solubilities.

Results and Discussion

Listed in Table 12 are the solubilities for various salts in sulfolane as determined by neutron activation analysis. These solubilities are expressed in millimoles of salt per liter of saturated solution. Unfortunately, the densities of the saturated solutions were not measured and hence an exact conversion of these values to the molal concentration scale is not possible. The results from each activation are tabulated as well as the average value. The errors appearing with each result under the column marked "solubility" are the errors in solubility due only to counting statistics. The error associated with each average value reported is the absolute experimental standard deviation for all of the results. With a little calculation, it can be seen that the relative standard deviations generally range between 2 and 6%. This is what may be expected from INAA techniques without elaborate sample handling.

The solubility trend of the alkali chlorides in sulfolane parallels that for water and other hydroxylic solvents. For the alkali metal

Table 12. Solubilities of some chloride and perchlorate salts in sulfolane at 40°C.

Compound	Solubility (millimoles/l)	Average	Compound	Solubility (millimoles/l)	Average
LiCl	365 ± 15 361 ± 13 365 ± 11 353 ± 10	361 ± 5	$MgCl_2$	24.0 ± 0.9 24.0 ± 0.9	24.0 ± 0.0
			$CaCl_2$	4.4 ± 0.2 4.5 ± 0.2 4.8 ± 0.2 4.6 ± 0.2	4.6 ± 0.2
NaCl	0.83 ± 0.08 0.92 ± 0.08	0.88 ± 0.06			
KCl	0.53 ± 0.06 0.53 ± 0.03	0.53 ± 0.00	$SrCl_2$	1.06 ± 0.05 1.08 ± 0.05 1.01 ± 0.05 1.08 ± 0.05	1.06 ± 0.04
RbCl	0.86 ± 0.05 0.81 ± 0.05	0.84 ± 0.04			
CsCl	1.1 ± 0.2 1.1 ± 0.2	1.1 ± 0.00	$BaCl_2$	0.12 ± 0.02 0.15 ± 0.02 0.13 ± 0.01 0.12 ± 0.01	0.13 ± 0.02
TlCl	0.41 ± 0.04 0.38 ± 0.04	0.40 ± 0.02			
$CdCl_2$	1.39 ± 0.09 1.46 ± 0.06 1.49 ± 0.07 1.41 ± 0.06	1.44 ± 0.05	AgCl	0.12 ± 0.02 0.19 ± 0.02 0.16 ± 0.02 0.18 ± 0.02	0.16 ± 0.03
			$NaClO_3$	40 ± 2 33 ± 2	36 ± 5
$KClO_4$	88.9 ± 4 90 ± 3	89.5 ± 0.8	$NaClO_4$	990 ± 33 972 ± 39	981 ± 13
$Mg(ClO_4)2$	362 ± 34 381 ± 30 352 ± 22 357 ± 21	363 ± 13	p-chloro-thiophenol	672 ± 31 659 ± 25 669 ± 20 668 ± 18	667 ± 5
NH_4Cl	0.47 ± 0.03 0.52 ± 0.03 0.50 ± 0.03 0.50 ± 0.02	0.50 ± 0.02	NH_4ClO_4	318 ± 13 305 ± 11 322 ± 9 320 ± 9	316 ± 8
$(CH_3)_4NCl$*	11.2 ± 0.7 8.2 ± 0.6	9.7 ± 2	$(CH_3)_4NClO_4$	64 ± 3 64 ± 3 61 ± 2 58 ± 2	62 ± 3
$(C_2H_5)_4NCl$	615 ± 25 605 ± 25 611 ± 16 591 ± 18	605 ± 10			
			$(C_2H_5)_4NClO_4$*	504 ± 18 533 ± 16	519 ± 21
$(C_3N_7)_4NCl$	450 ± 18 455 ± 18 452 ± 12 448 ± 13	451 ± 3	$(C_3H_7)_4NClO_4$	258 ± 11 274 ± 10 273 ± 8 270 ± 7	269 ± 7
			$(C_4H_9)_4NClO_4$	824 ± 42 826 ± 39 800 ± 24 790 ± 22	810 ± 18

* Salt used for solubility study was used as received from supplier, and interfering impurities were noted in gamma ray spectrum.

series, Li through Cs, sulfolane, water, methanol and ethanol show a minimum in molar solubility at KCl, and similar solubilities for the potassium and ammonium chlorides. In this respect the solubilities in sulfolane do not show a resemblance to those in SO_2 as suggested by Drago (30). In liquid SO_2 the solubility minima for the alkali chlorides and bromides are reached at sodium and the solubilities of the corresponding ammonium halides do not correspond closely to those of the potassium salts.

The similarity of the solubilities of ammonium chloride and potassium chloride in sulfolane and the dissimilarity in solubilities of these two salts in liquid sulfur dioxide cannot be readily explained in terms of a difference in solvent dielectric properties alone. However, the shift in the solubility minimum for the alkali metal chlorides to KCl in higher dielectric media such as sulfolane is qualitatively consistent with predictions based on Johnson's (47) equations relating variations in free energies of solution with cation size and solvent dielectric constant.

Solvent dielectric constant, while of some import in affecting the free energy of solvation of an ion, is not apparently the main factor in determining salt solubility in non-aqueous solvents. Attempts to quantitatively relate solubility and bulk solvent dielectric constant have repeatedly failed (70, 20). It would seem from this that specific solvent-solute interactions rather than simple electrostatic

considerations might play a predominant role in influencing solubility. The lack of correlation between solubility and bulk dielectric constant is apparent when one compares the solubilities of the alkali chlorides determined in this work for TMS with those for the same salts in dimethyl-sulfoxide (DMSO). The bulk dielectric constants for these two solvents are very similar ($\epsilon_{DMSO} = 46.6$ at 25°C, $\epsilon_{TMS} = 44.1$ at 40°C). Hence on the basis of the Born equation (8) or any of its modified versions using ion size adjustments, the free energy of solution for a salt or the solubility should be similar in both solvents. Shown in Table 13 are the molar solubilities of the alkali chlorides in TMS at 40°C and the molar solubilities of these salts in DMSO at 25°C. The values listed for DMSO were reported in the original reference on the molal concentration scale (70). To convert these values to the molar concentration scale, it was assumed that the saturated solutions were sufficiently dilute so that the differences in densities between the pure solvent and the saturated solutions were negligible. The solubility on the molar concentration scale can then be equated to the product of the solubility expressed on the molal scale and the density of the pure solvent. At 25°C the density of pure DMSO is 1.096 g/cc (51).

Table 13. Molar solubilities of the alkali chlorides in TMS and DMSO.

Salt	TMS (40°C)	DMSO (25°C)*
LiCl	0.361	2.34
NaCl	0.00088	0.085
KCl	0.00053	0.025
RbCl	0.00084	0.039
CsCl	0.0011	0.041

* Reference (70)

As one can see from the table, the solubilities of the alkali chlorides in TMS are one to two orders of magnitude smaller than those in DMSO. Furthermore, it is seen that the ratio of the salt solubilities in the two solvents is not constant. It is difficult to see how variations in activity coefficients at these concentrations and the moderate difference in temperature between the two experiments could drastically alter the observations. Hence it would appear that the bulk dielectric constant is not the primary factor governing solubility in these solvents.

The solubility trend for the series of anhydrous alkaline earth metal chlorides in sulfolane does not exactly correspond to the trend in solubility for these salts in water. As can be seen from Table 13, a steady decrease in solubility in TMS is observed with increasing cation size. For water a local maximum in solubility is reached at calcium for this series of salts. However, the solubility trend in sulfolane is in agreement with the observed trend in the free energies of solution for these salts in aqueous solution (80). The apparent

difference between the order of solubilities and free energies of solution in water for this series can perhaps be attributed to the formation of a new solid magnesium chloride hydrate phase. If such a hydrate phase were to form before the equilibrium between the anhydrous salt and the solution phase were attained, magnesium chloride would appear to be less soluble than the calcium salt.

The much higher solubility of the tetraalkylammonium chloride salts over the alkali and alkaline earth metal chlorides in sulfolane is to be expected. The lattice energies for the tetraalkylammonium chlorides are generally considerably smaller than those of the metal salts. Thus the solvation energies required to dissolve the crystal lattice are much less, resulting in higher solubilities. The very low heat of fusion of sulfolane coupled with the large heat of vaporization of the solvent suggests that there is little difference between the liquid state and the crystalline solid. The tetraalkylammonium salts are known to be solvent structure breakers. Thus by introducing the large, bulky tetraalkylammonium salts and disrupting the "ordered liquid," there also should be a large positive entropy change favoring dissolution of these salts. The high solubilities and degree of dissociation of these salts (25) in sulfolane will be quite useful to electrochemists studying electrode reactions in this solvent.

The solubility product can often be used to furnish a rough estimate of the solubility of a sparingly soluble salt. If side reactions

involving the ions formed in the dissolution process are not absent, the solubility product can still be combined with the equilibrium constants for the side reactions to estimate the solubility. The lack of solubility products and formation constants in sulfolane does not allow one to calculate many solubilities. However, recently a study of the equilibria between silver and halide ions was undertaken and the solubility products for a few silver halide salts and the formation constants for silver halide complexes have been reported (26, 3). It is of interest to compare the solubility of one of these salts, silver chloride, measured in this work, with the solubility estimate made from the solubility product and the various equilibrium constants.

Benoit et al. (3) found that two equilibria could be used to describe the potentiometric titration of chloride ion with silver ion in sulfolane. The equilibrium reactions used to describe their titration curve were:

$$AgCl\ (solid) \longrightarrow Ag^+ + Cl^- \qquad pK_{so} = 18.38$$

$$Ag^+ + Cl^- \longrightarrow AgCl_2^- \qquad \log \beta_2 = 20.19$$

The values for K_{so} and β_2 listed above are for the ionic strength used in the titration, which was approximately 0.001. Benoit claimed that their potentiometric titration work failed to show any evidence for the existence of any soluble complexes other than the mononuclear dihalide silver species, $AgCl_2^-$. Benoit's conclusions about the

formation of a single silver complex for chloride and bromide agree with the conclusions reached by Della Monica et al. (26) for bromide and thiocyanate. For the larger iodide ion, though, Della Monica reports that a polynuclear complex, $Ag_3I_4^-$, is the single complex formed. Thus, for a TMS solution saturated with AgCl, the following mass balance equation should apply.

$$C_{TCl} = (Cl^-) + 2\,(AgCl_2^-)$$

The parentheses in the above equation indicate molar concentration and C_{TCl} refers to the total concentration of chloride in the solution and hence to the molar solubility, s_{AgCl}, of AgCl.

If one neglects activity coefficients and assumes that the only species present in the saturated solution are Ag^+, Cl^-, and $AgCl_2^-$, a rough estimate of the solubility of silver chloride can be calculated from the following equation:

$$s_{AgCl} = \frac{(K_{so} + 2\,\beta_2 K_{so}^2)}{(K_{so} + \beta_2 K_{so}^2)^{1/2}}$$

where K_{so} and β_2 are equilibrium constants for the reactions shown above. By substituting values for K_{so} and β_2 into the above expression, the predicted molar solubility of AgCl in sulfolane at 30°C is found to be 1.04×10^{-8}. This is approximately 4 to 5 orders of magnitude smaller than was found experimentally. Although Benoit's

potentiometric work was carried out at 30°C and the solubility reported in this work was at 40°C, it does not seem likely that this moderate difference in temperature between the two experiments could account for such an incredible difference between the predicted and observed solubilities. It seems equally unreasonable that the observed difference could be produced by variations in activity coefficients.

To explain the large difference between the predicted and observed solubilities of AgCl, it seems necessary to postulate the existence of another silver species in a solution saturated with AgCl. It will be recalled that only two silver species, Ag^+ and $AgCl_2^-$, were used in computing the solubility. This was done because Benoit and Della Monica could find no evidence for the existence of other complexes from their potentiometric and conductometric work and could quite satisfactorily describe the potentiometric titration curve of chloride ion with silver ion using only two equilibria. The evidence for higher complexes than $AgCl_2^-$ in nonaqueous solvents with high dielectric constants like sulfolane is indeed scant. Likewise, there is no evidence for the existence of polynuclear complexes between silver and chloride ions at this time. The only silver species remaining, then, that could reasonably be considered to exist in high enough concentration to explain the large difference between the expected solubility and the observed value is the non-charged, monohalide complex, AgCl.

Formation constants for the AgCl complex species in other non-aqueous solvents have been reported (11, 17) and they are substantial, of the order of 10^{15} for propylene carbonate and dimethylformamide. Thus considering the following equilibria to apply to a saturated solution of AgCl a new expression for the molar solubility can be derived.

$$AgCl\ (solid) \rightleftharpoons Ag^+ + Cl^- \qquad pK_{so} = 18.38$$

$$Ag^+ + Cl^- \rightleftharpoons AgCl\ (solution) \qquad \log \beta_1 = ?$$

$$Ag^+ + 2\ Cl^- \rightleftharpoons AgCl_2^- \qquad \log \beta_2 = 20.19$$

The expression is

$$s_{AgCl} = \frac{(K_{so} + 2\ \beta_2\ K_{so}^2)}{(K_{so} + \beta_2\ K_{so}^2)\ I/2} + \beta_1\ K_{so}$$

which is similar to the previous solubility expression except for the additional term, $\beta_1\ K_{so}$. Knowing what the molar solubility is for AgCl from experiment and using Benoit's values for K_{so} and β_2, one can calculate β_1. When the appropriate substitutions are made and the expression is solved for β_1, β_1 is found to be 3.84×10^{14}. This value for β_1 in sulfolane is comparable to that reported for this reaction in propylene carbonate (11).

While β_1 is quite large on an absolute scale, it is relatively small compared to β_2. Its effect, then, on the predicted shape of the potentiometric titration curve for the titration of chloride ion with silver ion should be small. That is, the shape of the titration curve

predicted by Benoit should not be much different from that predicted when the formation of the AgCl complex is taken into consideration. To confirm this, expressions were derived for calculating the titration curve allowing for the existence of the AgCl complex. A plot of the calculated titration curve considering both AgCl and $AgCl_2^-$ complexes formation is shown in Figure 26. The calculations were performed assuming the same experimental conditions employed by Benoit in his work. Also plotted in this figure are the data from the real experiment and the data generated by Benoit considering only $AgCl_2^-$ formation.

Rather than plot cell potentials versus the volume of silver solution added, it was found more convenient to calculate and plot the cell potential versus ϕ where ϕ is a parameter that expresses the fraction of material titrated. ϕ is simply the ratio of the number of moles of silver ion added to the number of moles of chloride ion initially present. The derivation of the expressions relating ϕ to the silver ion activity (or concentration if we assume that the activity coefficients of the species in solution are unity) is somewhat similar to that used by Butler (12) in relating ϕ to (Ag^+) in the Leibig titration. The present derivation, however, is more rigorous than Butler's in that no a priori assumptions regarding the relative levels of the complexes are made. The complete development of the expressions used to describe the potentiometric titration of Cl^- with Ag^+ in

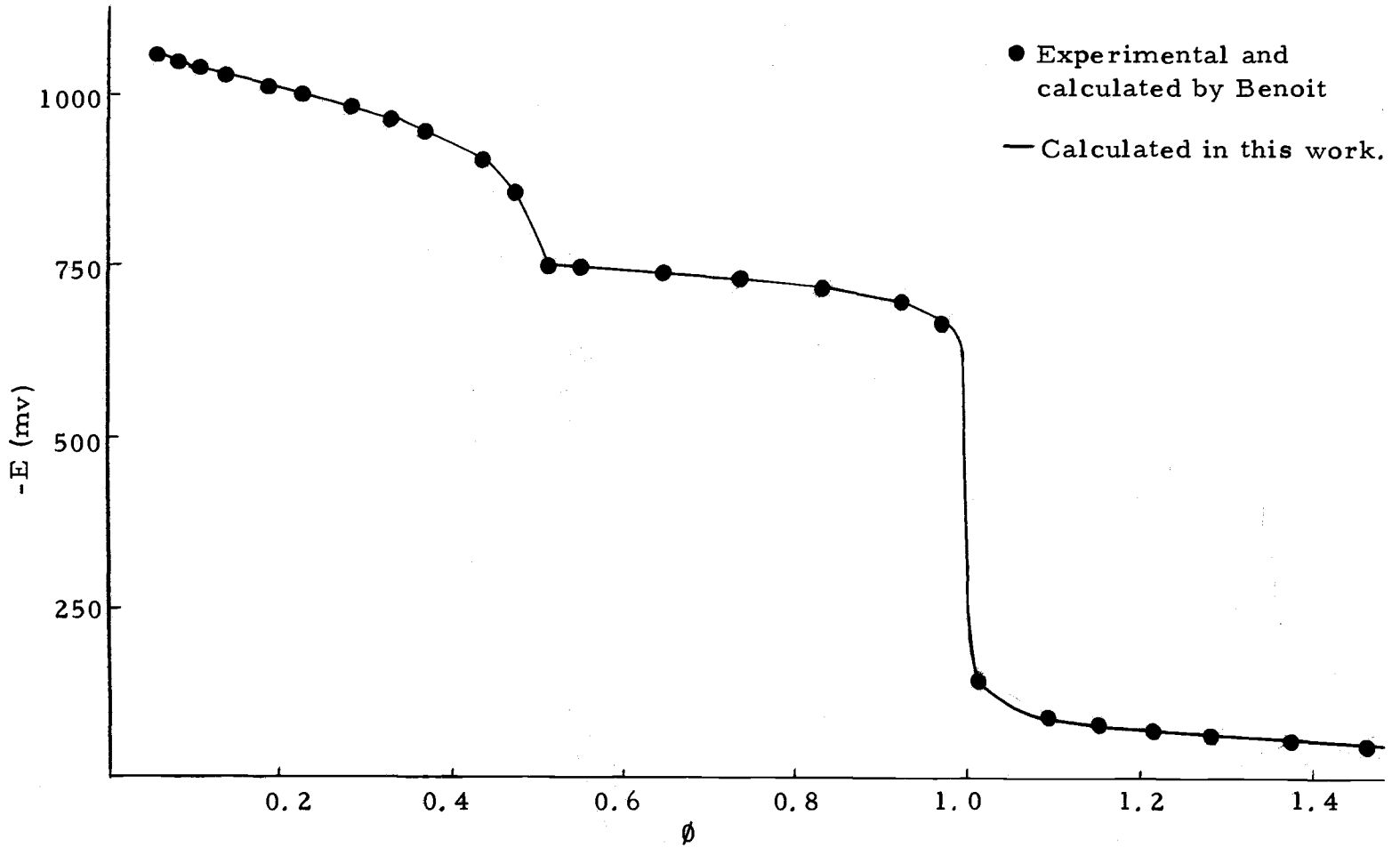

Figure 26. Potentiometric titration of chloride with silver ion in TMS.

sulfolane can be found at the end of this appendix along with a listing of the Fortran program used to perform the required calculations.

The titration curve computed taking into account the formation of the monohalide complex is not detectably different from that predicted by Benoit and fits his experimental data equally well, as shown in Figure 25. This is as intuitively expected. The magnitude of β_1 is relatively small compared to that of β_2 and to the reciprocal of K_{so} and thus should have little effect on the shape of the titration curve.

```
      PROGRAM TITRAT
C THIS PROGRAM CALCULATES THE POTENTIOMETRIC TITRATION CURVE
C FOR THE TITRATION OF CL ION WITH AG ION IN SULFOLANE
      DIMENSION SI(1000), AG(1000), CLX(1000), E(1000)
      B1 = 3.83E+14
      B2 = 1.55E+20
      EO = 100.
      SI = .01
      CL = .01045
      SOK = 4.17E-19
      CAG = .01755
      CCL = .01045
      N = 0
      DO 1 J = 1, 10000
    2 CL = CL - CL*.01
      X = 1. - B2*CL*CL
      Y = 1. + B1*CL + B2*CL*CL
      Z = X/Y
      XSI - (1. - CL/CCL)/(1. + CL/CAG - Z)
      DELTA = (XSI - SI(N))/SI(N)
      IF(DELTA .LT. .01)2, 3
    3 IF(XSI .GT. .5)5, 4
    4 N = J
      SI(N) = XSI
      G = SI(N)*CCL/(1. + SI(N)*CCL/CAG)
      AG(N) = G/Y
      E(N) = EO + 8314*303*ALOG(AG(N))/96487
      CLX(N) = CL
    1 CONTINUE
    5 AAG = AG(N)
      DO 9 K = 1, 10000
    6 AAG = AAG + AAG*.01
      T = SOK/AAG - AAG + SOK*SOK*B2/AAG
      XSI = (CCL - T)/(CCL + T*CCL/CAG)
      DELTA = (XSI - SI(N))/SI(N)
      IF(DELTA .LT. .01)6, 7
    7 IF(XSI .GT. 1.55)99, 8
    8 N = N + 1
      SI(N) = XSI
      AG(N) = AAG
      E(N) = EO + 8314*303*ALOG(AAG)/96487
      CLX(N) = SOK/AAG
    9 CONTINUE
   99 DO 21 L = 1, N
      IF((L+120) .GT. N)999, 21
   21 WRITE(20, 10) SI(L), AG(L), CLX(L), E(L), SI(L+120), AG(L+120)
     1, CLX(L+120), E(L+120)
   10 FORMAT(2('       'F7.4, 2('       'E10.3)'       'F7.1))
  999 CALL EXIT
      END
```

Derivation of Expressions for Describing the Potentiometric Titration of Tetraethylammonium Chloride with Silver Perchlorate in Sulfolane

Equations (A39) - (A41) are mass balance expressions that must apply throughout the titration, and Equation (A42) is a definition.

$$C_{Ag} V_{Ag} = [V_{Cl} + V_{Ag}] [(Ag^+) + (PPt) + (AgCl) + (AgCl_2^-)] \quad (A39)$$

$$C_{Cl} V_{Cl} = [V_{Cl} + V_{Ag}] [(Cl^-) + (PPt) + (AgCl) + 2(AgCl_2^-)] \quad (A40)$$

$$(Et_4N^+) + (Ag^+) = (Cl^-) + (AgCl_2^-) + (ClO_4^-) \quad (A41)$$

$$\phi = \frac{C_{Ag} V_{Ag}}{C_{Cl} V_{Cl}} = \frac{(ClO_4^-)}{(Et_4N^+)} \quad (A42)$$

C_{Ag} and C_{Cl} refer to the concentrations of the titer and titrant. V_{Ag} and V_{Cl} are the volumes of the titer and titrant. The parentheses around the ions and complex species indicate molar concentration. (PPt) is defined as the number of moles of precipitate per liter of solution; it is treated as a pseudo solute.

The titration can be conveniently divided into two parts. The first portion of the titration is one in which no AgCl precipitate is formed while the second portion consists of the part of the titration in which the precipitate is present.

Part I (PPt) = 0

For this portion of the titration curve, one must derive an expression for ϕ in terms of (Cl^-) and various constants. Start with Equation (A41) and replace (ClO_4^-) by means of Equation (A42).

$$(Et_4N^+) + (Ag^+) = (Cl^-) + (AgCl_2^-) + (Et_4N^+)\,\phi$$

Solve for ϕ.

$$\phi = 1 + \left[\frac{(Ag^+) - (Cl^-) - (AgCl_2^-)}{(Et_4N^+)}\right] \tag{A43}$$

Since $(Et_4N^+) = \dfrac{C_{Cl}\,V_{Cl}}{V_{Ag} + V_{Cl}}$

$$\phi = 1 + \left[\frac{[(Ag^+) - (Cl^-) - (AgCl_2^-)]\,[V_{Ag} + V_{Cl}]}{C_{Cl}\,V_{Cl}}\right] \tag{A44}$$

Replace $(AgCl_2^-)$ with $\beta_2\,(Ag^+)\,(Cl^-)^2$ and rearrange.

$$\phi = 1 + \left[\frac{(Ag^+)\,[1 - \beta_2(Cl^-)^2] - (Cl^-)\quad[V_{Ag} + V_{Cl}]}{C_{Cl}\,V_{Cl}}\right] \tag{A45}$$

Now one must get ride of (Ag^+) in Equation (A45) so rewrite Equation (A39) replacing (AgCl) and $(AgCl_2^-)$ with expressions involving (Ag^+), (Cl^-) and an equilibrium constant. Remember that for this portion of the titration curve (PPt) = 0. Thus Equation (A39) can be rewritten as follows:

$$C_{Ag}V_{Ag} = [V_{Ag} + V_{Cl}]\,[(Ag^+) + (Ag^+)(Cl)\beta_1 + (Ag^+)(Cl^-)^2\,\beta_2]$$

Solve for (Ag^+).

$$(Ag^+) = \left[\frac{C_{Ag} V_{Ag}}{V_{Cl} + V_{Ag}}\right] \left[\frac{1}{1 + \beta_1(Cl^-) + \beta_2(Cl^-)^2}\right] \tag{A46}$$

Combine Equations (A45) and (A46) to get an expression for $\emptyset$ that does not explicitly contain (Ag^+).

$$\emptyset = 1 + \left[\frac{C_{Ag} V_{Ag}}{C_{Cl} V_{Cl}}\right] \left[\frac{1 - \beta_2(Cl^-)^2}{1 + \beta_1(Cl^-) + \beta_2(Cl^-)^2}\right] - \frac{[V_{Ag} + V_{Cl}](Cl^-)}{C_{Cl} V_{Cl}} \tag{A47}$$

But since $V_{Ag} = \frac{\emptyset C_{Cl} V_{Cl}}{C_{Ag}}$ (from Equation (A42))

$$\emptyset = 1 + \emptyset \left[\frac{1 - \beta_2(Cl)^2}{1 + \beta_1(Cl) + \beta_2(Cl^-)^2}\right] - \frac{\emptyset(Cl^-)}{C_{Ag}} - \frac{(Cl^-)}{C_{Cl}} \tag{A48}$$

Solve Equation (A48) for $\emptyset$.

$$\emptyset = \frac{\frac{1 - (Cl^-)}{C_{Cl}}}{1 + \frac{(Cl^-)}{C_{Ag}} - \left[\frac{1 - \beta_2(Cl)^2}{1 + \beta_1(Cl) + \beta_2(Cl^-)^2}\right]} \tag{A49}$$

One can now calculate $\emptyset$ for various levels of free chloride ion, but one still needs an expression for (Ag^+) in terms of $\emptyset$ and (Cl^-) to calculate the first portion of the potentiometric titration curve. By

substituting $\frac{\phi C_{Cl} V_{Cl}}{C_{Ag}}$ for V_{Ag} in Equation (A46), one can obtain Equation (A50).

$$(Ag^+) = \left[\frac{\phi C_{Cl}}{1 + \phi \frac{C_{Cl}}{C_{Ag}}}\right] \left[\frac{1}{1 + \beta_1 (Cl^-) + \beta_2 (Cl^-)^2}\right] \quad \text{(A50)}$$

which relates (Ag^+) to ϕ and (Cl^-). Applying the Nernst relation to Equation (A50), the cell potential can be calculated for various levels of free chloride ion up to the point where silver chloride begins to precipitate. Precipitation should first occur for values of ϕ between 0.4999 and 0.5000 if local silver ion excesses can be avoided.

Part II

Equation (A50) does not apply to the second half of the titration because of the presence of AgCl precipitate and hence a new expression relating ϕ and (Ag^+) must be developed. By combining Equations (A39) and (A40) which apply throughout the entire titration, one can obtain Equation (A51).

$$C_{Cl} V_{Cl} - C_{Ag} V_{Ag} = [V_{Cl} + V_{Ag}] [(Cl^-) - (Ag^+) + (AgCl_2^-)] \quad \text{(A51)}$$

Since the solution is now in equilibrium with solid AgCl, the (Cl^-) can be replaced with $K_{so}/(Ag^+)$ and using β, $(AgCl_2^-)$ can be replaced with $\frac{K_{so}^2 \beta_2}{(Ag^+)}$. Making these substitutions in Equation (A51), one obtains Equation (A52).

$$C_{Cl} V_{Cl} - C_{Ag} V_{Ag} = [V_{Cl} + V_{Ag}] \left[\frac{K_{so}}{(Ag^+)} - (Ag^+) + \frac{K_{so}^2 \beta_2}{(Ag^+)} \right] \quad (A52)$$

Substituting $\frac{\phi C_{Cl} V_{Cl}}{C_{Ag}}$ for V_{Ag} in Equation (A52), rearranging and solving for ϕ, Equation (A53) can be obtained.

$$\phi = \frac{C_{Cl} - \left[\frac{K_{so}}{(Ag^+)} - (Ag^+) + \frac{K_{so}^2 \beta_2}{(Ag^+)} \right]}{C_{Cl} + \left[\frac{C_{Cl}}{C_{Ag}} \right] \left[\frac{K_{so}}{(Ag^+)} - (Ag^+) + \frac{K_{so}^2 \beta_1}{(Ag^+)} \right]} \quad (A53)$$

All that one has to do now is to calculate ϕ for various values of (Ag^+) and use the Nernst relation to obtain the cell potential. A plot of the cell potential versus ϕ then represents the titration curve for the second half titration.